INFORMATION TO USERS

This manuscript has been reproduced from the microfilm master. UMI films the text directly from the original or copy submitted. Thus, some thesis and dissertation copies are in typewriter face, while others may be from any type of computer printer.

The quality of this reproduction is dependent upon the quality of the copy submitted. Broken or indistinct print, colored or poor quality illustrations and photographs, print bleedthrough, substandard margins, and improper alignment can adversely affect reproduction.

In the unlikely event that the author did not send UMI a complete manuscript and there are missing pages, these will be noted. Also, if unauthorized copyright material had to be removed, a note will indicate the deletion.

Oversize materials (e.g., maps, drawings, charts) are reproduced by sectioning the original, beginning at the upper left-hand corner and continuing from left to right in equal sections with small overlaps.

Photographs included in the original manuscript have been reproduced xerographically in this copy. Higher quality 6" x 9" black and white photographic prints are available for any photographs or illustrations appearing in this copy for an additional charge. Contact UMI directly to order.

ProQuest Information and Learning
300 North Zeeb Road, Ann Arbor, MI 48106-1346 USA
800-521-0600

Université d'Ottawa · University of Ottawa

AN EXPERIMENTAL STUDY AND NUMERICAL SIMULATION OF SAND-STEEL INTERFACE BEHAVIOUR

Baocheng Li, B. Eng.

A Thesis
Submitted to the School of Graduate Studies and Research
Under the Supervision of

Dr. Erman Evgin

in partial fulfillment of the requirement for the degree of
Master in Applied Science in Civil Engineering

Department of Civil Engineering
University of Ottawa
Ottawa, Ontario
Canada K1N 6N5

May 2001

The Master in Applied Science in Civil Engineering is a joint program between Carleton University and the University of Ottawa, which is administered by the Ottawa-Carleton Institute for Civil Engineering

ABSTRACT

In a soil-structure interface test, the soil sample consists of two parts: the soil mass and the interface layer. In the previous experimental investigations of the soil-structure interface problems, the soil deformation in the interface layer was not measured separately from the soil deformation in the soil mass. Consequently, most of the previous numerical interface models were based on the combined deformation of the interface layer and soil mass.

The main objective of this research was to determine the stress-deformation behaviour of soil in the interface layer. The existing interface apparatus, C3DSSI, was set up to measure separately the tangential displacement due to the deformation of the sand sample, which included the soil mass and the interface layer, and the displacement due to sliding at the contact surface. Digital photography was used effectively to determine the deformations of sand in the interface layer separate from the sand mass. Experiments showed that strain localization takes place in the interface layer and the thickness of the interface layer increases gradually as the shear stress increases during a test.

A Fortran program for Lade's model was written to simulate numerically the sand-steel interface behaviour. The simulation consisted of two sections: the simulation of the behaviour of the sand mass, and the simulation of the sand behaviour in the interface zone. Comparisons were made between the results of the numerical modelling and the experimental results. These comparisons showed that Lade's work hardening model can be used with moderate success for the simulation of interface behaviour.

ACKNOWLEDGEMENTS

The author wishes to express his sincere thanks to his supervisor, Dr. Erman Evgin, for his continuous encouragement, general advice, and financial support throughout the program of research.

The technical assistance provided by the support staff, R. J. Moore, is gratefully acknowledged. Also special thanks to the fellow graduate student, Julio Angel Infante Sedano for his help.

The author would like to thank his parents, brothers and sister, for their encouragement and financial support. Finally, it is the author's wife, Yan Gao, whose encouragement and patience made this Master study successful.

TABLE OF CONTENTS

LIST OF TABLES

LIST OF FIGURES

CHAPTER 1
INTRODUCTION

1.1 Statement of Problem

In many geotechnical engineering problems, soils interact with structural members. Examples of soil-structure interaction problems include foundations of buildings, storage tanks, bridges, buried pipes and culverts, retaining walls, tunnels, and offshore platforms.

For the solution of a soil-structure interaction problem, the magnitude of load transferred at the interface has to be known. The interface is defined as a thin layer of soil next to the surface of the structural member. The behaviour of the soil in the interface layer is influenced by the surface roughness of the structural member, therefore, it is significantly different than the behaviour of the soil in the soil mass. In order to improve the present understanding of load transfer between soils and structures it is necessary to determine experimentally the behaviour of soil in the interface zone.

In the past, experimental investigations were conducted on soil-structure interfaces to obtain reliable estimates of soil-structure interface behaviour. Potyondy (1961) first performed a comprehensive series of direct shear type interface tests to determine the skin friction between different types of soils and construction materials. Since then more and more investigations have been carried out using various interface-testing devices. The most commonly used device is the direct shear type device (e.g., Potyondy 1961; Desai et al. 1985; Boulon and Plytas (1986). Yoshimi and Kishida (1981) used a ring torsion device to overcome the disadvantages of the direct shear type apparatus such as non-uniformity of

stresses and strains within the specimen. A simple shear type device was used for monotonic loading (Uesugi and Kishida 1986) and cyclic loading (Uesugi et al. 1989) of interfaces. The simple shear type device allows the measurement of sliding displacement between a structural material and soil as well as shear deformation of the soil mass. Simple shear type device allows the measurement of sliding displacement between a structural material and soil as well as shear deformation of the soil mass. Fakharian and Evgin (1996) developed a computer-controiled apparatus to study the behaviour of interfaces under three-dimensional monotonic and cyclic loading conditions. The interface apparatus is referred to as cyclic 3-Dimensional testing of interfaces (C3DI) whenever the direct shear box is used as the soil container, or cyclic 3-Dimensional simple shear testing of interfaces (C3DSSI), if the simple shear box is employed.

Previous research studies have provided information on the influence of various parameters on shear strength parameters and stress-displacement characteristics of interfaces. These parameters include: surface roughness of the structural material, composition and moisture content of soil, relative density, magnitude of normal stress, and boundary conditions in the direction normal to the interface plane.

On the numerical analysis side of investigations of soil-structure interface behaviour, several interface models have been developed (Fishman and Desai, 1987; Boulon and Plytas, 1986; Vardoulakis, 1994). However, there are still some uncertainties about the interface behaviour and the reliability of existing constitutive models. In the development of most constitutive models, the behaviour of soil in the interface layer was not separated from the behaviour of soil in the soil mass. Only a limited number of research work presently exists on observations of sample deformation and the shear band formation in the interface zone (Yoshimi and Kishida, 1981; Uesugi and Kishida, 1986).

For the development of a new mathematical model it is essential to obtain the stress-deformation behaviour of soil in the interface layer separate from the behaviour of soil in the soil mass.

The purpose of this thesis is to explore the above issue in some detail, using experimental methods as well as a numerical method.

1.2 Research Objectives

The main objectives of this thesis are as follows:

1. To determine experimentally the behaviour of soil in the interface layers.

2. To develop a mathematical model for the behaviour of interfaces.

1.3 Scope of Research

In order to achieve the above objectives, the following studies were conducted in this research:

1. A series of sand-steel interface tests were carried out using C3DSSI apparatus under constant normal stress boundary conditions. Modifications were made on this apparatus to observe the development of the stress-deformation response of sand-steel interface system. The measurements produced the information needed for the development of the mathematical model.

2. A digital camera was used to take pictures of the deformed shape of the interface layer at different stages. These pictures were then digitized by using a computer program named "digitizer" to obtain the deformation curves and the magnitude of slip at each stage.

3. A series of drained triaxial tests were performed on sand samples with various initial relative densities under four different confining pressures. The experimental data were used to obtain the parameters of Lade's model. Comparisons were made between the experimental data and the results of simulations using Lade's model.

4. Lade's model was used to develop a mathematical model for sand-steel interfaces.

1.4 Outline of Thesis

The thesis is organized in the following way:

Chapter 2 presents a literature review on the experimental investigations of soil-structure interface behaviour. Presently available interface testing apparatuses, their characteristics, and observed interface behaviour are discussed.

In Chapter 3, the behaviour of an interface between sand and steel under constant normal stress conditions was investigated. The effects of normal stress and initial relative density on the behaviour of the interface were examined.

Chapter 4 introduced the digitization method for the analysis of sand deformations. First, a brief literature review was presented concerning the observation of particle movement. The modification of C3DSSI apparatus and procedures for the analysis of sand deformations by a digitization method were described in detail. The sand deformation curves at different stages were presented.

Chapter 5 gives a literature review of some constitutive models, such as Cam-Clay model, Nor-sand model, Cosserat model, and Lade's Model. These models were considered in the development of a mathematical model for soil-structure interface behaviour. This review includes the advantages and disadvantages of various existing interface models and constitutive relations.

Chapter 6 presents a detailed description of Lade's model. First the experimental data from triaxial tests are presented in detail. The data are then used in the determination of the parameters for Lade's model. Finally these parameters were used to simulate the relationships of deviator stress vs. axial strain as well as the volumetric strain vs. axial strain for triaxial tests. Advantages as well as limitations of Lade's model are presented in this chapter.

Chapter 7 describes the procedures, using Lade's model, for modelling the behaviour of sand-steel interfaces. Then the modelling results for the soil mass as well as for the interface zone are presented. Finally, the comparisons are given between the results of the numerical modelling and the experimental data presented earlier in Chapter 4.

Chapter 8 presents the conclusions of the present research and the suggestions for further studies.

CHAPTER 2
EXPERIMENTAL OBSERVATIONS OF INTERFACE BEHAVIOUR: LITERATURE REVIEW

2.1 Devices Used for Interface Testing

2.1.1 Direct Shear Type Device

The direct shear testing of interfaces is similar to direct shear testing of soils. A hollow box, which contains the soil specimen, rests on a construction material. The load in the normal direction is applied by a loading platen to the top of the soil sample. The horizontal load is gradually increased to shear the interface.

Potyondy(1961) used a direct shear type soil container to determine the coefficient of friction between different types of soils and construction materials. Both strain-controlled and stress-controlled tests were conducted. The specimens of construction materials were placed in the lower portion of the box, and the soil was placed in the upper half.

Desai *et al.* (1985) also used a direct shear type device to study the friction between sand and steel/concrete under the conditions of repeated loading (Fig. 2.1a). The bottom half of the box, which was made from steel plates, had a square cross-section and with inner dimensions of 410 × 410 mm. One of the materials such as concrete, ballast, rock was inserted in the bottom half. The top part consisted of a square box (310 × 310 mm) and contained the other material. Thus, an interface of 310 × 310 mm was created at the junction (Fig. 2.1b).

The direct shear type apparatus is simple in sample preparation and in test procedures. However, the major shortcomings of this apparatus are: (1) the development of heterogeneity in the sample along the direction of shear as the test progresses; (2) the stress concentration at the ends; (3) a loss of material between the half boxes or the half box and the plate; (4) a tilting of the half box resulting an additional friction; and (5) the difficulty of separating the interface sliding displacement and the displacement due to soil deformation.

2.1.2 Simple Shear Type Device

Uesugi and Kishida (1986a) developed a simple shear type device. It measures not only sliding displacement between steel and soil but also shear deformation of soil mass. As shown in Fig. 2.2, the container of sand specimen was a stack of rectangular 2 mm thick aluminium plates with 400 × 100 mm space in the middle. The surface of each plate was lubricated to allow the container to follow the shearing deformation of sand with minimum frictional resistance. The contact surface between steel and sand was originally 400 mm in length and 100 mm in breadth. Because the steel plate was longer than the friction surface, the area of friction surface remained constant during a test even after sliding occurred. The simple shear type apparatus solves the problem of separation between sliding displacement and shear deformation of soil sample. But, the stress non-uniformity still exists in the simple shear tests.

2.1.3 Annular Shear Type Device

The annular shear device was used by Brumund and Leonards (1973) for experimental study of static and dynamic friction between sand and typical construction materials. The test configuration is shown schematically in Fig 2.3. It consists of a cylinder of sand encased in a rubber membrane with a 28.6 mm diameter, 356 mm long rod located along its axis. By evacuating air from within the membrane, a normal stress was applied to sand-rod interface that ranged from 8.6 to 86 kPa. The rod was then caused to slip relative to the sand by

gradually applying static forces to the rod in the axial direction. The coefficient of friction between sand and different materials such as steel, Teflon, cement mortar, and graphite was measured by using this apparatus.

2.1.4 Ring Torsion Type Device

Huck *et al.* (1973) and Huck and Saxena (1981) conducted some experimental investigation on soil-concrete interface phenomena by using a ring torsion apparatus. Soil samples were confined inside and outside by standard membranes and were in contact with the lower and upper concrete rings which were held by steel holders.

A ring torsion apparatus used by Yoshimi and Kishida (1981a,b) is shown in Fig.2.4. First, dry sand was rained into an annular container lined with 0.3 mm thick rubber membrane, and the top surface of the sand was levelled with a suction device. Then a ring shaped metal specimen was placed on the sand as the construction material. A static torque was applied to shear the interface under a constant normal load applied with weights. The circumferential and vertical displacements of the metal ring were measured, by using x-ray radiography. The deformation of sand and slippage at the soil-metal contact was also measured in some tests.

The geometry of the device allows unlimited circumferential displacement, and reduces somewhat the non-uniformities, due to edge effect, of normal and shear stresses at the contact surface and within the soil sample. The sliding displacement and the displacement due to shear deformation were distinguished by using x-ray photography. The ring torsion type apparatus is a complicated system in terms of sample preparation and measurement of shear displacements.

2.1.5 Plane Strain Apparatus

Tejchman and Wu (1995) used a plane strain type apparatus for friction measurement between a sand specimen and a steel plate. The cross section of the sand specimen was 40 ×

80 mm. A wooden wedge with an angle of 67.5° against the horizontal was covered with a steel plate. The angle of the wooden wedge was chosen to be the inclination of the mobilized plane according to the Coulomb failure criterion. The wooden wedge was placed at the bottom of the sand mould. The wedge and the sand specimen were enclosed by a rubber membrane, and confined between two rigid platens. The whole set-up was placed into a chamber with pressure supplied by pressurized air and kept constant throughout the test. The vertical driving force was applied by moving the loading piston downwards. The plane strain apparatus has the advantage that all stress components in the plane of shearing can be determined. But there are still some disadvantages such as stress concentration at the end of the specimen and the decreasing shear surface during the displacement. After the experiments were terminated, the volume change along the steel plate observed by means of x-rays. A dark region marked the dilated zone on the radiographs, because dense sand absorbed more x-rays than loose sand.

2.1.6 3-D Apparatus

Most soil-structure interface testing devices generally measure two-dimensional interface behaviour. Many soil-structure interfaces in engineering practice, however, are subjected to three-dimensional loading. For example, the wind, waves, ice, and ocean currents result in combined repeated axial and lateral loads on offshore gravity structures; power transmission lines are subjected to loads caused by wind and earthquakes, resulting in repeated loads on their foundations. The solutions of these problems require that the interface tests be conducted in three-dimensional mode. Fakharian and Evgin (1993, 1996) developed a computer-automated apparatus for monotonic and cyclic testing of interfaces between soil and structural materials under three-dimensional stress conditions. Both direct shear type and simple shear type soil containers were used. Either displacement-controlled or load-controlled test can be conducted simultaneously in all three directions. The simple shear box consists of a stack of 2 mm thick anodized, Teflon coated, square shape aluminium plates. Two identical ball screw stepper motors are used to directly apply the tangential forces to the contact surface in two orthogonal directions. A motorized air regulator, which is operated by

a built-in stepper motor, adjusts the pressure for the E / P actuator to apply load in the normal direction. The sliding displacement can be distinguished from the shear deformation of the soil mass. The control and data-acquisition are performed by a closed-loop computer controlled system. Therefore, various interface-shearing paths can be realized.

Fakharian (1996) summarized the advantages and disadvantages for each type of device both in performance and also reliability of results, which is presented in Table 2.1.

2.2 Typical Test Results

Depending on the application requirements, either shear strength parameters or stress displacement relations of the interface might be of interest. Shear strength parameters include adhesion, usually denoted by C_a, and angle of friction between soil and structural material, denoted by δ. These parameters are normally required for instability investigation of practical engineering problems such as retaining walls and piles. However, for rigorous and realistic analysis of soil-structure systems, the stress-displacement relations are essential. Fu (1998) summarized the existing soil-structure interface test results, which is shown in Table 2.2. According to the tests listed in this Table, typical test results and effects of some influencing factors are summarized in the following subsections.

Table 2.1 Advantages and Disadvantages of
Existing Interface Testing Devices (after Fakharian, 1996)

Device Type	Advantage	Disadvantage
Direct Shear	Most easily available; Simple system; Simple preparation; Simple procedure.	Unable to separate sliding displacement with shear deformation displacement of sand mass; Stress concentration at ends.
Simple Shear	Constant interface area; Simple preparation; Simple procedure; Displacement factors can be measured separately; Reliable cyclic test results.	Stress concentration at ends.
Annular Shear	Geometrically similar to skin friction of piles and friction of steel reinforcements.	Normal stress on interfaces unknown; Stress concentration at ends.
Ring Torsion	Endless ring interface; No stress concentration at ends; Constant interface area; Large displacement possible.	Complicated system; Difficult to prepare uniform sand mass in a ring shape; Difficult to finish surface roughness of metal ring uniformly.
Plane Strain	All stress components in the plane of shearing be determined	Stress concentration at ends; Decreasing shear surface during deformation; Validity of results only in the range of high cell pressures.

Table 2.2 Description of Some Existing Soil-Structure Interface Tests

(After Fu, 1998)

Conducted by	Apparatus	Loading conditions	Sample dimensions	Soil properties	Structural material
Potyondy (1961)	Direct shear type, strain- and stress-controlled, 2-D	Monotonic, constant normal stress	A = 6×6 cm^2 and 9×9 cm^2	(1) Sand, low and high D_r, dry and saturated (2) Clay, medium PI (3) Mixture of 50% sand and 50% clay	(1) Mild steel, smooth and rough (2) Wood, shaped by planning (3) Concrete, smooth and rough
Brumund and Leonards (1973)	Annular shear type, stress-controlled, 2-D	Static and dynamic (step-type force), constant normal stress	d = 1 1/8 in or 2 in, L = 10 in, h = 3 - 3 7/8 in	(1) Uniformly graded sand, D_r = 90%, Dry (2) Crushed sand, D_r = 90%, Dry	(1) Plain steel (2) Teflon coated steel (3) Graphite coated steel (4) Plain smooth mortar (5) Teflon coated smooth mortar (6) Graphite coated smooth mortar (7) Plain rough mortar
Huck et al. (1973) Huck and Saxena (1981)	Ring simple shear torsion type, 2-D	Static and dynamic, constant normal stress	d_{in} = 12.7 cm, d_{out} = 17.7 cm, h_{sand} = 2.5 cm	(1) Ottawa sand, D_r = 80% (2) Edgar plastic Kaolin clay, ϖ = 5.5%	Concrete, rough and smooth
Yoshimi and Kishida (1981a,b)	Ring simple shear torsion type, displacement-controlled, 2-D	Static, R_t = 0.6 mm/min, constant normal stress or constant volume	d_{in} = 24 cm, d_{out} = 28.8 cm, h = 0.9 - 4.2 cm	Sands, 3 kinds, D_r = 40% - 90%, Dry	Steel, brass, and aluminium, smooth to rough
Acar et al. (1982)	Direct shear type, deformation-controlled, 2-D	Static, constant normal stress		Quartz sand	(1) Steel, smooth (2) White pine without irregularities (3) Concrete
Boulon and Plytas (1986) Boulon and Nova (1990)	Direct shear type (circular shaped shear box), 2-D	Monotonic, constant normal stress, constant volume, and constant normal stiffness	d = 10 cm and 6 cm	Hostun sand, dense, coarse - medium, dry	Metal plate, rough
Uesugi and Kishida (1986a) Kishida and Uesugi (1987)	Direct and simple shear type, displacement-controlled, 2-D	Static, constant normal stress	A = 400×100 mm^2, h = 10 - 29 mm	Sands 3 kinds, D_{50} = 0.15 - 0.62 mm, D_r = 90%, Dry	Low-carbon steel, smooth to rough
Uesugi and Kishida (1986b)	Direct and simple shear type, displacement-controlled, 2-D	Static, constant normal stress	A=100×40 mm^2 h = 24 mm (17 mm for direct hear box)	Sands 3 kinds, D_{50} = 0.16 - 1.82 mm,	Low-carbon steel, smooth to rough
Uesugi et al (1988)	Simple shear type, stress- and displacement-controlled, 2-D	Static, constant normal stress	A = 400×100 mm^2, h = 30 mm	Seto sand, D_r = 90%, Dry	Low-carbon steel, smooth to rough
Uesugi et al (1989)	Simple shear type, displacement-controlled, 2-D	Monotonic, R_t = 1 mm/min, repeated, constant normal stress	A = 100×40 mm^2, h = 24 mm	Sands, 3 kinds, D_r = 90%, almost dry	Low-carbon steel, smooth to rough
Uesugi et al (1990)	Simple shear type, displacement-controlled, 2-D	Monotonic, R_t = 1 mm/min, repeated, two-way (sinusoidal), constant normal stress	A = 100×40 mm^2, h = 24 mm	Toyoura sand, Seto sand, Air-dried	Concrete, two kinds of cement mortars, R_{max} = 6 - 50 μm (L = 0.2 mm)
Tejchman and Wu (1995)	(a) Direct shear type, displacement-controlled, 2-D (b) Modified plane strain type, displacement-controlled, 2-D	(a) Static, constant normal stress (b) Static, varying normal stress	(b) Width = 4 cm, height = 8 cm	Karlsruhe sand, D_{50} = 0.45 - 0.50 mm, Dry	Steel, smooth to rough
Paikowsky et al. (1995)	Direct and simple shear type, displacement-controlled, 2-D	Static, R_t = 1.3 mm/min, constant normal stress and constant volume	A = 40×12.5 cm^2	Ottawa sand, Dry	Steel, smooth to rough

2.2.1 Shear Strength Parameters

Coulomb's law of friction has been widely used in physics and engineering. If a material, such as soil is in contact with another material like a steel plate, Coulomb's law of friction is stated by the equation: $F = \mu \cdot N$, where F is the frictional force required to induce relative displacement at the contact surface, μ is the coefficient of friction, and N is the normal force between the two materials. Assume that the friction angle between the steel plate and soil is δ. By dividing the normal force and shear force by the contact surface area, the normal stress and shear stress can be obtained. If there is also adhesion, c, between the soil and the plate, the Mohr-Coulomb failure criterion can be written as $\tau_f = c + \sigma_n \cdot \tan \delta$, where τ_f and σ_n are the shear stress and normal stress at failure on the contact surface, respectively. The Mohr-Coulomb failure criterion is represented in Fig. 2.5 in which δ is the slope of failure envelope and C_a is the intercept between the failure envelope and the τ axis.

Generally speaking, the shear strength of an interface under a constant normal stress and monotonic shearing condition could be influenced by the parameters such as: type of surface material; surface roughness; moisture content and relative density of soil; grain size distribution of soil; magnitude of normal stress; and rate of shearing. The first elaborate study to recognize the importance of these parameters was conducted by Potyondy (1961). Based on a series of tests between different soils (sand and clay) and construction materials, he found that four major factors determine the skin friction: the moisture content of soils, the roughness of the surface, the composition of soils, and the intensity of normal load.

Based on a series of tests by direct shear device, Acar *et al.* (1981) concluded that relative density of sand and normal stress influence the angle of friction between sand and structural materials such as steel, wood and concrete. Angle of friction was high for low normal stress and high relative densities as illustrated in Fig 2.6. They concluded that such effects are negligible for practical purposes.

By employing an annular shear type device, Brummund and Leonards (1973) found that the coefficient of friction increases with the surface roughness and angularity of the sand grains. They also found that in the case of unlubricated surfaces, the dynamic coefficient of friction is about 20 percent greater than the static coefficient.

Yoshimi and Kishida (1981a,b), Uesugi and Kishida (1986a) and others pointed out the importance of the influence of surface roughness on the frictional resistance. On the basis of a series of simple shear type interface tests between various types of dry sand and steel plates, Uesugi and Kishida(1986a,b) concluded that the type of sand and the surface roughness of steel had significant influence on the coefficient of friction. The influence of the normal stress (98 kPa to 980 kPa) and the mean grain size of sand (0.55 to 0.62 mm and 0.15 to 0.19 mm) were not so significant.

2.2.2 Stress-Displacement Relations

Four parameters are normally measured during an interface test, i.e. normal stress, σ_n, shear stress, τ, volume change or normal displacement, v, and shear displacement, u. For the common case of constant normal stress, shear stress and normal displacement variations are usually plotted against shear displacement.

Yoshimi and Kishida(1981) reported some test results between steel and Tonegawa sand as shown in Fig. 2.7. A ring torsion apparatus was used in these experiments. Uesugi and Kishida (1986a) reported similar results for the interfaces between steel and Toyoura sand, obtained from a simple shear type device, as shown in Fig. 2.8. The results from both sets of tests indicate that the surface roughness significantly influences the peak and residual shear strengths. A more pronounced peak is observed from rough surfaces followed by strain softening until the shear stress levels off at the residual shear strength.

Volume change (or normal displacement) results indicated some initial compression for smooth surfaces, whereas rough surfaces exhibited a substantial dilation after the initial

compression (Fig. 2.7 and 2.8). As explained earlier, one of the advantages of both the simple shear type and ring torsion devices is the possibility of distinguishing between sliding displacement and shear deformation of soil at the interface. Separation of shear deformation of sand and sliding displacements are shown in Fig. 2.9a and Fig. 2.9b, respectively, for the results of Fig. 2.8.

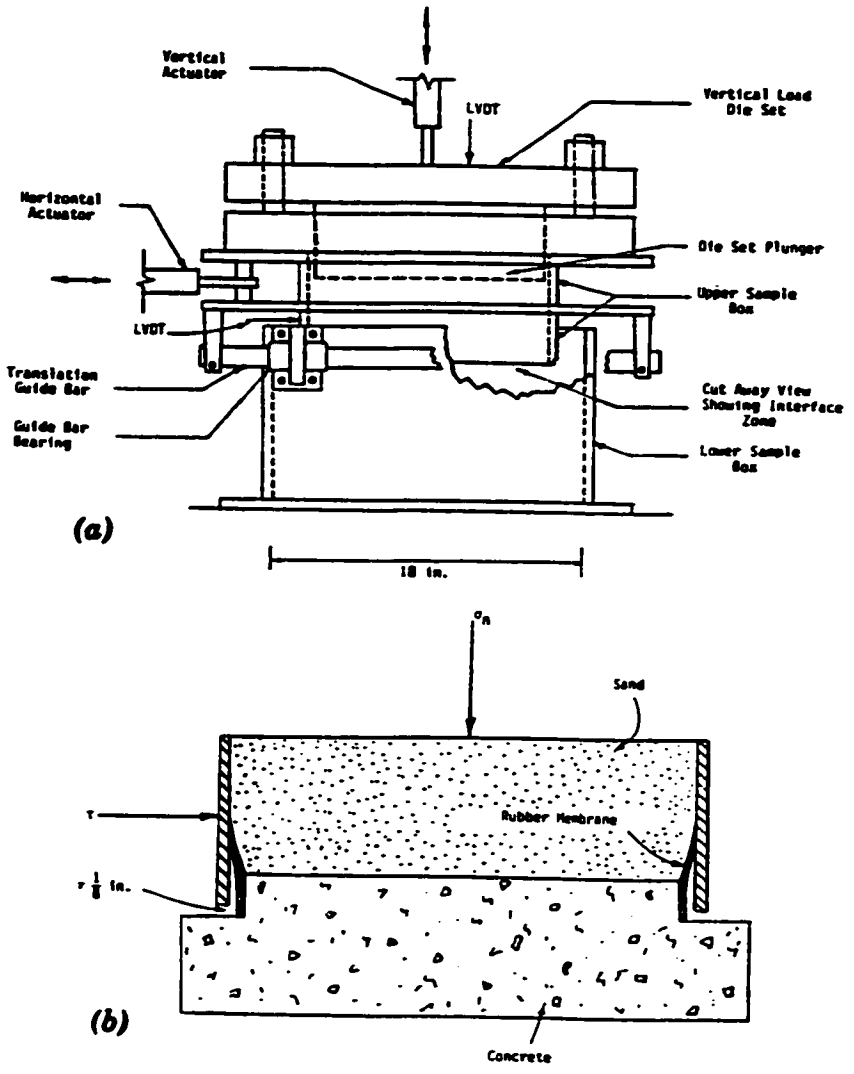

FIG. 2.1 Desai's direct shear type device

(a) Test box; (b) Schematic of the membrane arrangement

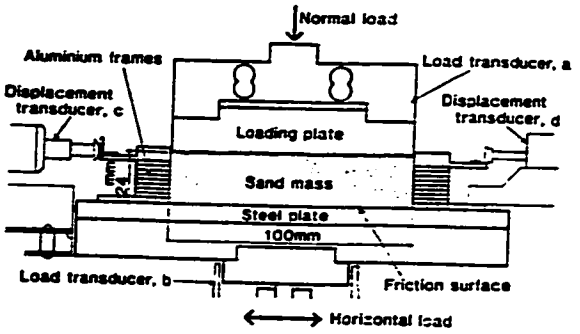

FIG. 2.2 Simple shear type apparatus (After Uesugi and Kishida, 1986b)

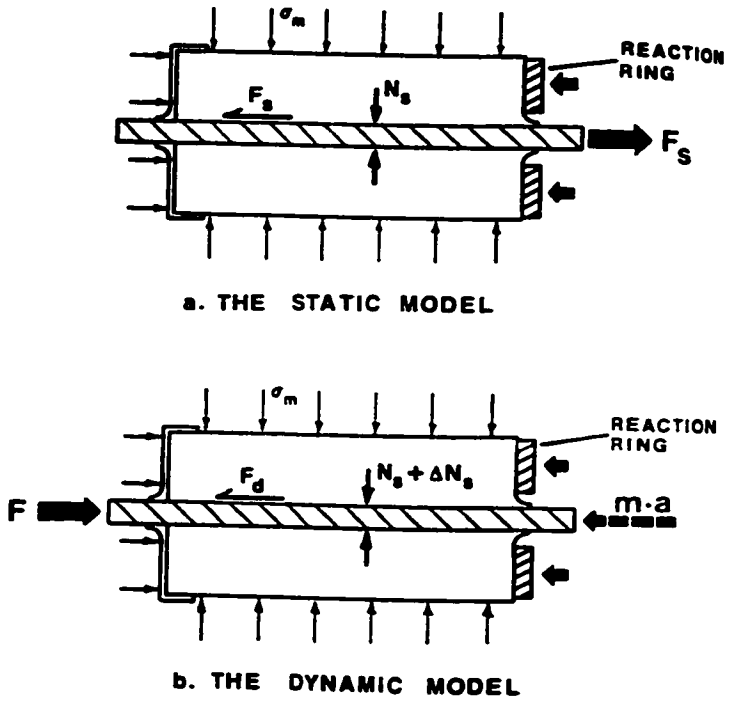

FIG.2.3 Annular shear type device (After Brummund and Leonards, 1973)

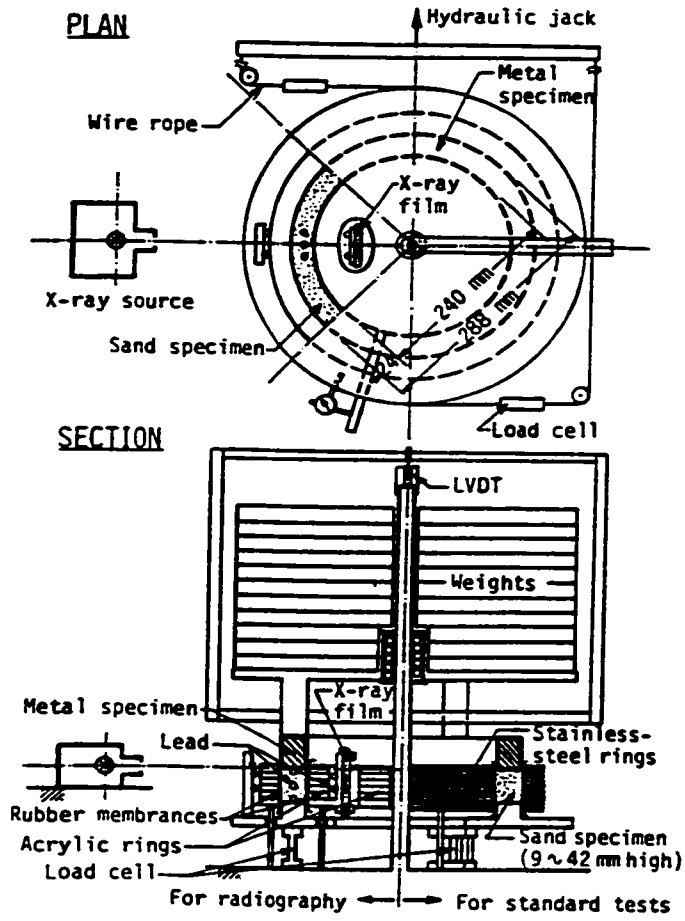

FIG. 2.4 Ring torsion apparatus (After Yoshimi and Kishida, 1981)

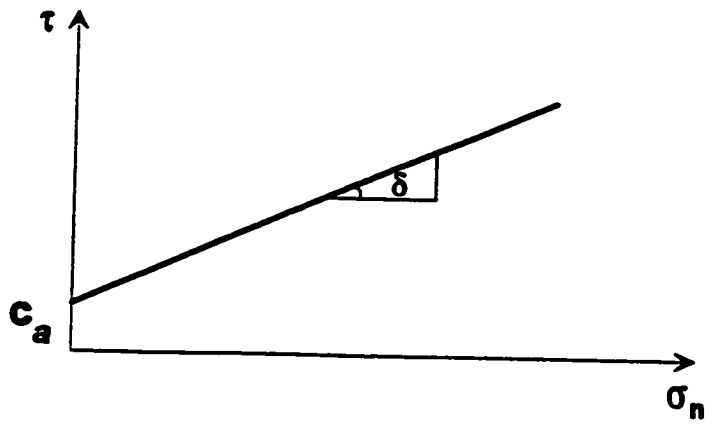

FIG. 2 5 Mohr-Coulomb failure criterion

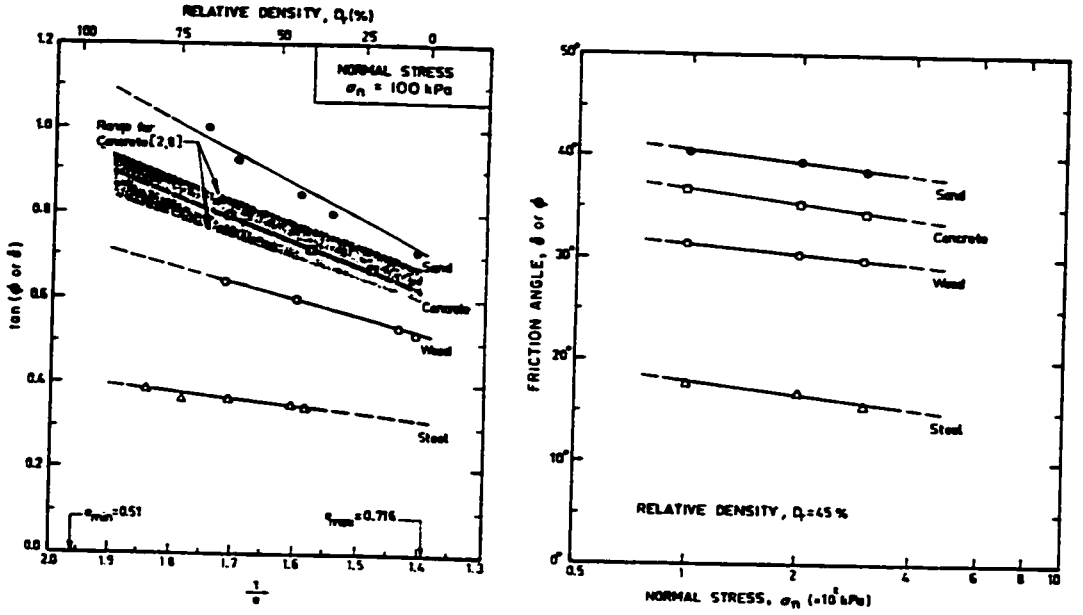

FIG. 2.6 Variation of skin friction (shear strength) with relative density and normal stress (After Acar *et al.*, 1982)

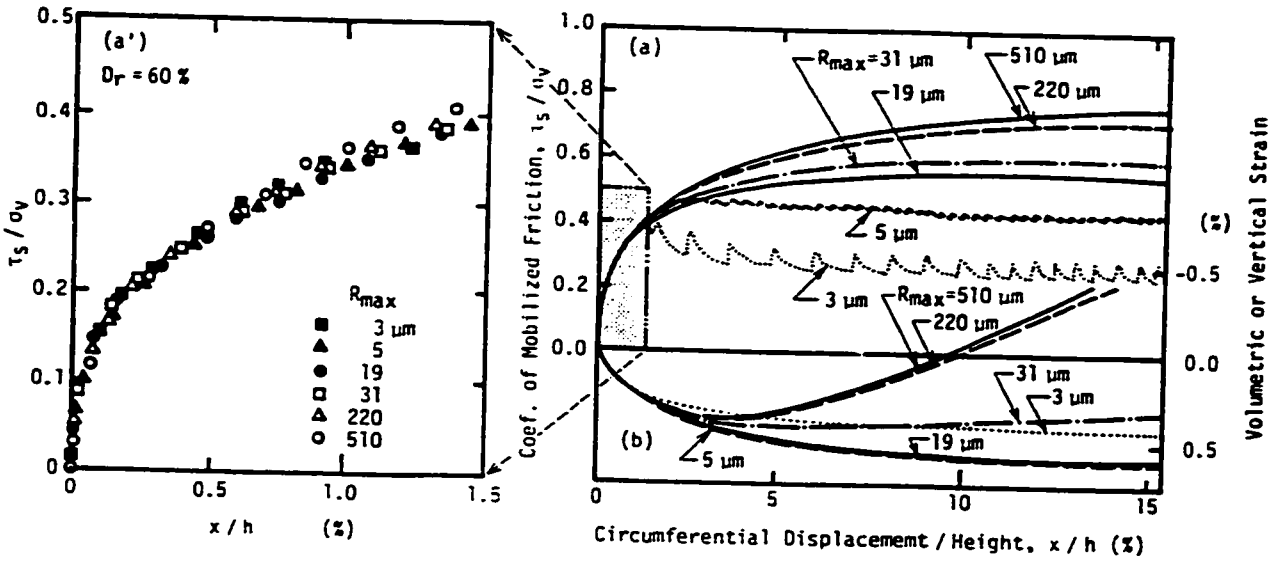

FIG.2.7 Interface test results between steel and Tonegawa sand

(After Yoshimi and Kishida, 1981)

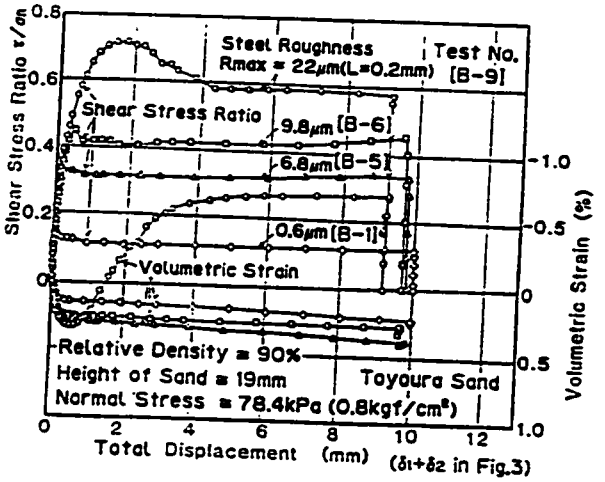

FIG.2.8 Interface test results between steel and Toyoura sand

(After Uesugi and Kishida, 1986a)

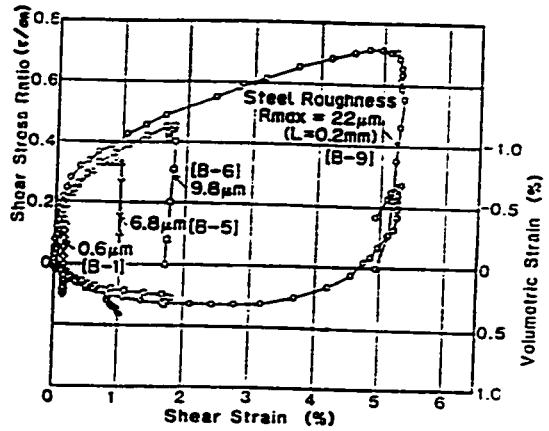

(a)

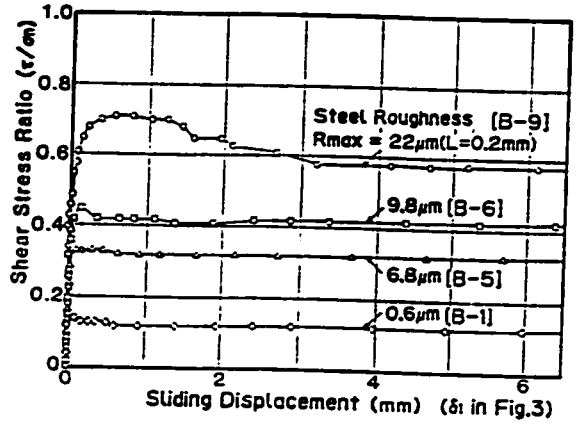

(b)

FIG.2.9 Decomposition of results of Fig. 2.8

(a) Shearing deformation of sand sample

(b) Sliding displacement at the steel-sand contact surface

CHAPTER 3
EXPERIMENTAL OBSERVATIONS OF SAND-STEEL INTERFACE BEHAVIOUR

This chapter first describes the materials used throughout this study. And then the automated 3-D interface apparatus C3DSSI (i.e., Cyclic 3-Dimensional Simple Shear testing of Interfaces) is introduced. Subsequently the specimen preparation is described. Finally the influences of normal stress as well as initial relative density on the stress-displacement relations of the interface are presented.

3.1 Interface Materials

- **Sand**

  Two types of air-dried quartz sand were used in this study. The general properties of the sands are given in Table 3.1. The maximum and minimum void ratios are determined using the ASTM standards D4253-93 and D4254-91, respectively. The grain size distributions are illustrated in Figure 3.1.

- **Structural Material**

  In this investigation, a 300 × 300 mm low carbon steel plate was used as the structural material. The rough surface was obtained by uniformly sand-blasting the smooth plate to increase the roughness of the surface to 25 μm for sampling length of L = 0.8 mm.

Table 3. 1 Properties of Sands

Sand type	Mean grain size D_{50} (mm)	Maximum unit weight γ_{max} (kN/m^3)	Minimum unit weight γ_{min} (kN/m^3)	Maximum void ratio e_{max}	Minimum void ratio e_{min}	Coefficient of Uniformity C_u
Medium Crushed Quartz	0.6	16.05	13.09	1.024	0.651	2.09
Coarse Crushed Quartz	1.4	15.84	13.16	1.014	0.673	1.72

3.2 Description of C3DSSI Interface Apparatus

An automated 3-D apparatus C3DSSI that was developed by Evgin and Fakharian (1996) was used in this study. The schematic view of this apparatus is shown in Figure 3.2. The operation of the interface apparatus and the data acquisition are automated by a computer-controlled system. The apparatus consists of three major parts:

1) Loading System
   - Reaction frame
   - Vertical loading unit (pneumatic actuator)
   - Horizontal loading unit (stepper motors)
2) Soil Containers
   - Simple shear type soil container
   - Direct shear type soil container
3) Data Acquisition and Computer Control System
   - Load cells
   - Displacement transducers
   - Interface unit
   - Computer
   - Menu-form software

A pneumatic actuator is used to apply the normal load on the interface. The operation of this actuator is controlled by a computer to impose a constant normal stress. The tangential forces are applied to the interface plane through an X-Y loading table by using the ball screw stepper motors, which are capable of applying displacement- or load-controlled shear in both x- and y-directions independently. In this study, displacement-controlled tests were used with a velocity of 1 mm/min at which the loading table moved horizontally only in x-direction.

This apparatus has both direct shear type and simple shear type soil containers. In this study, simple shear type soil container was used which was capable of measuring both sliding displacement between steel plate and soil as well as shear deformation of soil sample. A stack of 1 mm thick anodized square aluminium plates with an inside area of 100 ×100 mm is placed on the steel plate which has an area of 300 × 300 mm. Since the steel plate is longer than the soil surface, the area of contact surface remains constant as the displacement continues to increase. The bottom of the aluminium container is covered with foam to minimize the leakage of sand during shearing. In addition, a 0.25 mm thick sheet of Teflon is glued to the bottom of the foam layer as shown in Figure 3.3 to minimize the friction between the steel plate and the aluminium box. The magnitude of normal stress was maintained constant during the process of shearing. The normal displacement, shear stress, and tangential displacements were recorded at 5-second intervals.

The C3DSSI apparatus was equipped with two transducers measuring the tangential loads (in the x and y directions) and five LVDTs monitoring the tangential and normal displacements. In this study, only two transducers and three LVDTs were in operation. Load transducers were used to measure the tangential load in the x direction as well as the normal load in the vertical direction. Two of the three LVDTs were used to measure the tangential displacement in the x direction to distinguish between the sliding displacement (slip) along the contact surface and the soil deformation. The other LVDT measured the change of sand height (i.e., the normal displacement of the top of the soil sample).

Figure 3.4 illustrates the schematic diagrams of tangential displacements. The total tangential displacement, δ_{total}, is measured as the relative displacement between the top aluminium plate

and the steel specimen. LVDT-X1 was used for this purpose. The shear deformation of sand, δ_{soil}, is measured by LVDT-X2, which reads the relative movement between the top and bottom aluminium plates. The sliding displacement, $\delta_{sliding}$, at the soil-steel interface is the difference between δ_{total} and δ_{soil}.

3.3 Sample Preparation

To prepare the sand samples for each test, the aluminium stack of plates (simple shear type soil container) is positioned at the centre of the steel plate. The sand is rained into the container at a desired density by one of the methods described below. A suction device is used to level the top surface of the sand sample. The plate is then fixed on top of the loading table of the interface-testing device, and the loading platen is moved downward to touch the sand surface.

In this study there are three methods to prepare sand with the desired density.

1) Scooping Method

   By means of this method, only the loose sand samples can be prepared. The sand is taken gently by using a spoon and then placed into the container.

2) Low-Falling Height Single-Sieve Pluviation Method

   A small raining device was designed to obtain a uniform loose to medium dense sand samples. The device has outside dimensions of 100×100 mm. At its bottom many holes were drilled. During the preparation of samples, the raining device was first placed inside the soil container and was in touch with the steel plate. Sand was spooned into the device gently and uniformly. The raining device was then slowly lifted up so that the sand could rain into the shear box. The top of the sand samples was finally levelled by suction. After applying the initial normal stress of 5 kPa, which resulted from the weight of the loading platen, an initial relative density of 43% to 48% was achieved using this method.

3) Medium-Falling Height Single-Sieve Pluviation Method

In this method, a Perspex prism with inside dimensions of 100×100 mm and with a total height of 300 mm was placed on top of the soil container. A sieve (opening 4.0 mm) with inside dimensions of 100×100 mm was placed inside the prism at an adjustable height to the soil container. During the preparation of samples, a soft plastic sheet was first placed on the sieve, and the sand was spooned uniformly onto the plastic film. Then film was removed rapidly and the sand rained down into the soil container. The top of the sand was levelled by suction. Considering the weight of the loading platen, an initial relative density of 87% to 89% could be obtained. The drop height was 25 cm.

The sample preparation is continued as described next. In order to align the stacks of aluminium plates (simple shear box) in vertical direction, the 1mm thick aluminium plates were piled up around a dummy sample as shown in Figure 3.5. A hollow area is made on top of the dummy sample, which is slightly larger than the cross-section of loading platen. While the loading platen was lowered, the dummy sample and the stack of aluminium plates around it were moved horizontally until the loading platen fit into the hollow part of the dummy sample. In this way the soil container plates were positioned correctly. Then the stack of plates was pressed down by four clamps at the corners to prevent any movement that would cause misalignment.

The steel plate together with the soil container plates were moved out of the apparatus. The dummy sample was removed, and then the sand was rained into the container. The top part of sand was levelled off by means of suction. Then the steel plates together with the soil container were placed back in the apparatus. After lowering the loading platen and placing it on the sand surface, the clamps for holding the stack of plates were removed. The steel specimen was fixed to the loading table by four bolts at the corners and the desired normal load was applied by the pneumatic actuator. Finally the LVDTs were mounted to measure the tangential displacements. The sample was ready for testing.

3.4 Test Results and Influential Factors

Series of interface tests were carried out using the C3DSSI apparatus. Figure 3.6.a and 3.6.b show the plots of shear stress versus tangential displacement and normal displacement versus tangential displacement, respectively, for the interface between the sand blasted steel plate and medium crushed quartz sand with initial relative density of 88.2% under the normal stress of 100 kPa.

Figure 3.6a indicates that the peak shear stress was 65 kPa, which corresponds to a tangential displacement of 0.6 mm. After the peak, the shear stress decreased and approached a residual shear stress of 61 kPa. From Figure 3.6c it can be seen that the variation of normal displacement exhibited a small amount of compression at first, followed by dilation, which is typical for an interface between a rough surface and dense sand. The test data also show that the peak strength was reached near the point of inflection of the normal displacement curve (Fig. 3.6c).

Figure 3.6d shows that the major portion of shear deformation of sand took place before the peak shear strength was reached. Thereafter, the shear deformation of the sand was negligibly small while the sliding displacement at the contact surface continued as was shown in Figure 3.6b. This observation indicated that the shear strength of the soil mass was higher than the shear strength at the contact surface. Otherwise, the shear failure would have occurred within the sand mass. The peak shear strength of this sand (at 93% initial relative density) was measured to be 93.3 kPa ($\tau = \sigma_n \tan\phi$, $\sigma_n = 100$ kPa, $\phi = 43°$).

Figure 3.6b indicates that the peak shear strength was reached at a sliding displacement of 0.28 mm. At this point, the deformation of sand mass was 0.32 mm. The summation of these two values would result in the total tangential displacement of 0.6mm as shown in Figure 3.6a. These results are in good agreement with those reported by Uesugi and Kishida (1986) for the interface between Toyoura sand and steel plate.

3.4.1 Effect of Normal Stress

Several tests were conducted by using the interface between the sand blasted steel plate and medium crushed quartz sand under normal stresses of 100 kPa and 300 kPa. The initial relative densities of sand were 88.2% and 45.7%. The results are presented in Figures 3.7.

Figure 3.7a and 3.7b show the plots of shear stress-tangential displacement and normal displacement-tangential displacement, respectively, for dense sand (Dr = 88.2%) samples. Similar plots for medium dense sand (Dr = 45.7%) are shown in Figures 3.7c and 3.7d. A well-pronounced peak is observed in dense sand results, whereas medium dense samples exhibited a less pronounced peak. Dense sand compressed first, followed by dilation during shearing, and the rate of dilation was lower at high normal stresses. Medium dense sand, however, did not indicate dilation.

The normalized results of Figures 3.7a and 3.7c are illustrated in Figures 3.8a and 3.8b, for dense and medium dense sands, respectively. The maximum stress ratio, i.e., the coefficient of friction, $(\frac{\tau}{\sigma_n})_{max}$, was the same for different normal stresses and the residual stress ratio was 0.61. For the medium dense samples, the maximum stress ratio was higher at the low normal stress. The peak was less pronounced than that of dense samples and the residual stress ratio was 0.49.

Comparisons between test results for dense and medium sands under different normal stresses are presented in Figure 3.9. From Figure 3.9b it can be clearly seen that, for medium dense samples, a greater sliding displacement was required to mobilize the peak shear stress for a higher normal stress (e.g. 1.85 mm for 300 kPa and 0.75 mm for 100 kPa). This trend was not observed in dense sand.

3.4.2 Effect of Initial Relative Density of Sand

The effects of different initial relative densities on the stress-displacement relations of the interface are also shown in Figure 3.9. The peak strength was higher at higher densities. Figure 3.9d indicates that the sand deformation increased with the decrease of relative density.

Normalized results for Figure3.9 are illustrated in Figures 3.10. Figures 3.10b indicates that the sliding displacements were about the same under different normal stresses for the same initial relative density. A similar trend is observed in plots of stress ratio versus sand displacement in Figure 3.10c.

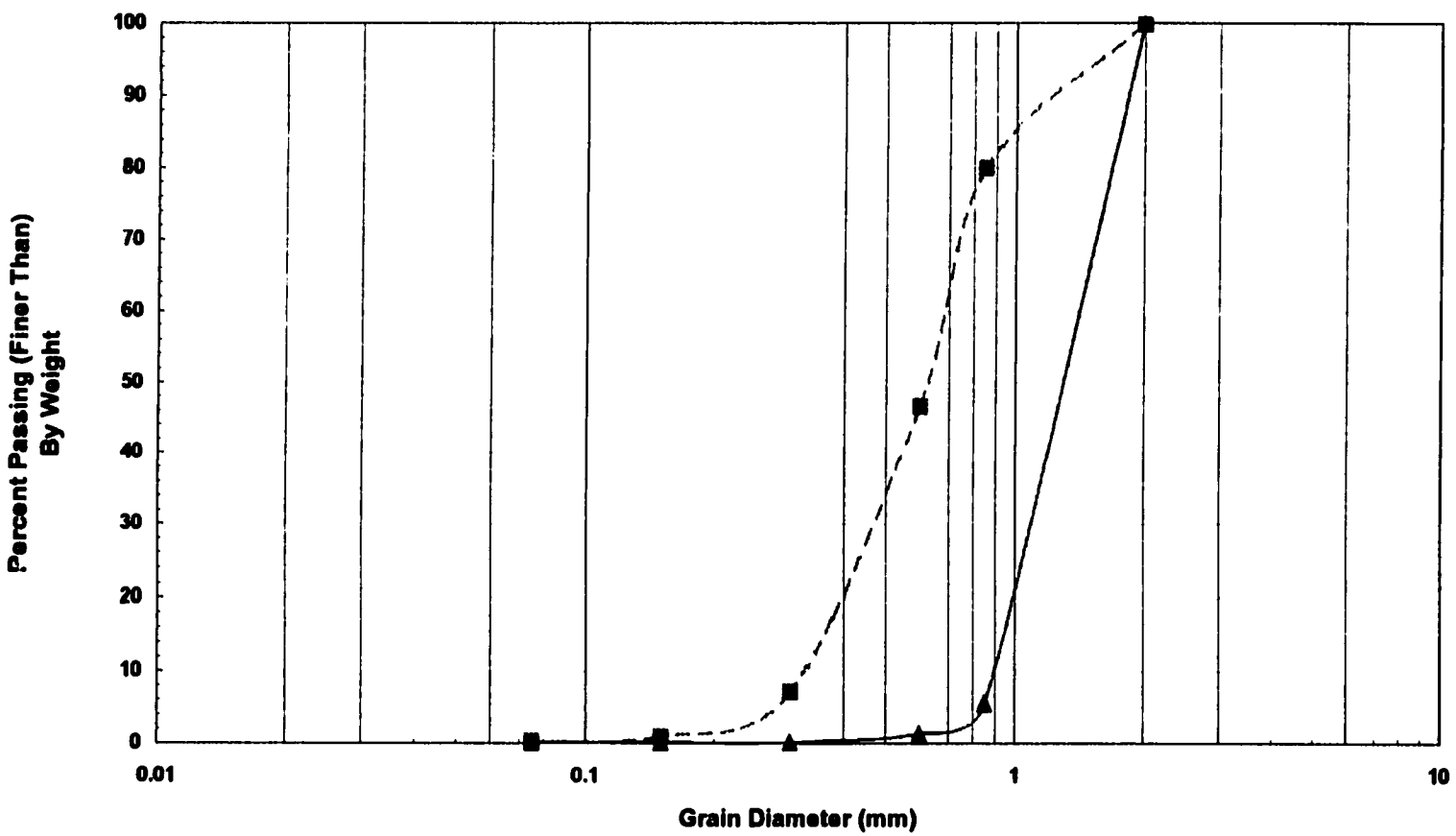

FIG. 3.1. Sieve analysis

Medium Crushed Quartz
Coarse Crushed Quartz

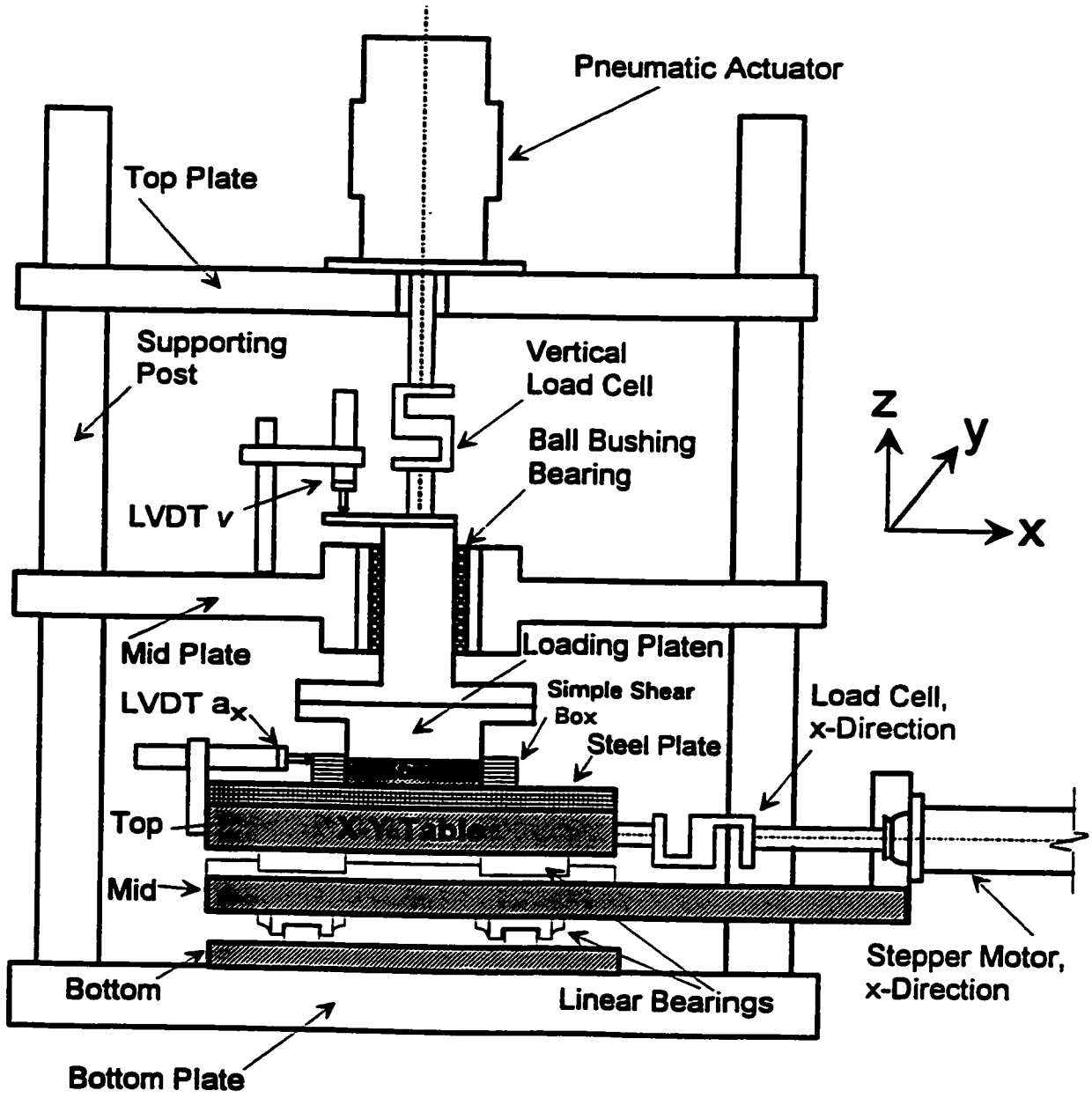

FIG.3.2 Schematic view of apparatus C3DSSI

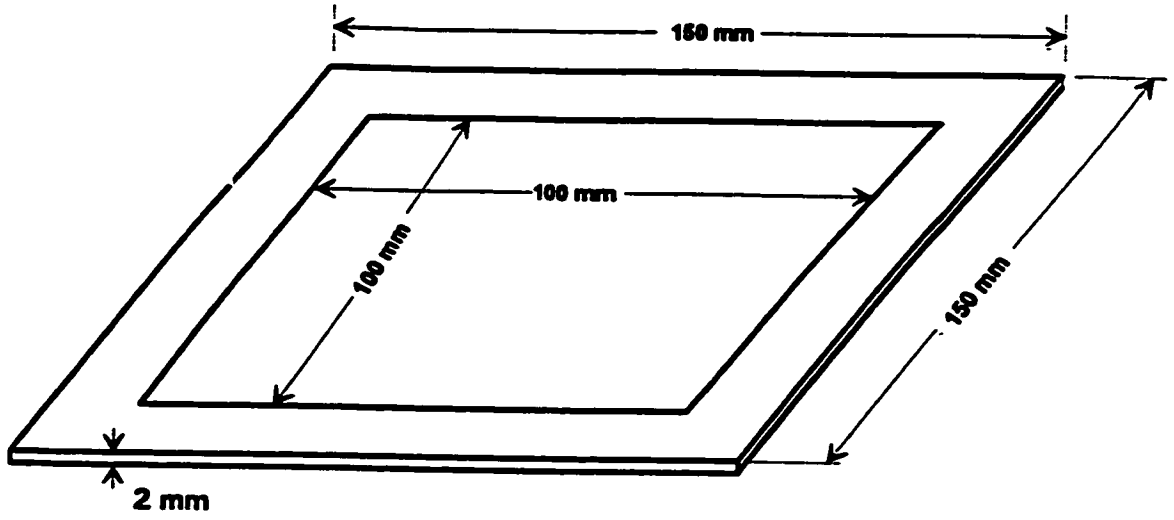

FIG.3.3 Teflon coated aluminum plates used in the simple shear box

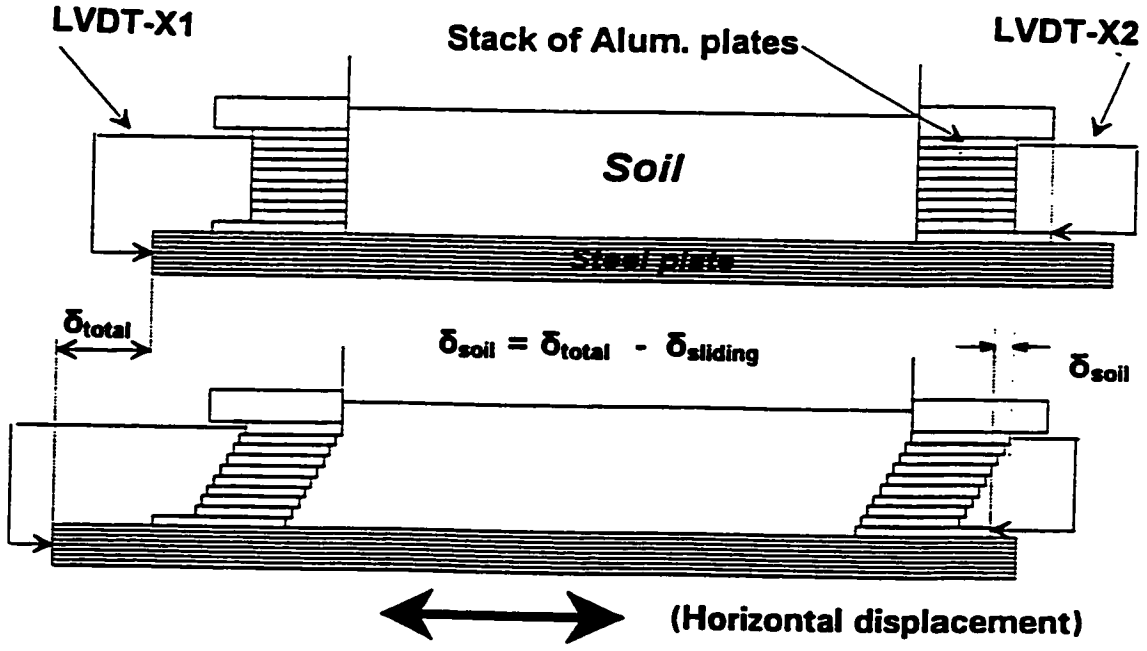

FIG.3.4 Schematic diagrams of tangential displacement

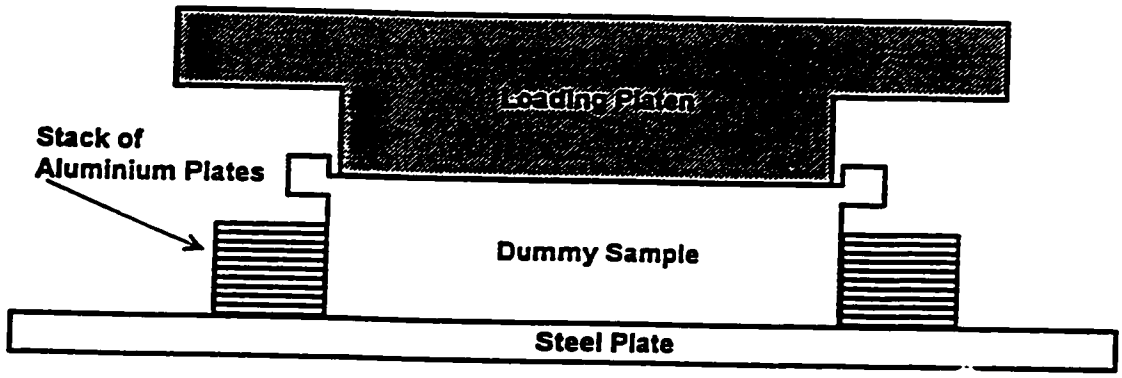

FIG.3.5 Aligning and positioning of the stack of plates by the dummy sample

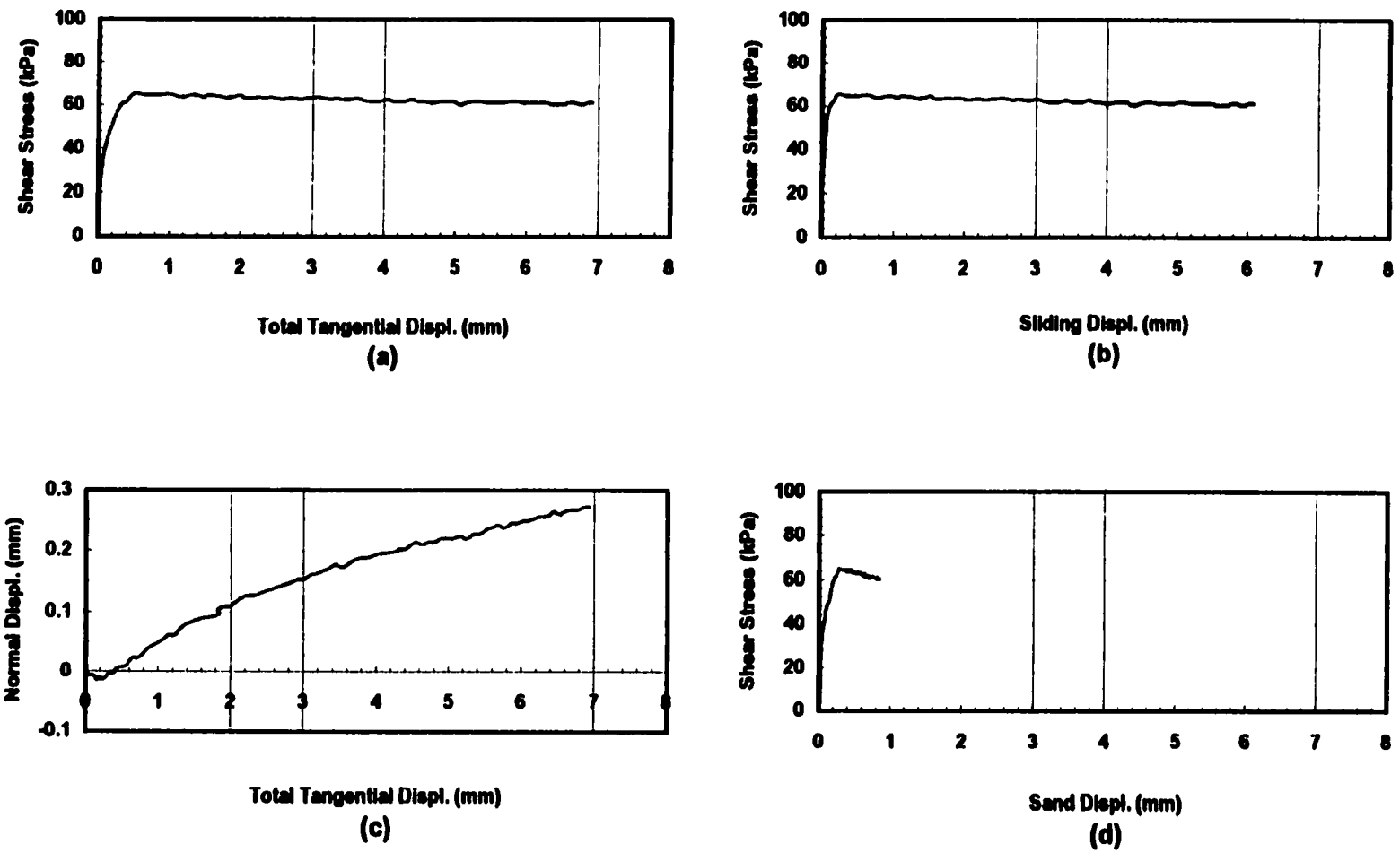

FIG. 3.6 Constant normal stress test result

Surface: Sand blasted steel plate
Sand: Medium crushed quartz, Dr = 88.2%
Normal Stress = 100 kPa

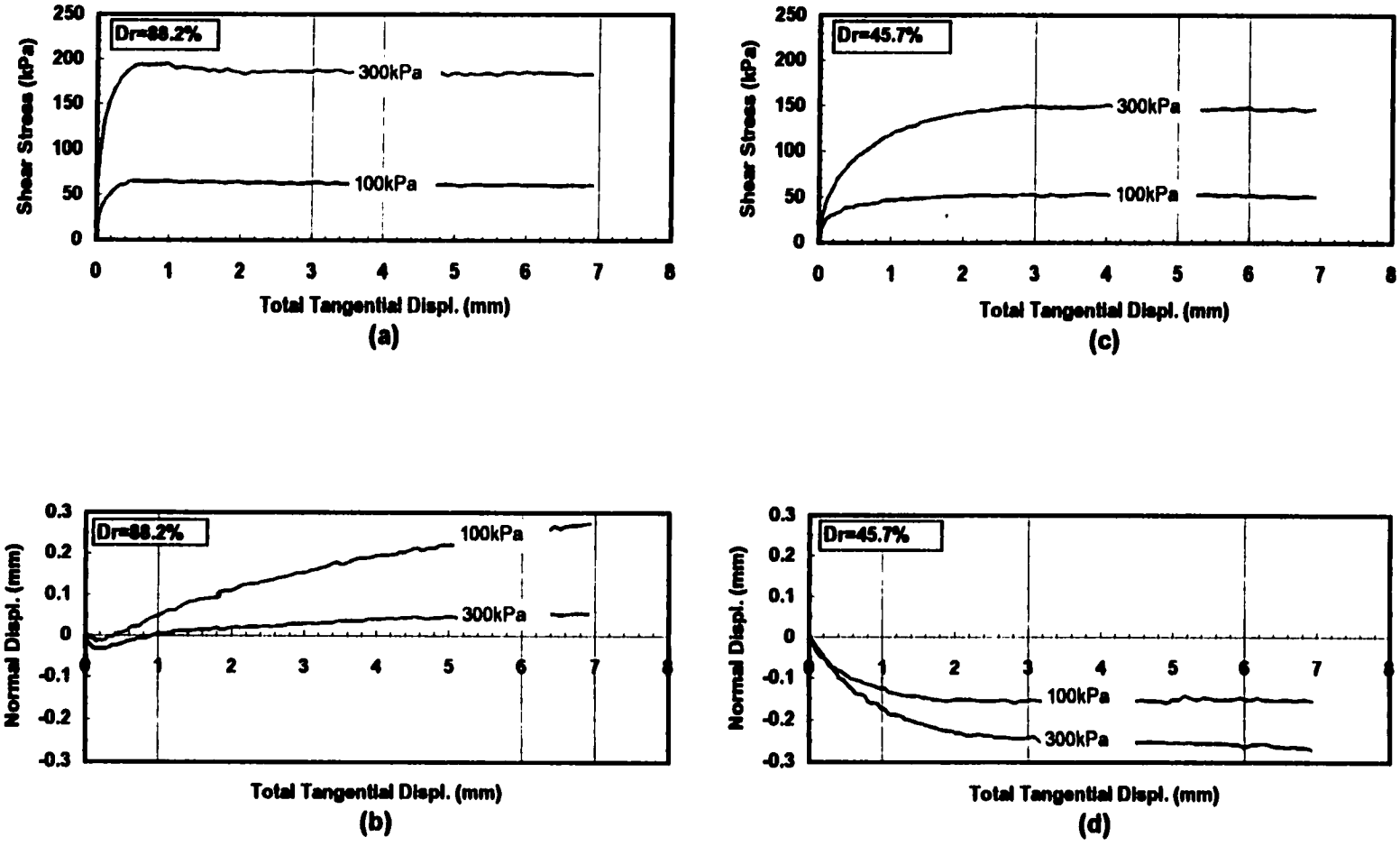

FIG. 3.7 Comparisons between test results under different normal stresses

Surface: Sand blasted steel plate
Sand: Medium crushed quartz, Dr = 88.2% and 45.7%
Normal stress = 100 kPa and 300 kPa

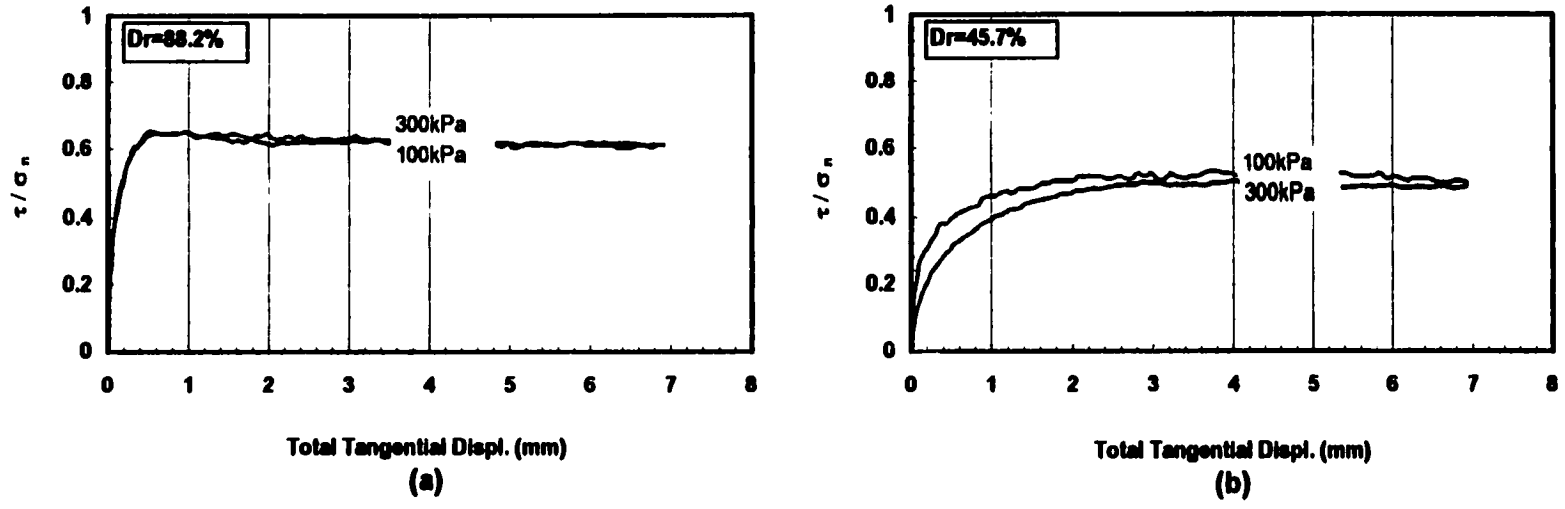

FIG. 3.8 Normalized results of FIG. 3.7a and 3.7b

Surface: Sand blasted steel plate
Sand: Medium crushed quartz, Dr = 88.2% and 45.7%
Normal stress = 100 kPa and 300 kPa

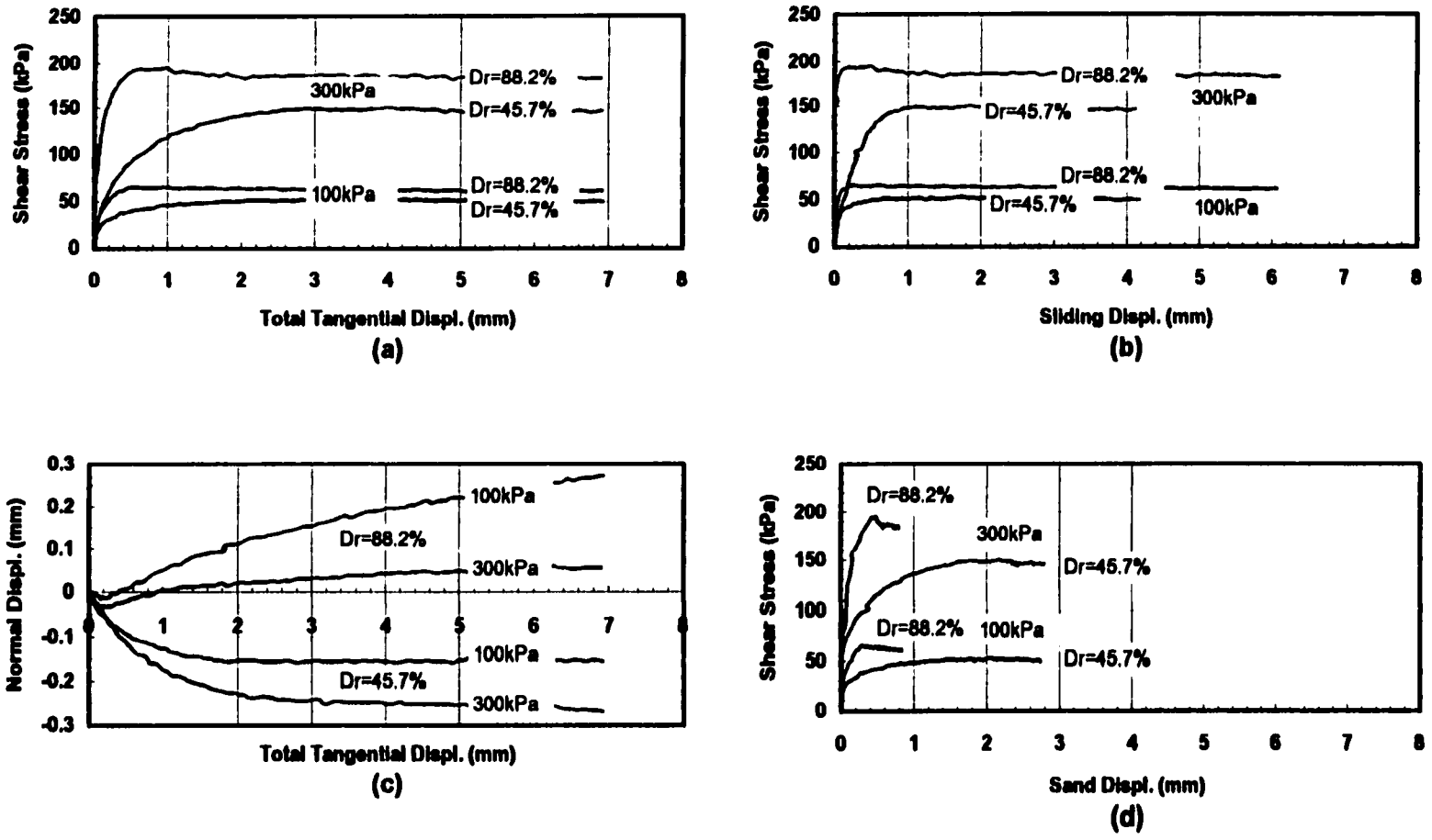

FIG. 3.9 Comparisons between test results with different densities under different normal stresses

Surface: Sand blasted steel plate

Sand: Medium crushed quartz, Dr = 88.2% and 45.7%

Normal stress = 100 kPa and 300 kPa

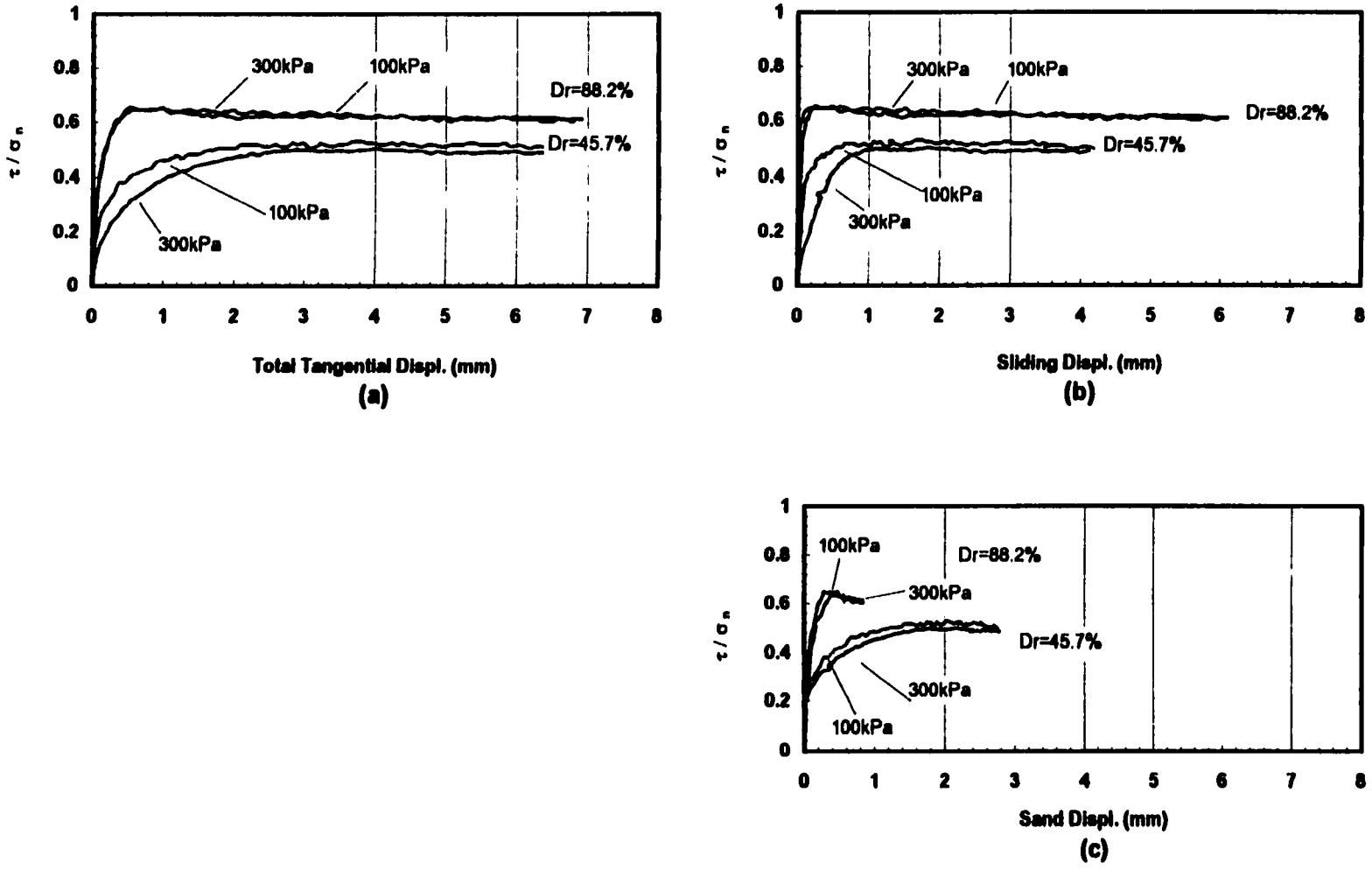

FIG. 3.10 Normalized results of FIG. 3.9

Surface: Sand blasted steel plate
Sand: Medium crushed quartz, Dr = 88.2% and 45.7%
Normal stress = 100 kPa and 300 kPa

CHAPTER 4

OBSERVED MOVEMENTS OF SAND PARTICLES IN INTERFACE TESTS

The measurement of particle movements provides an important contribution to the understanding of the behaviour of interfaces between sand and steel plates. This chapter consists of four sections. The first section contains a literature review on the measurements of particle movements. The second section describes the modifications made on the C3DSSI apparatus. The third and forth sections include the procedures and the results of the measurements made in the present study by using the modified apparatus.

4.1 Literature Review

Butterfield et al. (1970) used a stereo-photogrammetric method for measuring the displacement field in sand. Andrewes and Butterfield (1973) applied the method for measuring the displacement of sand particles. De Pater and Nieuwenhuis (1986) used the double-exposure photography technique to obtain the displacements of sand particles. They calculated the displacements from the interference pattern formed by directing a laser beam through the negative.

Yoshimi and Kishida (1981a) used the X-ray photography method to measure the particle displacements in an interface test. They showed that the tangential displacement of the interface consisted mostly of slip for smooth surfaces. While for rough surfaces, the

displacement consisted mostly of shear zone distortion along the interface. Until the shear stress exceeded about 85% of the maximum value, the slip movement and the shear zone displacement remained almost at zero. The sand deformed uniformly throughout its height.

Uesugi and Kishida and Tsubakihara (1988) described a method for observing the particle movements near the interface between sand and steel plates. They used a simple shear type apparatus with minor modifications. The soil container was equipped with a glass window for observing the particle movements near the interface. Close-up photographs were taken of the sand-particles at specified time intervals during the sand-steel interface tests. The change in particle coordinates gave the displacement history of particles. Following conclusions were drawn from this investigation. Before the peak frictional resistance, there was little sliding at the interface. The sand mass deformed uniformly. At the peak, the interface started sliding. Along a rough interface, the particles slipped, rolled and moved up and down. Along a smooth surface, on the other hand, sand mass slipped without large deformation. A shear zone formed in the sand along a rough surface during sliding. The shear zone has a maximum stress ratio τ / σ_n lower than that of the same sand in a dense state. When τ / σ_n of the shear zone is lower than the coefficient of friction at yield μ_y, τ / σ_n becomes the upper-limit of the coefficient of friction. Thus, the stress ratio becomes lower with the progress of shear zone formation. This explains the reduction in shear resistance during the interface sliding. There is no formation of shear zone when the interface is smooth.

Uesugi and Kishida and Tsubakihara (1988) illustrated the components of the tangential displacement schematically, which is shown in Figure 4.1. The total tangential displacement δ consisted of the interface sliding δ_1 (evaluated as the relative displacement between the steel and the bottom aluminium plate) and the displacement due to the shear deformation of sand mass δ_2. Furthermore, δ_1 was divided into two parts, the net interface sliding and the displacement due to the shear zone distortion in the sand along the rough interface. When the interface is smooth, the displacement of steel relative to the bottom plate is nearly equal to the net interface sliding.

4.2 Apparatus Modifications

In the present study, the total tangential displacement δ_{total} consists of the displacement due to sliding, $\delta_{sliding}$, and the displacement resulting from the deformation of sand, δ_{sand}. It is assumed that the sand in the sample container can be divided into two parts, i.e., the sand mass at the upper part and the interface layer at the lower part near the contact surface. The objective of this study is to separate δ_{sand} into two parts, i.e., the displacement due to the sand mass deformation, δ_{mass}, and the displacement due to the deformation within the interface layer, $\delta_{interface}$.

Some modifications were made on the C3DSSI apparatus to facilitate the observation of the development of sand deformation during all stages of tests. A new soil container was built. On one of the vertical faces of the stack of aluminium plates, two vertical straight lines 5.0 cm apart were drawn. The thickness of the plates was reduced from 2 mm (Fakharian, 1996) to 1 mm. The stack of aluminium plates was lubricated to allow the sand container to follow the deformation of the sand mass with minimum frictional resistance. When the sand was sheared, the stack of aluminium plates changed their relative positions, i.e., the lines on the aluminium plates were no longer on the same line. These results provided the necessary information for the determination of the shear deformation in the sand samples.

4.3 Description of Measurement Procedure

During the experiments, a digital camera was used to take photographs of the lines on the vertical wall of the aluminium plates. Data-exchange software was installed in the computer in order to transfer the images of photographs into the computer. "Digitizer" software was used to digitize the images and to form Microsoft Excel data. The procedures are described in detail as follows.

4.3.1 Taking Photographs

A digital camera (Pentax Digital Still Camera EI-C90) was placed in front of the two straight lines, which were drawn, using an exacto knife, on the vertical front face of the stack of aluminium plates. The camera lens was placed at a distance of 25 mm from the aluminium plates. Series of photographs were taken to record the changes of the relative positions of the lines. The macro-shooting mode of the camera was used to take pictures because the lines were very narrow. Pictures were taken at designated intervals when the total tangential displacement δ_{total} reached 0.0 mm, 0.05 mm, 0.2 mm, 0.5 mm, 0.8 mm, 1.2 mm, 2.0 mm, 3.0 mm, 4.0 mm, 5.0 mm, 6.0 mm, and 7.0 mm. The images of the pictures were saved temporarily in the camera as JPEG files.

4.3.2 Data Communication

The software named "Daisy Collage and ISL_CAM (32-bit version)" was installed in the computer in order for the digital camera to use the "ISL_CAM" PC-Camera data exchange utility. By using the data exchange utility, the JPEG files were transferred to the computer as series of bmp files.

4.3.3 Digitizer and Excel Software

The software "Digitizer" was used for processing the bmp files. The advantage of this software was that, the images of the lines could be digitized and transferred to Microsoft Excel numerical data. Charts could be easily obtained in Excel software, which exactly demonstrate the shape of the lines on the elevation of the stack of aluminium plates.

After the steps mentioned above, the shape of the lines for each aluminium plate at different stages was successfully represented by a series of Excel curves. The resolution of the camera is 0.04 mm.

4.4 Observation Results

The results of a test between the sand blasted steel plate and medium crushed quartz sand under the normal stress of 100 kPa were presented first. The initial relative density of sand was 88.2%. Figure 4.2 shows a series of photographs. The positions of the lines at 12 different stages can be seen in these photographs which were taken when the total tangential displacement δ_{total} reached 0.0 mm, 0.05 mm, 0.2 mm, 0.5 mm, 0.8 mm, 1.2 mm, 2.0 mm, 3.0 mm, 4.0 mm, 5.0 mm, 6.0 mm, and 7.0 mm. Figure 4.3 shows the development of sand deformation. Curves represent 12 different stages shown in Figure 4.2.

Before the stress ratio reached the coefficient of friction at the interface, there was a small amount of soil displacement (nearly 0.32 mm). Before stage 4 (when δ_{total} was less than 0.5 mm), the tangential displacement curves could be idealized almost as linear lines. The interface layer between the medium crushed quartz sand and a sand blasted steel plate has not been formed at the beginning of interface testing. After stage 4, the changes in the slopes of the curves demonstrated nonlinearity, which indicated the beginning of the formation of the interface layer. For example, from stage 5 to stage 9, i.e., δ_{total} ranged from 0.8 mm to 4.0 mm, the non-linear part of the curves were almost 2.0 mm thick; while from Stage 10 to Stage 12, the non-linear part grew to 3 mm, which represents an increase in the thickness of the interface layer during one experiment.

Figures 4.4, 4.6, and 4.8 show the photographs of the development of the sand deformation at different stages for the interface between a sand blasted steel plate and medium crushed quartz sand under the normal stresses of 100 kPa and 300 kPa, respectively. The initial relative densities were 45.7% and 88.2%. Figures 4.5, 4.7, and 4.9 show the development of sand deformation curves corresponding to different conditions. The interface thickness at different stages was obtained. For example, Figure 4.5 shows that, when the initial relative density was Dr = 88.2% and the normal stress was σ_n = 300 kPa, the interface layer was formed at stage 9, i.e., when δ_{total} = 4.0 mm. The thickness of the interface layer was 2mm at this stage.

For medium dense sand, under the condition of σ_n = 100 kPa as shown in Figure 4.7, the interface layer was formed at stage 4 (δ_{total} = 0.5 mm) with the thickness of 2 mm; then the thickness increased continuously in the following steps. At stage 7 (δ_{total} = 2.0 mm), the thickness of the interface was 3 mm; at stage 9 (δ_{total} = 4.0 mm), the thickness was 4 mm; at stage 12 (δ_{total} = 7.0 mm), the thickness grew to 4.5 mm. Figure 4.9 shows the development of the curves under the condition of σ_n = 300 kPa. The interface was formed at stage 5 (δ_{total} = 1.2 mm) with the thickness being equal to 4 mm; at stage 9 (δ_{total} = 4.0 mm), the interface thickness was 4 mm; at stage 12 (δ_{total} = 7.0 mm), the thickness grew to 7 mm.

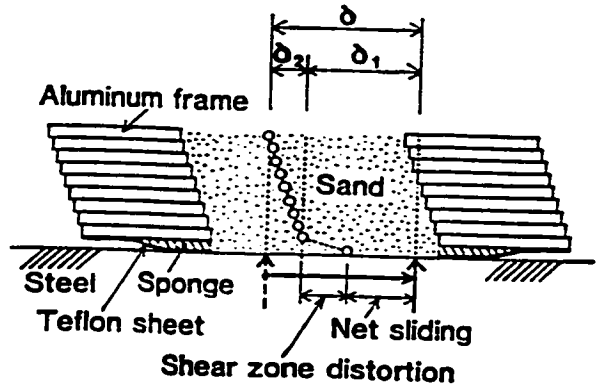

FIG.4.1 Components of the tangential displacement

(After Uesugi *et al.*, 1988)

(a) Stage 1

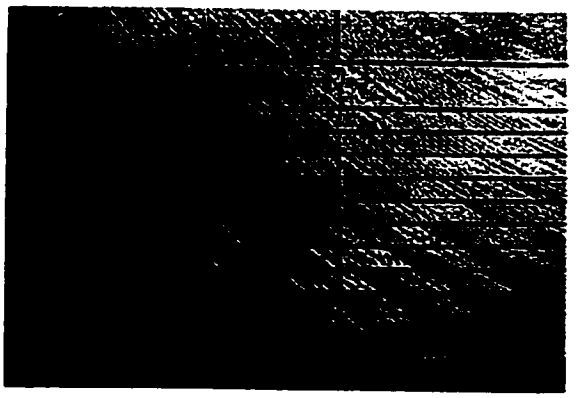

(b) Stage 2

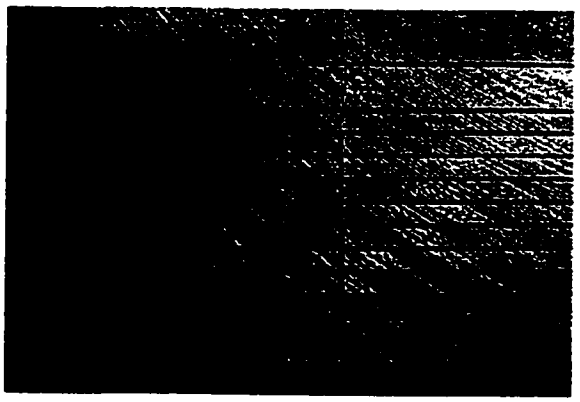

(c) Stage 3

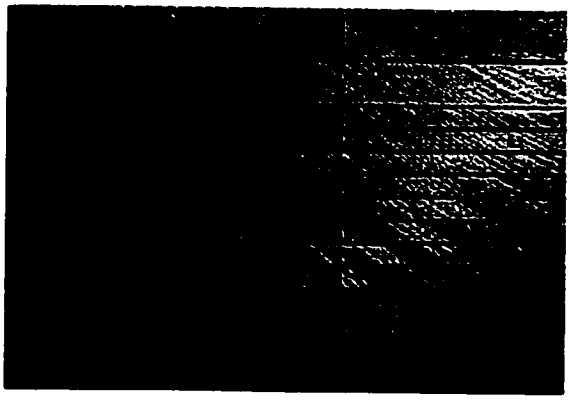

(d) Stage 4

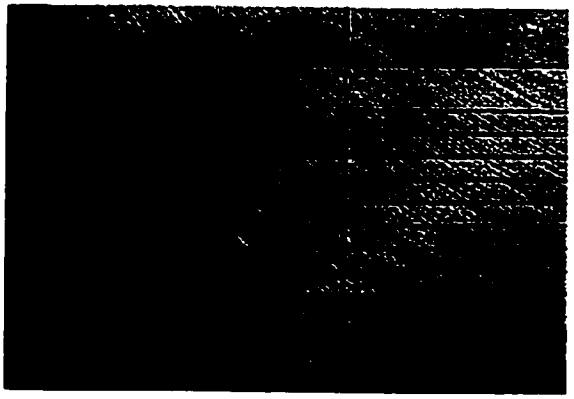

(e) Stage 5

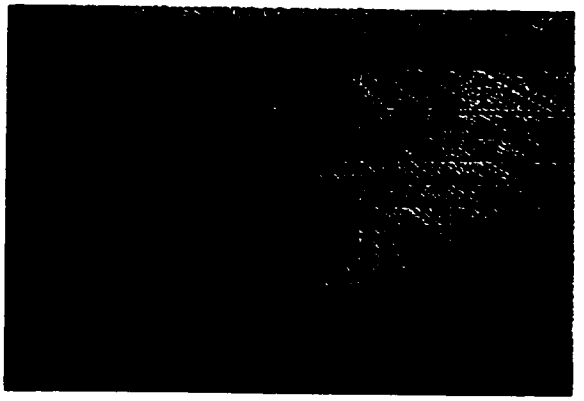

(f) Stage 6

FIG 4.2 Photographs of sand deformation development

Surface: Sand blasted steel plate
Sand: Medium size crushed quartz, Dr = 88.2%
Normal Stress = 100 kPa

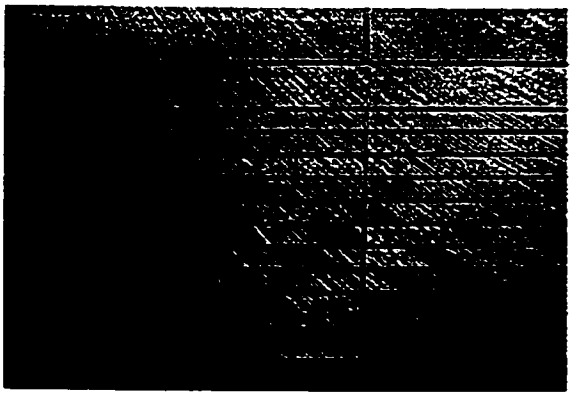

(g) Stage 7

(h) Stage 8

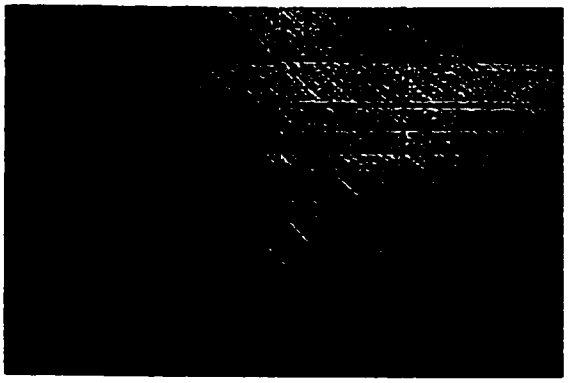

(i) Stage 9

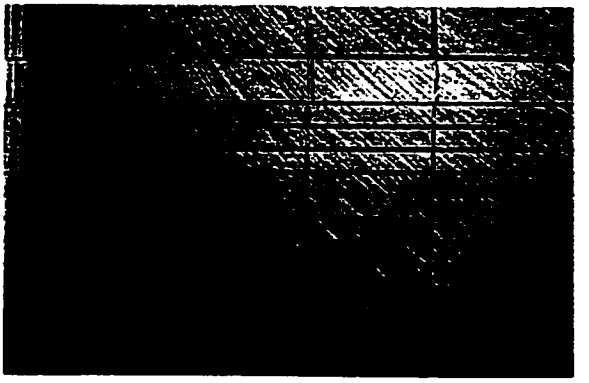

(j) Stage 10

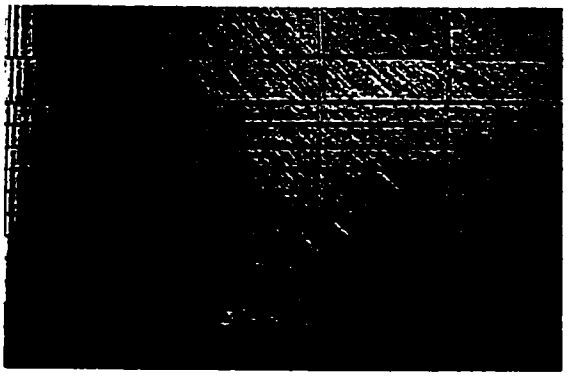

(k) Stage 11

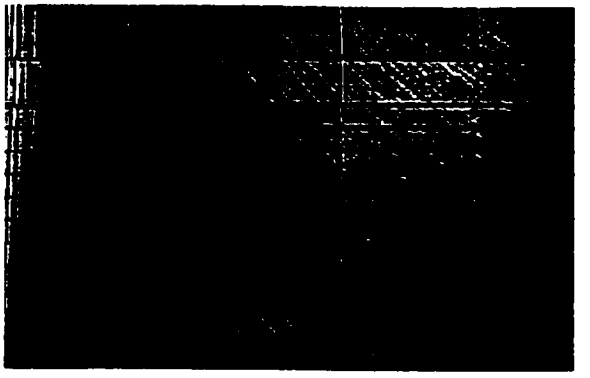

(l) Stage 12

FIG 4.2 (Continued) Photographs of sand deformation development

Surface: Sand blasted steel plate
Sand: Medium size crushed quartz, Dr = 88.2%
Normal Stress = 100 kPa

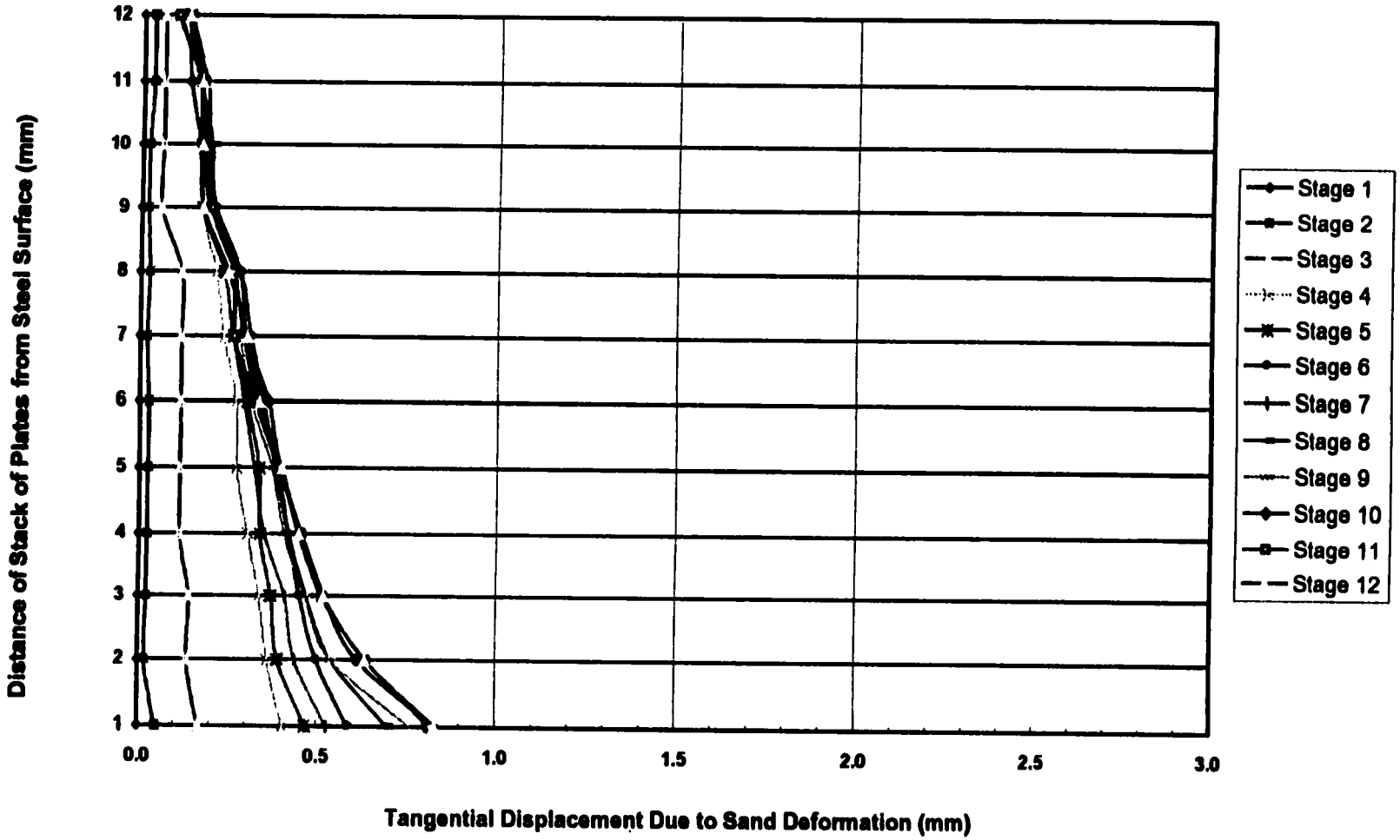

FIG 4.3. Sand deformation development curves

Surface: Sand blasted steel plate
Sand: Medium size crushed quartz, Dr = 88.2%
Normal Stress = 100 kPa

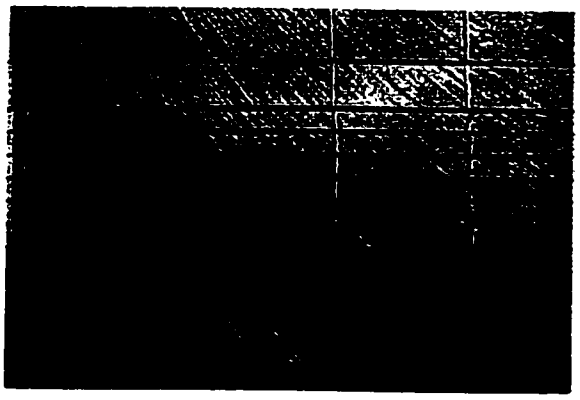

(a) Stage 1

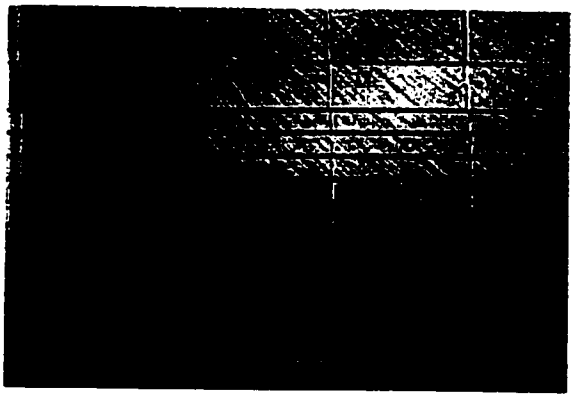

(b) Stage 2

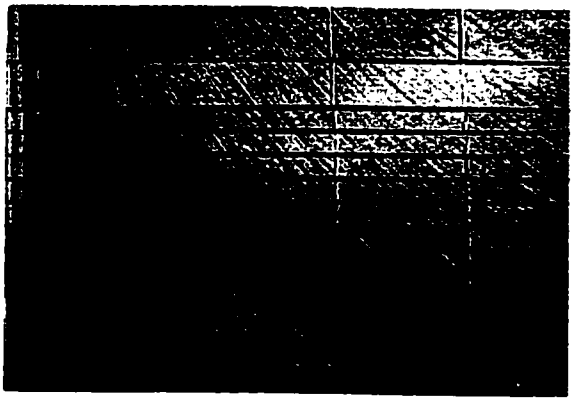

(c) Stage 3

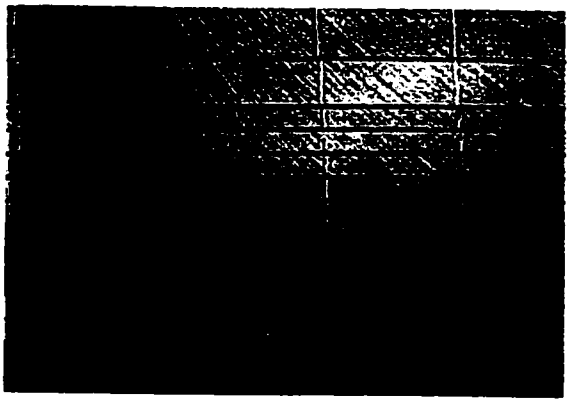

(d) Stage 4

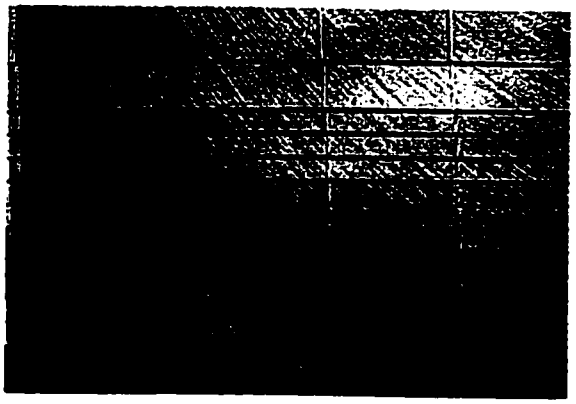

(e) Stage 5

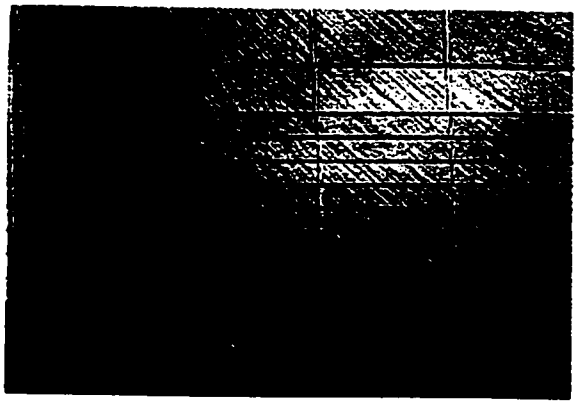

(f) Stage 6

FIG 4.4 Photographs of sand deformation development

Surface: Sand blasted steel plate
Sand: Medium size crushed quartz, Dr = 88.2%
Normal Stress = 300 kPa

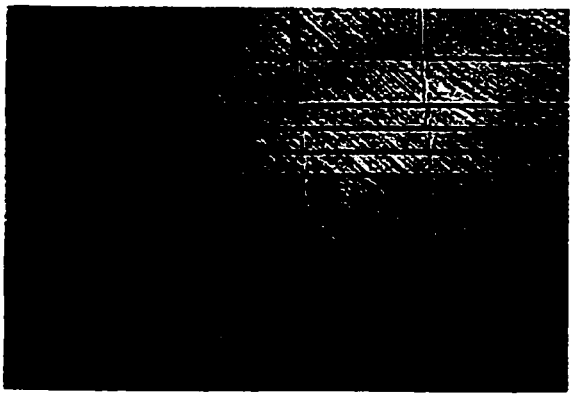

(g) Stage 7

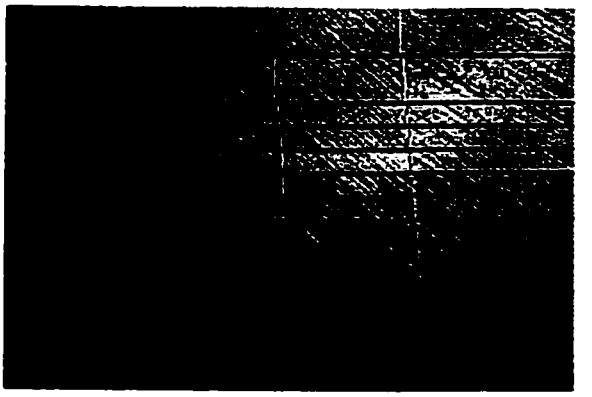

(h) Stage 8

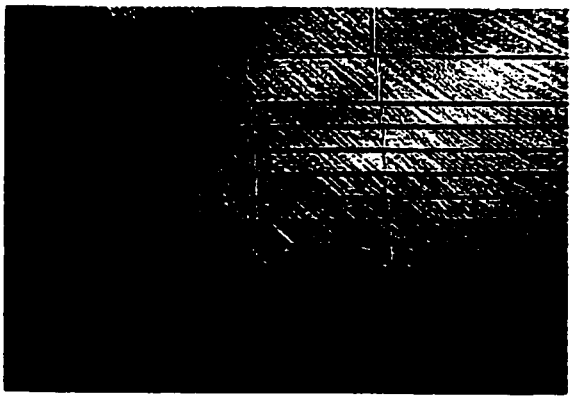

(i) Stage 9

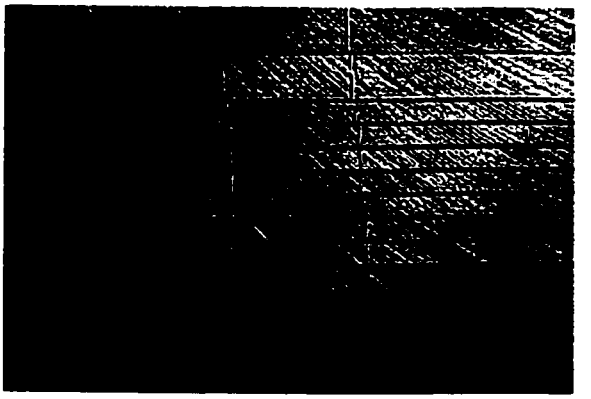

(j) Stage 10

(k) Stage 11

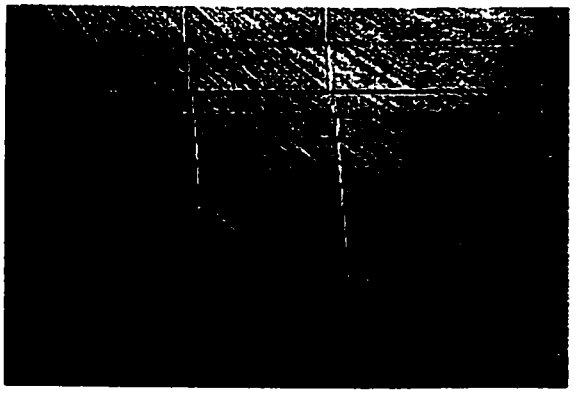

(l) Stage 12

FIG 4.4 (Continued) Photographs of sand deformation development

Surface: Sand blasted steel plate
Sand: Medium size crushed quartz, Dr = 88.2%
Normal Stress = 300 kPa

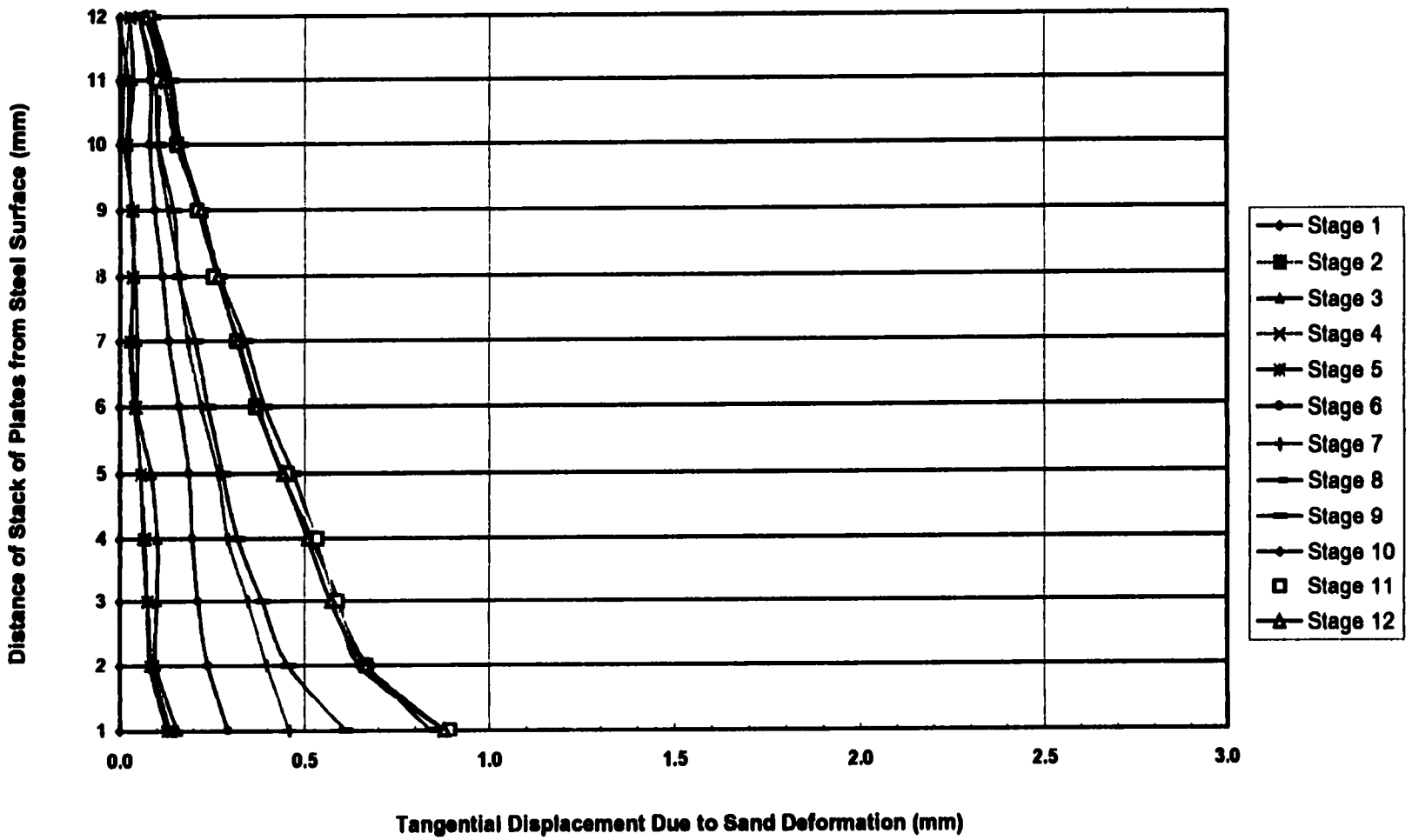

FIG 4.5. Sand deformation development curves

Surface: Sand blasted steel plate
Sand: Medium size crushed quartz, Dr = 88.2%
Normal Stress = 300 kPa

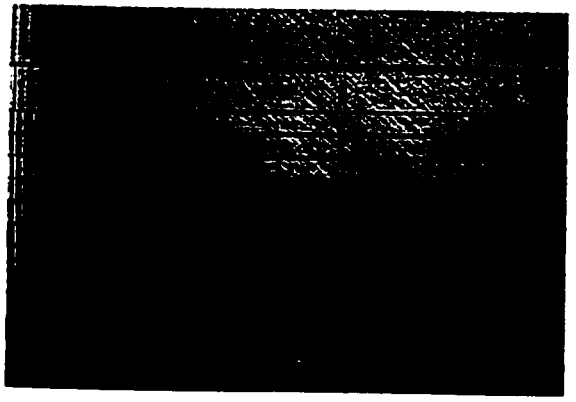

(a) Stage 1

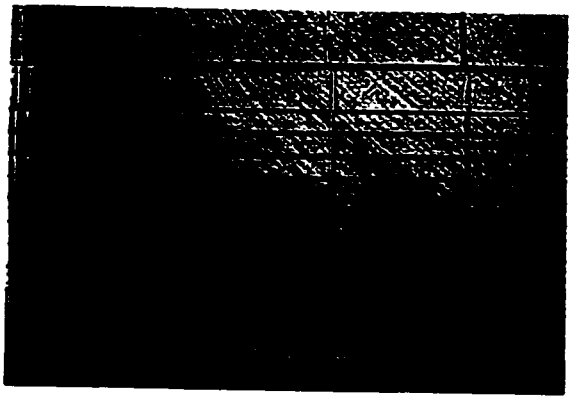

(b) Stage 2

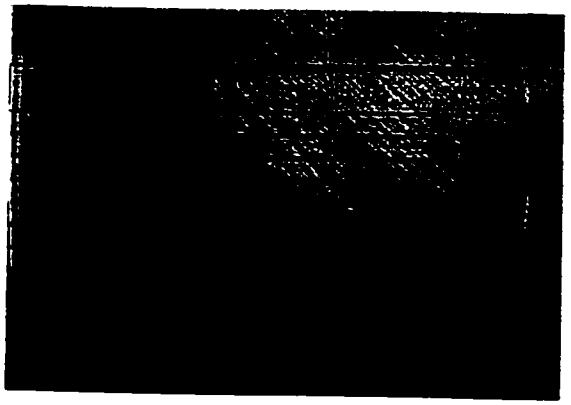

(c) Stage 3

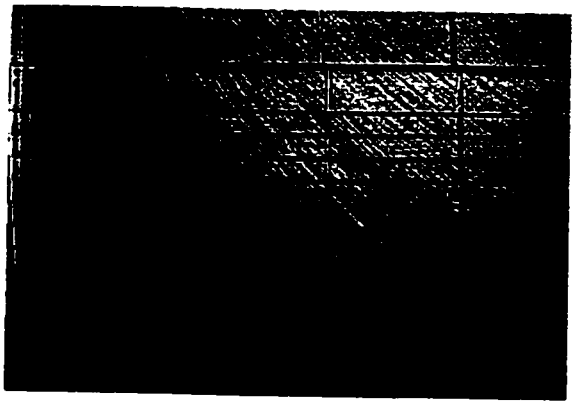

(d) Stage 4

(e) Stage 5

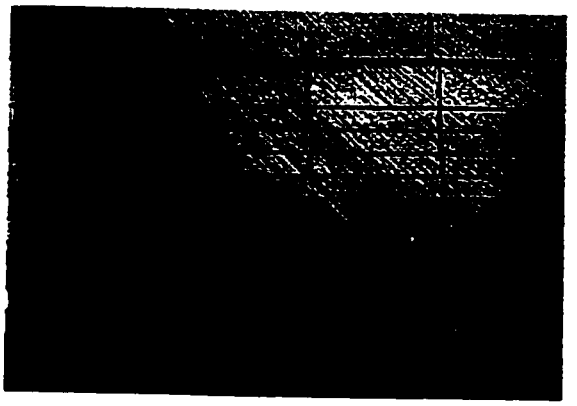

(f) Stage 6

FIG 4.6 Photographs of sand deformation development

Surface: Sand blasted steel plate
Sand: Medium size crushed quartz, Dr = 45.7%
Normal Stress = 100 kPa

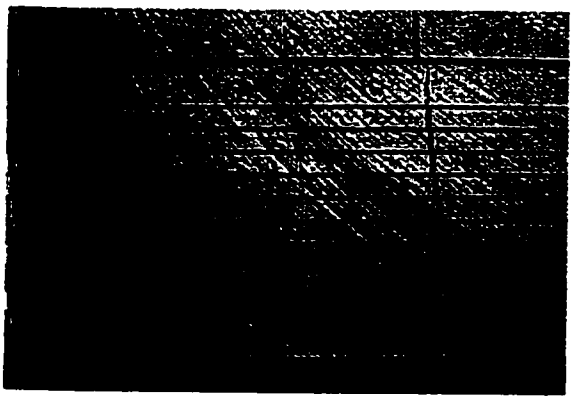

(g) Stage 7

(h) Stage 8

(i) Stage 9

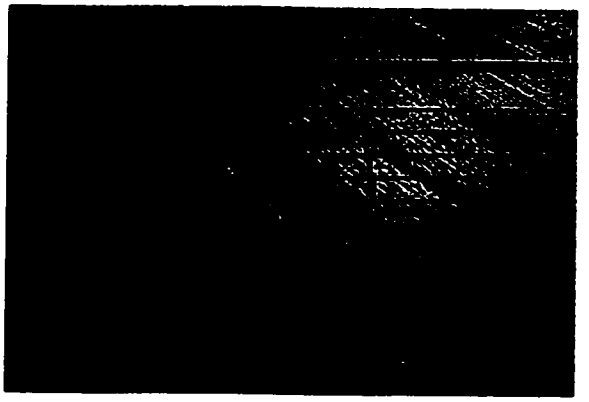

(j) Stage 10

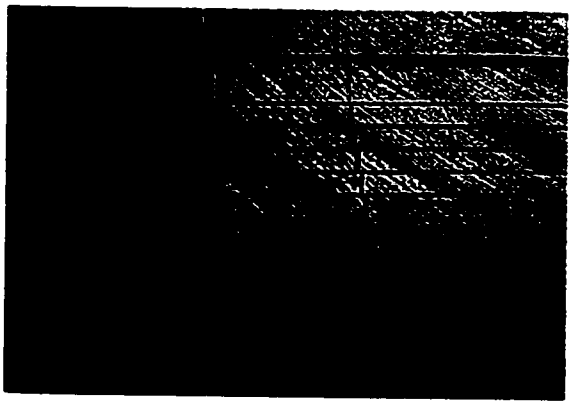

(k) Stage 11

(l) Stage 12

FIG 4.6 (Continued) Photographs of sand deformation development

Surface: Sand blasted steel plate
Sand: Medium size crushed quartz, Dr = 45.7%
Normal Stress = 100 kPa

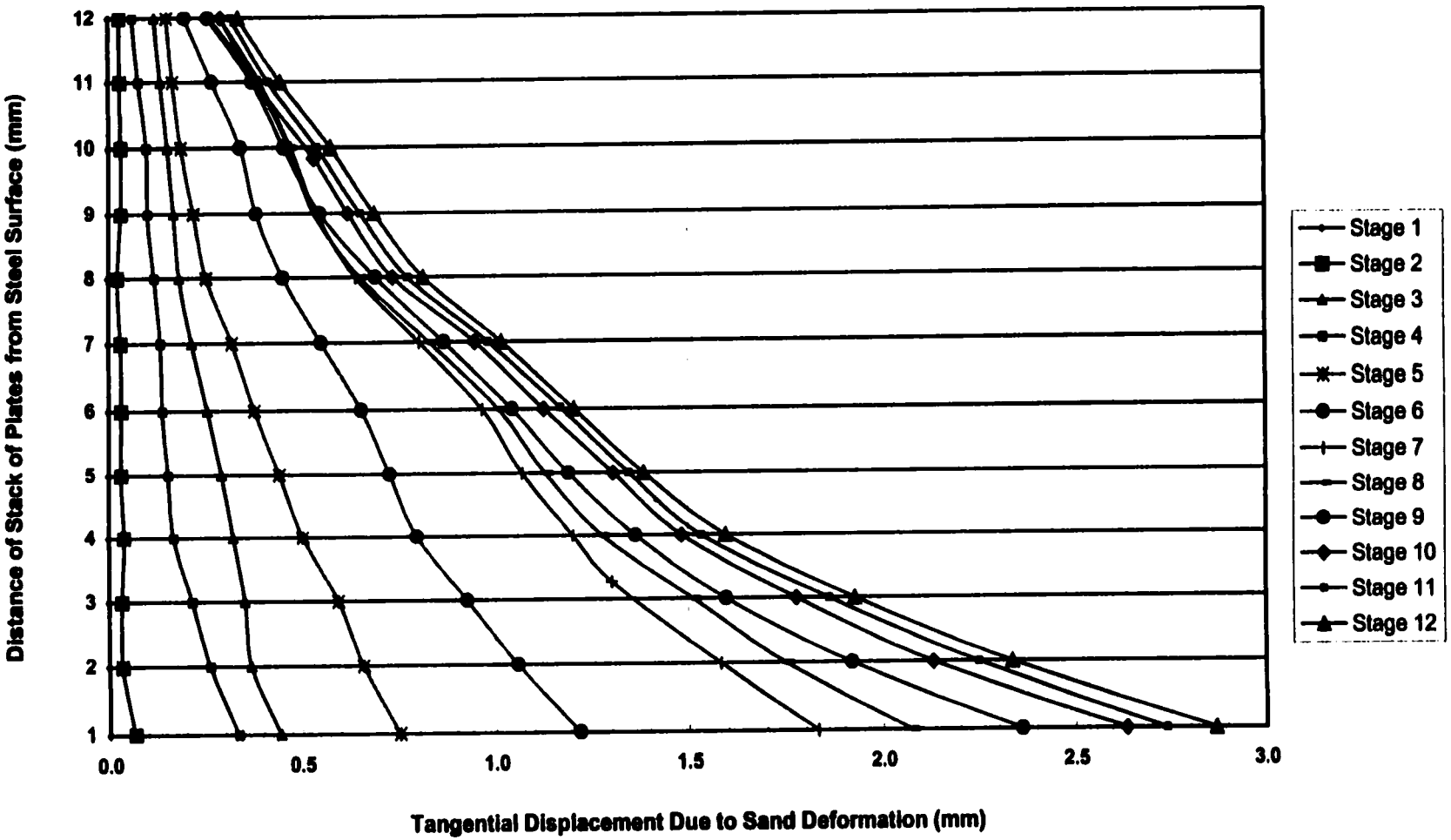

FIG 4.7. Sand deformation development curves

Surface: Sand blasted steel plate
Sand: Medium size crushed quartz, Dr = 45.7%
Normal Stress = 100 kPa

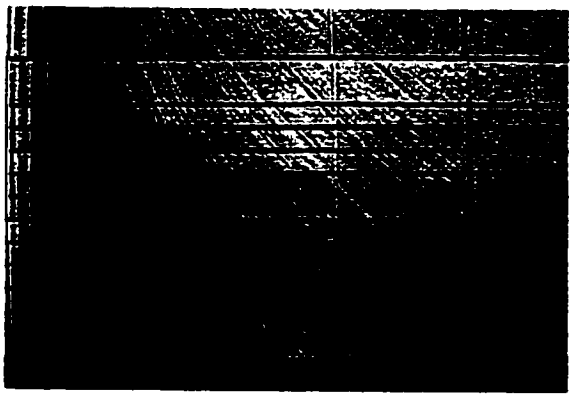

(a) Stage 1

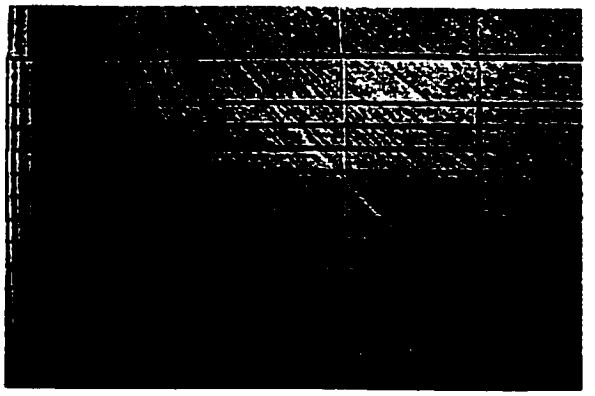

(b) Stage 2

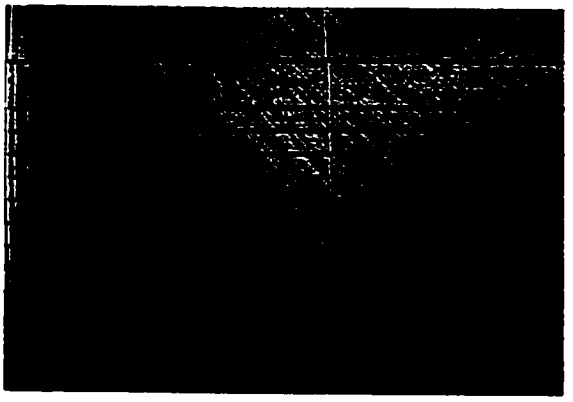

(c) Stage 3

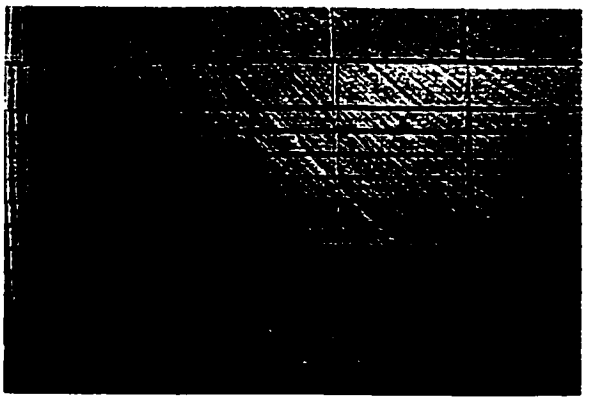

(d). Stage 4

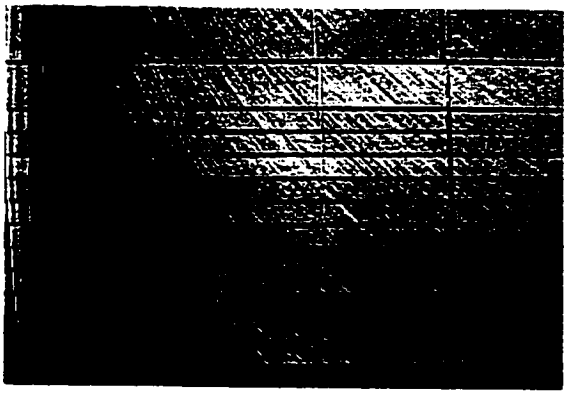

(e) Stage 5

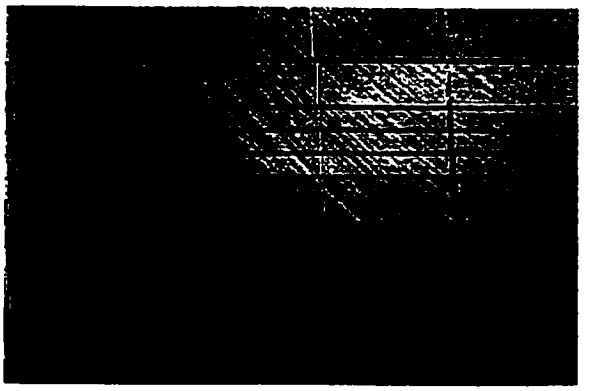

(f) Stage 6

FIG 4.8 Photographs of sand deformation development

Surface: Sand blasted steel plate
Sand: Medium size crushed quartz, Dr = 45.7%
Normal Stress = 300 kPa

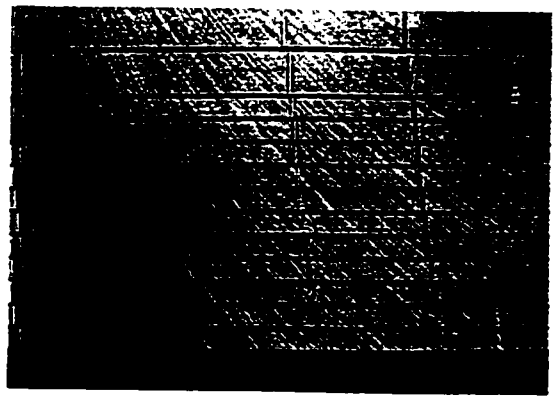

(g) Stage 7

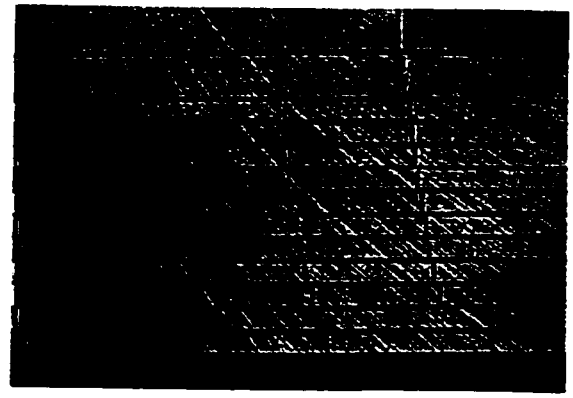

(h) Stage 8

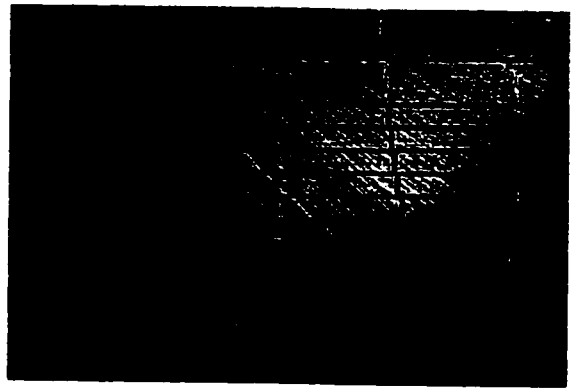

(i) Stage 9

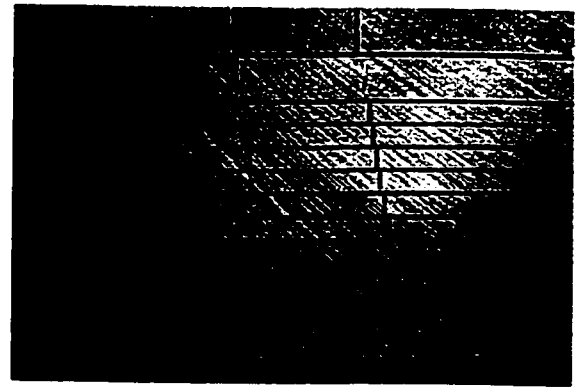

(j) Stage 10

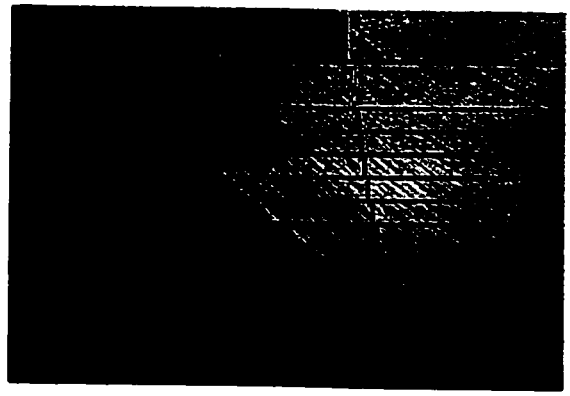

(k) Stage 11

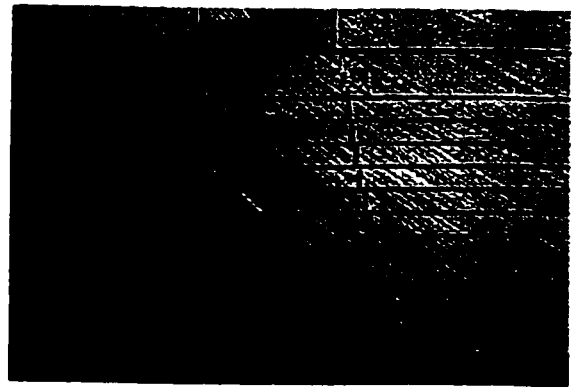

(l) Stage 12

FIG 4.8 (Continued) Photographs of sand deformation development

Surface: Sand blasted steel plate
Sand: Medium size crushed quartz, Dr = 45.7%
Normal Stress = 300 kPa

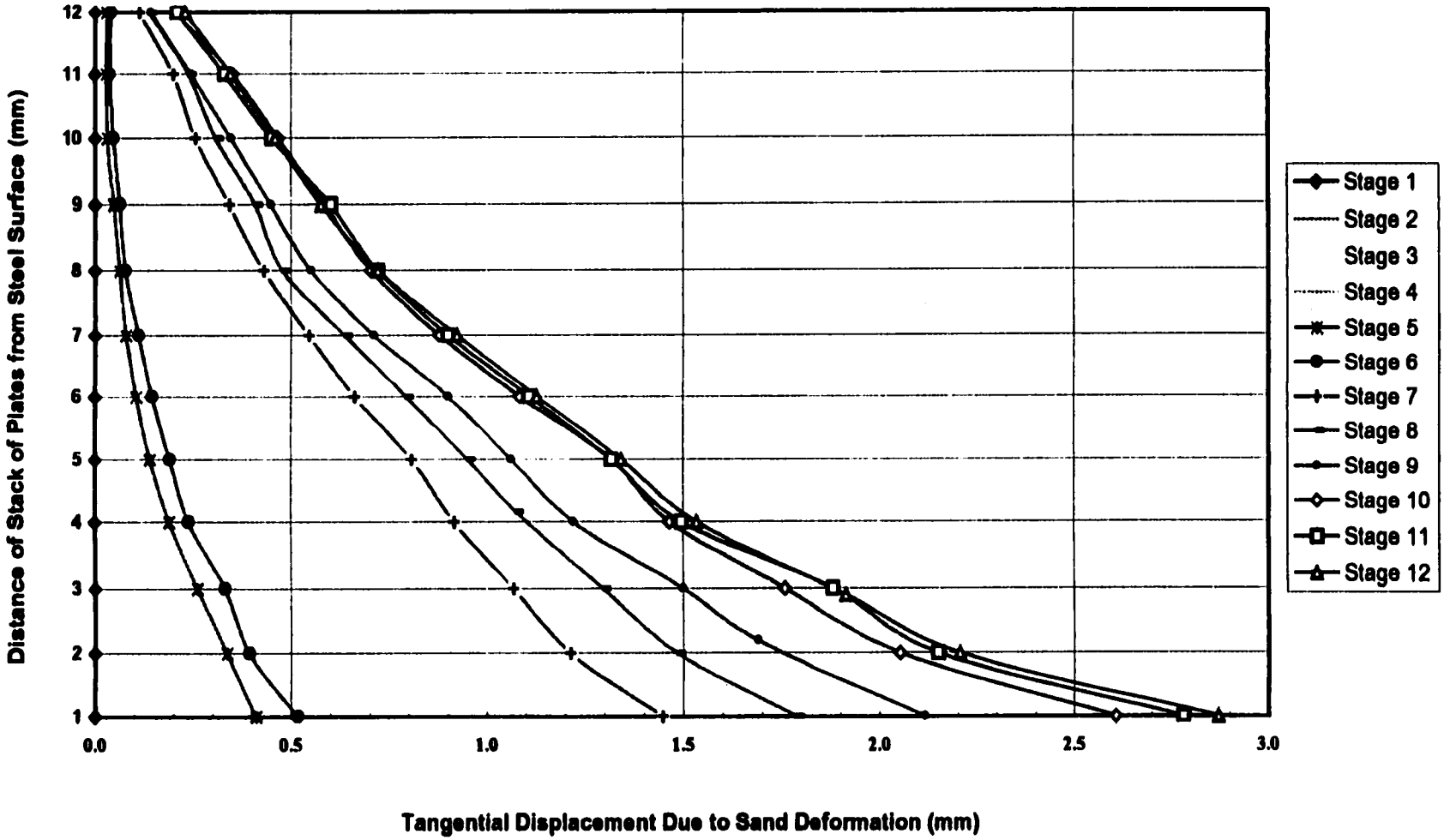

FIG 4.9. Sand deformation development curves

Surface: Sand blasted steel plate
Sand: Medium size crushed Quartz, Dr = 45.7%
Normal Stress = 300 kPa

CHAPTER 5
CONSTITUTIVE MODELS FOR SOIL-STRUCTURE INTERFACE BEHAVIOUR: LITERATURE REVIEW

In this chapter, major developments in constitutive relations for the numerical simulation of soil-structure interface behaviour are briefly reviewed. A short description of a Mohr-Coulomb type model, a non-linear elastic model, an elasto-plasticity based model, and the hyperbolic model are provided. Finally, Lade's model is described in detail.

5.1 Mohr-Coulomb Type Model

The Mohr-Coulomb failure criterion can be applied to interfaces similar to that of soils. The shear behaviour of the interface before failure is considered as rigid or elastic for practical applications. This is the simplest, yet frequently used model for the behaviour of interfaces.

The rigid-plastic model does not account for shear and normal displacements before failure or slip occurs. The elastic-perfectly plastic models consider the shear displacement, but lack the possibility of considering the non-recoverable (plastic) deformations. Both models are poor in terms of modeling the normal displacements and post-peak behaviour of interfaces. The major advantage of such models is simplicity and applicability to some conditions like those without hardening effects. But they are not suitable for granular materials in which work hardening, non-recoverable displacements before failure, and non-linearity and post-peak softening are common.

5.2 Non-linear Elastic Model

In order to account for non-linearity involved in interface behaviour, non-linear elastic models have been used for interface modeling. The hyperbolic simulation is a common practice both in soil and interface modeling. Ramberg and Osgood (1943) proposed a curve fitting procedure for description of stress-strain curves by three parameters. Streeter *et al.* (1974) used the Ramberg-Osgood model for defining cyclic behaviour of soils and Idriss et al. (1978) used it for cohesive soils. The same model with some modifications was applied for interfaces subjected to cyclic loads by Desai *et al.* (1985). The Ramberg-Osgood model simulates the interface behaviour as a piece wise non-linear elastic response. As a result, although unloading and reloading are included, inelastic deformations are not included in the sense of the theory of plasticity. The model also lacks the ability of considering the normal displacements at the contact surface.

5.3 Direction Type Model

A direction dependent constitutive relation was proposed by Boulon and Plytas (1986). This 2-D model was developed on the basis of the experimental results from direct shear tests with constant normal stress or constant volume testing conditions. A path dependent interpolation rule was applied and the incremental shear and normal stresses of the interface were related to the incremental shear and normal displacements:

$$\begin{Bmatrix} \dot{w} \\ \dot{u} \end{Bmatrix} = \begin{bmatrix} \frac{\partial \dot{w}}{\partial \dot{\tau}} & \frac{\partial \dot{w}}{\partial \dot{\sigma}_n} \\ \frac{\partial \dot{u}}{\partial \dot{\tau}} & \frac{\partial \dot{u}}{\partial \dot{\sigma}_n} \end{bmatrix} \cdot \begin{Bmatrix} \dot{\tau} \\ \dot{\sigma}_n \end{Bmatrix} \qquad (5\text{-}1)$$

Where $\dot{w}$ and $\dot{u}$ are shear and normal displacement increments and $\dot{\tau}$ and $\dot{\sigma}_n$ are shear and normal stress increments, respectively.

The coupling between normal and shear behaviour was derived automatically from the interpolation function. This model has been employed for the analysis of soil-structure interaction problems, such as axially loaded piles by Boulon and Plytas (1986).

5.4 Elasto-Plasticity Based Models

Except the direction type model explained in section 5.3, all other constitutive models for interface behaviour ignore the normal response of the interface, thus ignore the coupling effects of shear and normal displacements. The concept of theory of plasticity was applied to account for the coupling between normal and shear behaviour. The first attempt towards the application of theory of plasticity for interface modeling was made by Ghaboussi and Wilson (1973). The cap plastic model was applied to joints in rocks; the perfectly plastic yield surface was used to limit shear stresses; a strain-hardening cap was applied to control dilatancy. Therefore, the components of normal strain and shear strain could be divided into elastic and plastic parts.

An elasto-plastic constitutive model was developed by Fishman and Desai (1987) and Desai and Fishman (1991) for hardening behaviour of rock joints with associative and non-associative flow rules. The same model was modified by Navayogarajah *et al.* (1992) for monotonic and cyclic behaviour of interfaces between sand-steel and sand-concrete. The modified model was applied and expanded by Fakharian (1996) to simulate the behaviour of interfaces under the 2-D and 3-D monotonic loading conditions.

In the following subsections, Cam-Clay model, Nor-Sand model, and discrete element method (DEM) are summarized briefly.

5.4.1 Cam-Clay Model

The Cambridge theories are known under the umbrella term of Cam Clay. Cam Clay is a theoretical model for soil behaviour. It combines the theories of critical state soil mechanics and the idea of a state boundary surface with the theories of plasticity, including yielding, hardening and plastic flow. Schofield and Wroth (1968) described the original Cam Clay model while Roscoe and Burland (1968) described the modified Cam Clay. Actually all the theories within the Cam Clay family are basically similar. Soil is taken to be frictional with logarithmic compression. The state boundary surface is taken as a yield surface and as a plastic potential surface, and hardening is related to the plastic volumetric strains. Based on the concepts of the flow rule and plastic potential from plasticity theory, the Cam Clay model was developed using simple curve fitting procedures. The principal differences between the various members of the Cam Clay family are in the precise equations for the yield surface. For example, in the original Cam Clay model the yield surface is a logarithmic spiral while in the modified Cam Clay model the yield surface is elliptical.

5.4.2 Nor-Sand Model

Jefferies (1993) and Been and Jefferies (1991) developed a generalized Cambridge-type constitutive model, Nor-sand, for dilatant soil from the fundamental axioms of critical state theory. Nor-sand is generalized using two axioms. First, a unique locus, which is called the critical state locus, CSL, exists in q, p, e space such that soil can be deformed without limit at constant state of stress and constant void ratio. q is defined as σ_1- σ_3, p is the mean stress and e is the void ratio. Second, the critical state locus forms the ultimate condition of all distortional processes in soil, so that all monotonic distortional stress state paths tend to end at this locus. Some assumptions were made which include: a single yield surface exists in the stress space at any instant; stress is coaxial with strain increment; strain increment is normal to the yield surface.

Nor-Sand captures the influence of void ratio and confining stress on the constitutive behaviour of sand. Initial void ratio and mean stress are explicitly included through the use of

a state parameter. Work-hardening must be constrained to maximum values to replicate the measured behaviour of sands; these maximum values forming limited hardening loci parallel to the critical state locus in the e-ln p space.

5.4.3 Discrete Element Method (DEM)

Numerical simulations of sand-steel interface tests were performed by Fu (1998) using the discrete element method (DEM). A two-dimensional discrete element program PFC^{2D} was used in the simulations. Some conclusions were given based on this method. It was mentioned that, the particles move not only in the tangential direction but also in the direction normal to the interface. The particles closer to the contact surface had larger horizontal displacements. Before the peak of frictional resistance, there was little sliding at the interface. The sand mass deformed uniformly and there was not a large increase in the sand volume. At the peak, the interface started sliding, and along a rough interface, the particles slipped, rolled and moved up and down. On the other hand, along a smooth interface, sand mass slipped without large deformation. A localized shear zone was formed in the sand within a thickness of 10 mm above the contact surface during sliding. A shear zone formation explains the reduction in frictional resistance during the interface sliding. When the interface was smooth, there was no formation of shear zone.

In the discrete element method, both rotations and translations of individual grains are monitored. The particle shape plays an important role in the simulations. The simulations using the peanut shape particle units produced better results than those using round particles for both strength and deformation behaviour of an interface under constant normal stress. The interface soil undergoes very large structural changes during the localized shear. The interface thickness could be visually determined by particle displacement. The particle displacement in an interface zone exceeds the value expected by extrapolating the displacement due to the shear deformation of sand mass. The interface thickness is usually within the range of 2 to 8 times the mean grain size.

It was also found out that, the relative density of sand in shear zone is lower than that of the sand before the interface failure. The lower density of sand in the shear zone results in the lower maximum shear stress ratio. Therefore the upper limit to the coefficient of friction decreases because of the shear zone formation.

Although the maximum shear strength can be simulated reasonably well, the numerical sample behaviour did not agree well with the experimentally observed behaviour before the peak shear strength is reached. Furthermore, the compressive deformation during shearing was not fully simulated.

5.4.4 Hyperbolic Model

Duncan and Chang (1970) developed a simple non-linear (hyperbolic) stress-strain relation based on the generalized Hooke's law and the Mohr-Coulomb failure criterion in order to include both displacement and failure in the analysis. This model was used for incremental analysis of embankments and excavations (Chang 1970, Duncan *et al.* 1970). Later it was found that stress-strain theories based entirely on assumed incremental elastic behaviour have apparent shortcomings in the prediction of soil response at high stress levels. The hyperbolic relationship has been found to be inadequate for accurate modeling of such effects as the influence of the intermediate principal stress, volume increases due to shear stress, and the strain softening.

5.5 Lade's Model

The elasto-plastic stress-strain theory described in Lade's model was developed on the basis of results of cubical triaxial tests on cohensionless soil. The parameters involved can be derived entirely from the results of a series of conventional triaxial compression tests.

Strain increments are assumed to have both elastic and plastic parts.

$$\Delta\varepsilon = \Delta\varepsilon^{e} + \Delta\varepsilon^{p} \qquad (5\text{-}2)$$

where $\Delta\varepsilon^e$ = the elastic strain increments

$\Delta\varepsilon^p$ = the plastic strain increments

In the following subsections, three basic requirements for Lade's model are described in detail.

5.5.1 Failure Criterion and Yield Surface

There must exist a yield surface such that when the soil is subjected to changes in stress represented by points inside that surface, the soil will deform elastically, whereas if the changes in stress tend to cross the yield surface, soil will simultaneously yield plastically and deform elastically. The yield surface expands as the soil is loaded to successively higher stress levels, and at failure the yield surface coincides with the failure surface. The equation of the failure criterion is:

$$I_1^3 - k_1 I_3 = 0 \qquad (5\text{-}3)$$

where k_1 is a constant whose value depends on the density of the sand

I_1 is the first stress invariant, $I_1 = \sigma_1+\sigma_2+\sigma_3$

I_3 is the third stress invariant, $I_3 = \sigma_1\cdot\sigma_2\cdot\sigma_3$

The yield surface is expressed by the following equation:

$$f = \frac{I_1^3}{I_3} \qquad (5\text{-}4)$$

where f is the stress level

In principal stress space the shape of a failure surface is conical, with the apex of the cone at the origin of the stress axes, as shown on the insert in Fig. 5.1. Cross sections of failure surfaces are shown on an octahedral plane in Fig 5.1a for friction angles in triaxial compression of 30°, 40°, and 50°. Fig. 5.1b shows the cross sections of the failure surfaces as well as the experimental results for comparison purpose.

The yield surface, which defines the boundary between states of stress where both elastic and plastic deformations occur and those where only elastic deformations occur, is assumed to have the same general shape as the failure surface. During continued loading the yield surface is assumed to expand symmetrically around the hydrostatic axis as stress level increases. The ultimate position of the yield surface, for which $f = k_1$, is the failure surface for the sand. During unloading and changes in stress for which the stress level is constant, the yield surface remains in the same position corresponding to the highest stress level previously applied to the sand.

Thus when a stress increment is applied to an element of sand in which the current values of stress define a point on the current yield surface, there are two possibilities: if $df > 0$, the sand yields plastically and f takes a new higher value; if $df \leq 0$, the sand undergoes only elastic deformation, additional yielding does not occur, and the value of f defining the position of the yield surface does not change.

5.5.2 Plastic Potential and Flow Rule

A flow rule is required which relates the relative magnitudes of the plastic strain increments to the stresses. The flow rule is derived from the requirements that the plastic strain increment direction should be normal to the plastic potential surface. There are infinite numbers of such surfaces. For perfect plasticity, the plastic potential surface is assumed to be the same as the yield surface. This implies much higher rates of dilation than are observed in tests on real soils. When the plastic potential surface is assumed to differ from the yield surface, i.e. when the flow rule is "non-associated", much better agreement between theory and experiment can be achieved. The plastic potential function is expressed in a form similar to the failure criterion:

$$g = I_1^3 - K_2 I_3 \qquad (5\text{-}5)$$

where K_2 is a constant for any given value of f

5.5.3 Work-Hardening Law

A work-hardening law is needed, from which the magnitudes of the plastic strain increments caused by given stress increments can be determined. The relationship between the work used to produce plastic yield and the stress level is termed the work-hardening law. The adoption of an isotropic hardening law implies that the yield surface expands uniformly and that the degree of hardening is independent of stress-path. According to the isotropic hardening hypothesis, the relationship between the total plastic work and the degree of hardening could be expressed as $W_p = F(f)$, where F is a monotonically increasing positive function. The plastic work could be calculated as:

$$W_p = \int \{ \sigma_{ij} \}^T \cdot d\varepsilon_{ij}^{\,p} \qquad (5\text{-}6)$$

where $\{ \sigma_{ij} \}^T \cdot d\varepsilon_{ij}^{\,p}$ is the plastic work done per unit volume during the plastic strain increment $d\varepsilon_{ij}^{\,p}$.

The increment in plastic work is calculated from:

$$\Delta W_p = \frac{a \cdot df}{\left(1 - r_f \dfrac{f - f_t}{k_1 - f_t}\right)^2} \qquad (5\text{-}7)$$

where $a = M\, Pa\, (\dfrac{\sigma_3}{pa})^l$

r_f, k_1, and f_t are the parameters in Lade's model

df is the difference in f between two successive stress states

The plastic stress-strain relationship may be expressed as:

$$\begin{Bmatrix} \Delta\varepsilon_x^p \\ \Delta\varepsilon_y^p \\ \Delta\varepsilon_z^p \\ \Delta\varepsilon_{yz}^p \\ \Delta\varepsilon_{zx}^p \\ \Delta\varepsilon_{xy}^p \end{Bmatrix} = \frac{K_2}{3(I_1^3 - K_2 \cdot I_3)} \cdot \Delta Wp \cdot \begin{Bmatrix} \frac{3}{K_2} \cdot I_1^2 - \sigma_y \cdot \sigma_z + \tau_{yz}^2 \\ \frac{3}{K_2} \cdot I_1^2 - \sigma_z \cdot \sigma_x + \tau_{zx}^2 \\ \frac{3}{K_2} \cdot I_1^2 - \sigma_x \cdot \sigma_y + \tau_{xy}^2 \\ \sigma_x \cdot \tau_{yz} - 2 \cdot \tau_{xy} \cdot \tau_{zx} \\ \sigma_y \cdot \tau_{zx} - 2 \cdot \tau_{xy} \cdot \tau_{zx} \\ \sigma_z \cdot \tau_{xy} - 2 \cdot \tau_{xy} \cdot \tau_{zx} \end{Bmatrix} \tag{5–8}$$

The elastic strain increment is calculated by:

$$\Delta\varepsilon_x^e = \frac{\Delta\sigma_x}{E_i} - \frac{v}{E_i} \cdot (\Delta\sigma_y + \Delta\sigma_z)$$

$$\Delta\varepsilon_y^e = \frac{\Delta\sigma_y}{E_i} - \frac{v}{E_i} \cdot (\Delta\sigma_x + \Delta\sigma_z)$$

$$\Delta\varepsilon_z^e = \frac{\Delta\sigma_z}{E_i} - \frac{v}{E_i} \cdot (\Delta\sigma_x + \Delta\sigma_y) \tag{5-9}$$

$$\Delta\varepsilon_{xy}^e = \frac{\Delta\tau_{xy}}{2 \cdot G}$$

$$\Delta\varepsilon_{yz}^e = \frac{\Delta\tau_{yz}}{2 \cdot G}$$

$$\Delta\varepsilon_{zx}^e = \frac{\Delta\tau_{zx}}{2 \cdot G}$$

The total strain increment is calculated by:

$$\Delta\varepsilon_x^t = \Delta\varepsilon_x^e + \Delta\varepsilon_x^p$$

$$\Delta\varepsilon_y^t = \Delta\varepsilon_y^e + \Delta\varepsilon_y^p \tag{5-10}$$

$$\Delta\varepsilon_{xy}^t = \Delta\varepsilon_{xy}^e + \Delta\varepsilon_{xy}^p$$

The total strain is the accumulation of the total strain increments.

$$\varepsilon_x = \Sigma\, \Delta\varepsilon_x^t$$

$$\varepsilon_y = \Sigma\, \Delta\varepsilon_y^t \tag{5-11}$$

$$\varepsilon_{xy} = \Sigma\, \Delta\varepsilon_{xy}^t$$

5.5.4 Advantages and Limitations

The stress-strain theory described here was developed by using the principles of elasticity and plasticity to simulate the non-linear and stress-dependent behaviour of cohesionless soils. It incorporates a new failure criterion and a yield criterion, a non-associated flow rule, and an empirical work-hardening law. The form of the yield criterion used in this theory was chosen as simple as possible in order to arrive at an uncomplicated stress-strain relationship. The values of the parameters can be evaluated using only the results of triaxial compression tests. These parameters may be used to calculate strains in this sand for any combination of stresses.

Compared to other available stress-strain theories, this theory has an improved capability for modeling several essential aspects of the stress-strain and strength characteristics of cohensionless soils, including the effects of the intermediate principal stress, shear-dilatancy effects, stress-path effects, and coincidence of stress increment and strain increment axes at low stress levels with transition to coincidence of stress and strain increment axes at high stress levels. Results of cubical triaxial tests, torsion tests, and tests performed using various stress-paths were analyzed using this theory and found that it is capable of predicting the behaviour of cohensionless soils for a wide range of loading conditions with reasonable accuracy.

Involved in this theory are some simplifying assumptions, which results in limitations in its capabilities in some aspects. The application of a hyperbolic curve fit for the work-hardening law implies that no decrease in strength occurs when large strains are produced in the sand. Thus, dense sand is assumed to work-harden, even at large strains, whereas the real behaviour exhibits strain softening after the peak stress level has been reached.

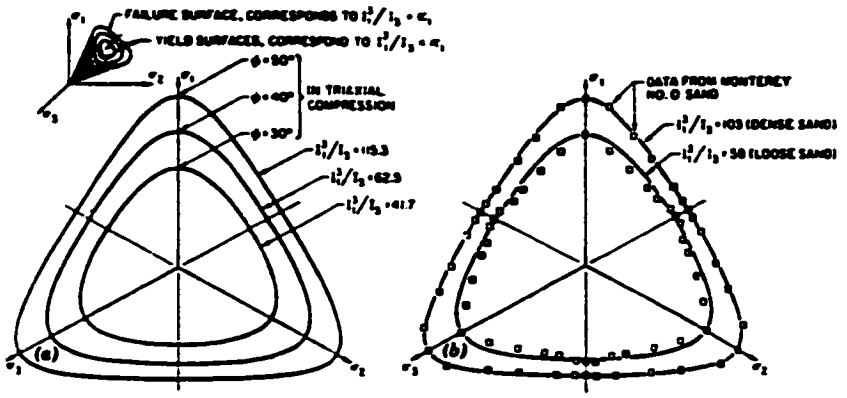

FIG.5.1 Failure surface in principal stress space (After Lade and Duncan, 1975)

(a) Shapes of failure and yield surface

(b) Comparison of failure surfaces and data obtained from experiment

CHAPTER 6

SIMULATION OF SAND BEHAVIOUR USING LADE'S MODEL

In this Chapter, first the experimental data from triaxial tests are presented in detail. The data are then used in the determination of the parameters for Lade's model. Subsequently these parameters were used in the simulation of deviator stress versus axial strain as well as the volumetric strain versus axial strain response of soil in triaxial tests.

6.1 Experimental Data from Triaxial Tests

Series of consolidated drained triaxial tests were conducted in this study. Medium size crushed quartz sand was used in the experiments. Very dense samples as well as medium dense samples were tested under four different confining pressures. Stress increments and volume changes were measured in each test. The results are presented in Figures 6.1 to 6.4. Mohr circles and p-q plots are presented in Figures 6.5 to 6.8.

Figures 6.1 shows the plots of deviator stress, σ_1-σ_3, versus axial strain, ε_1, for medium dense sand. The confining pressures, σ_3, were 100 kPa, 150 kPa, 250 kPa, and 350 kPa. The average initial relative density of the soil samples is 45.8%. The maximum deviator stresses were found to be 363 kPa at σ_3 = 100 kPa, 506 kPa at σ_3 = 150 kPa, 829 kPa at σ_3 = 250 kPa, and 1140 kPa at σ_3 = 350 kPa. The plots of volumetric strain, Δv, versus axial strain, ε_1,

under different confining pressures are shown in Figure 6.2. For small values of axial strain, the volumetric strain was compressive. As the axial strain increased, the sample started to dilate. The rate of dilation decreased with the increase of the confining pressure.

Figure 6.3 shows the deviator stress versus axial strain curves for dense sand. Figure 6.4 presents the volumetric strain versus axial strain curves. The average initial relative density was 89%. The peak deviator stresses were found to be 493 kPa at σ_3 = 100 kPa, 650 kPa at σ_3 = 150 kPa, 1072 kPa at σ_3 = 250 kPa, and 1500 kPa at σ_3 = 350 kPa. Dense sand samples exhibit higher peak deviator stress and larger dilatancy in comparison with medium dense sand.

Mohr circles corresponding to peak deviator stresses for medium dense sand in triaxial tests are plotted in Figure 6.5. The angle of internal friction ϕ of the medium crushed quartz sand was found to be 38.3°. Another method of finding ϕ is to use the slope of K_f line, which is plotted on a p-q diagram in Figure 6.6. Here the slope of K_f line ψ was found to be 31.6°. Using the relationship of $\sin\phi = \tan\psi$, the angle of internal friction ϕ was obtained to be 38°.

Mohr circles for dense sand are plotted in Figure 6.7. The slope of the failure envelope was 43.4°. K_f line was plotted in Figure 6.8 and ψ was 34.4°. Using the relationship of $\sin\phi = \tan\psi$, the angle of internal friction ϕ was found to be 43.1°.

6.2 Procedure for Parameter Determination

6.2.1 Initial Tangent Modulus E_i and $(\sigma_1 - \sigma_3)_{ult}$ Value

Triaxial compression tests provided a continuous record of axial strain, ε_1, and deviator stress, $(\sigma_1-\sigma_3)$. In order to obtain the initial tangent modulus, the values of ε_1 and $\frac{\varepsilon_1}{\sigma_1-\sigma_3}$ were plotted in transformed coordinates and a straight line is fitted to data points.

$$\frac{\varepsilon_1}{\sigma_1-\sigma_3} = a + b\,\varepsilon_1 \qquad (6\text{-}1)$$

where a = intercept of the straight line

b = slope of the straight line, $\frac{1}{b} = (\sigma_1-\sigma_3)_{ult}$

The data and best-fit lines are presented in Figures 6.9 and 6.10.

(1) Medium dense sand

In the transformed coordinates as shown in Figure 6.9, the trend lines are plotted for four tests with different confining pressures. The equations of the trend lines y = bx +a are listed below. Note that "y" represents $\frac{\varepsilon_1}{\Delta\sigma}$ and "x" represents ε_1.

σ_3 = 100 kPa: y = 0.002469x + 0.002409

σ_3 = 150 kPa: y = 0.001821x + 0.002086

σ_3 = 250 kPa: y = 0.001114x + 0.001715

σ_3 = 350 kPa: y = 0.000784x + 0.001332

The values of $E_i = \frac{1}{a}$ and $(\sigma1-\sigma3)_{ult} = \frac{1}{b}$ are listed in Table 6.1.

(2) Dense sand

The data and trend lines for dense sand are shown in Figure 6.10. The initial tangent modulus $E_i = \frac{1}{a}$ and $(\sigma1-\sigma3)_{ult} = \frac{1}{b}$ are calculated using the same procedure as for medium dense sand and the results are listed in Table 6.2.

σ_3 = 100 kPa: y = 0.001876x + 0.000897

σ_3 = 150 kPa: y = 0.001424x + 0.000818

σ_3 = 250 kPa: y = 0.000844x + 0.000614

σ_3 = 350 kPa: y = 0.000654x + 0.000428

Table 6.1: E_i and $(\sigma 1-\sigma 3)_{ult}$ values for medium dense sand

σ_3 (kPa)	$E_i = \frac{1}{a}$ (kPa)	$(\sigma_1-\sigma_3)_{ult} = \frac{1}{b}$ (kPa)
100	41511	405.02
150	47937	549.15
250	58309	897.67
350	75075	1275.5

Table 6.2: E_i and $(\sigma 1-\sigma 3)_{ult}$ values for dense sand

σ_3 (kPa)	$E_i = \frac{1}{a}$ (kPa)	$(\sigma_1-\sigma_3)_{ult} = \frac{1}{b}$ (kPa)
100	111483	533.1
150	122249	702.2
250	162866	1184.8
350	233645	1529.1

6.2.2 Deviator Stress at Failure

The deviator stress at failure $\Delta\sigma = (\sigma 1-\sigma 3)_f$ is obtained directly from the triaxial test data, and the results are presented in Table 6.3.

Table 6.3: Variations of $\Delta\sigma = (\sigma 1-\sigma 3)_f$ values with σ_3

	σ_3 = 100 (kPa)	σ_3 = 150 (kPa)	σ_3 = 250 (kPa)	σ_3 = 350 (kPa)
Medium Dense Sand	363	506	829	1140
Dense Sand	493	650	1072	1501

6.2.3 Modulus Number K_{ur} and Exponent n

The initial tangent moduli E_i for medium dense sand samples as well as for dense sand samples are obtained from Table 6.1 and 6.2. By using the equation below, parameters K_{ur} and n are obtained.

$$E_i = K_{ur} \cdot p_a \cdot (\frac{\sigma_3}{p_a})^n \qquad (6\text{-}2)$$

where p_a = atmospheric pressure = 101.3 kPa.

In order to find K_{ur} and n, the values of E_i are plotted against σ_3 on log-log scales. A straight line to the data is also fitted. These results are shown in Figure 6.11. The following results could be obtained:

(1) For medium dense sand

$$E_i = 401.9\ p_a (\frac{\sigma_3}{p_a})^{0.4576}$$

$K_{ur} = 401.9$

$n = 0.4576$

(2) For dense sand

$$E_i = 1033\ p_a (\frac{\sigma_3}{p_a})^{0.5807}$$

$K_{ur} = 1033$

$n = 0.5807$

6.2.4 Stress Level f and Maximum Value of Stress Level k_1

(1) Stress Level

Stress level is defined as:

$$f = \frac{I_1'^3}{I_3} \qquad (6\text{-}3)$$

where I_1 is the first stress invariant, $I_1 = \sigma_1+\sigma_2+\sigma_3$

I_3 is the third stress invariant, $I_3 = \sigma_1 \cdot \sigma_2 \cdot \sigma_3$

In the triaxial compression tests, $\sigma_2 = \sigma_3$

(2) k_1 = Constant = $f_{at\ failure}$

The determination of k_1 is explained by the following example. In the triaxial test with σ_3= 150 kPa for medium dense state, the principal stresses at failure are σ_1 = 656 kPa, σ_3= σ_2 = 150 kPa. By using the equation k_1 = constant = $f_{at\ failure} = \frac{I_1^3}{I_3}$, k_1 was calculated to be equal to 59.2.

Table 6.4: Variations of k_1 with σ_3

	σ_3 = 100 kPa	σ_3 = 150 kPa	σ_3 = 250 kPa	σ_3 = 350kPa	k_1 Mean Value
Medium Dense Sand	62.94	59.2	58.38	57.55	59.52
Dense Sand	84.09	73.94	73.2	73.2	76.1

The mean values of k_1, 59.52 for medium dense sand and 76.1 for dense sand, will be used as the parameters for the failure states.

6.2.5 Elastic and Plastic Strain Components

The strain increments $\Delta\varepsilon_1$ and $\Delta\varepsilon_3$, are divided into elastic and plastic components $\Delta\varepsilon_1^e$, $\Delta\varepsilon_3^e$, $\Delta\varepsilon_1^p$, and $\Delta\varepsilon_3^p$.

$\Delta\varepsilon_1$ = axial strain increment

$\Delta\varepsilon_v$ = volumetric strain increment

$\Delta\varepsilon_3$ = lateral strain increment $= \frac{\Delta\varepsilon_v - \Delta\varepsilon_1}{2}$

The incremental elastic strains for each load increment are related to the incremental stress changes for that increment by the generalized Hooke's law:

$$\Delta\varepsilon_3^{\,e} = \frac{1}{E_i}\cdot[\Delta\sigma_3 - \nu(\Delta\sigma_1 + \Delta\sigma_2)]$$

$$\Delta\varepsilon_1^{\,e} = \frac{1}{E_i}\cdot[\Delta\sigma_1 - \nu(\Delta\sigma_2 + \Delta\sigma_3)] \qquad (6\text{-}4)$$

where ν = Poisson's ratio

In the present study, $\Delta\sigma_2 = \Delta\sigma_3 = 0$, so:

$$\Delta\varepsilon_1^{\,e} = \frac{1}{E_i}\cdot\Delta\sigma_1$$

$$\Delta\varepsilon_3^{\,e} = -\frac{1}{E_i}\cdot\nu\cdot\Delta\sigma_1 = -\nu\cdot\Delta\varepsilon_1^{\,e} \qquad (6\text{-}5)$$

It should be mentioned here that, there is no plastic strains until f becomes equal to f_t (threshold of stress level). Therefore, E_i is used in the calculation of $\Delta\varepsilon_3^{\,e}$ and $\Delta\varepsilon_1^{\,e}$.

After the elastic strain increments, $\Delta\varepsilon_3^{\,e}$ and $\Delta\varepsilon_1^{\,e}$, are obtained, the plastic strain increments are calculated as:

$$\Delta\varepsilon_3^{\,p} = \Delta\varepsilon_3 - \Delta\varepsilon_3^{\,e}$$

$$\Delta\varepsilon_1^{\,p} = \Delta\varepsilon_1 - \Delta\varepsilon_1^{\,e} \qquad (6\text{-}6)$$

6.2.6 v^p, k_2, and A

(1) For the triaxial compression test, v^p is the ratio of $\Delta\varepsilon_3^{\,p}$ to $\Delta\varepsilon_1^{\,p}$:

$$v^p = -\frac{\Delta\varepsilon_3^{\,p}}{\Delta\varepsilon_1^{\,p}} \qquad (6\text{-}7)$$

(2) Another parameter in the model is k_2, which is expressed as:

$$k_2 = \frac{3\cdot I_1^{\,2}(1+v^p)}{\sigma_3(\sigma_1 + v^p\cdot\sigma_3)} \qquad (6\text{-}8)$$

This parameter is used in the plastic potential function which is given as:

$$g = I_1^3 - k_2 \cdot I_3 \qquad (6\text{-}9)$$

In Eq. 6-8, for a given stress level, the values of σ_3, σ_1, I_1, and v^p can be input, thus the k_2 values could be obtained. Figures 6.12 and 6.13 show the plot of the variations of k_2 with $f = \frac{I_1^3}{I_3}$ for triaxial compression tests performed on medium dense sand as well as dense sand with different confining pressures.

(3) As shown in Figures 6.12 and 6.13, the variation of k_2 is related to f by a simple linear equation:

$$k_2 = A\,f + 27\,(1\text{-}A) \qquad (6\text{-}10)$$

In this equation, A is the inclination of the straight line, which can be determined by plotting the data as shown in Figures 6.12 and 6.13.

For the case of medium dense samples shown in Figure 6.12, the equation representing a straight line was expressed as:

$$y = 0.3872x + 15.348$$

So the value of the parameter A is 0.3872 for medium dense sand.

For dense samples (see Figure 6.13), the equation relating k_2 to f was expressed as:

$$y = 0.4299x + 13.946$$

So the value of the parameter A is 0.43 for dense sand.

6.2.7 Plastic Work and Threshold Stress Level

The plastic work increments is expressed as:

$$\Delta W_p = \sigma_1 \Delta\varepsilon_1^p + \sigma_2 \Delta\varepsilon_2^p + \sigma_3 \Delta\varepsilon_3^p \qquad (6\text{-}11)$$

For the present study, $\sigma_2 = \sigma_3$, so:

$$\Delta W_p = \sigma_1 \Delta\varepsilon_1^p + 2\,\sigma_3 \Delta\varepsilon_3^p \qquad (6\text{-}12)$$

The total plastic work is obtained from:

$$Wp = \sum \Delta Wp \tag{6-13}$$

By plotting the values of stress level, f, against plastic work, Wp, the threshold stress level f_t is obtained. From Figure 6.14 and 6.15, the f_t value for medium dense sand and dense sand is 33 and 35, representatively.

6.2.8 Failure Ratio r_f

The relations between Wp and $(f - f_t)$ may be approximated by hyperbolae for which the following expression is used:

$$(f - f_t) = \frac{W_p}{a + d \cdot W_p} \tag{6-14}$$

The values of the coefficients *a* and *d* are determined by plotting the values of Wp versus $\frac{W_p}{f - f_t}$ on transformed axes, as shown in Figure 6.16 for medium dense sand and in Figure 6.17 for dense sand. The best-fit line is also shown in the plot. So:

a = intercept of the straight line

$\frac{1}{a}$ = initial slope of the Wp versus $\frac{Wp}{f - ft}$ relationship

d = slope of the straight line

$\frac{1}{d} = (f - f_t)_{ult}$

The values of $\frac{1}{a}$ and $\frac{1}{d}$ for medium dense and dense sand are presented in Table 6.5.

The failure ratio is calculated by:

$$r_f = \frac{k_1 - f_i}{(f - f_t)_{ult}} \tag{6-15}$$

The value of r_f is always less than unity. Consider for example the medium dense sand, when the confining pressure σ_3 = 150 kPa, $k_1 = f_{at\ failure} = (\frac{I_1'}{I_3})_{at\ failure} = 76.1$, $f_t = 37$, and $(f\text{-}f_t)_{ult} = \frac{1}{d} = \frac{1}{0.0299} = 33.444$. By substituting these values into the equation, r_f is calculated: r_f = (59.52-33)/33.22 = 0.793. Using the same procedure, the r_f values for different confining pressures for dense as well as medium dense sand are obtained (see Table 6.6).

Table 6.5: $\frac{1}{a}$ and $\frac{1}{d}$ values for medium dense and dense sand

σ_3 (kPa)	Medium Dense Sand		Dense Sand	
	$\frac{1}{a}$	$(f - f_t)_{ult} = \frac{1}{d}$	$\frac{1}{a}$	$(f - f_t)_{ult} = \frac{1}{d}$
100	7.61	35.84	11.22	64.52
150	2.92	33.44	6.08	51.02
250	1.79	31.65	3.03	52.08
350	1.4	29.94	1.887	49.26

The mean values of 0.81 and 0.767 are used for medium dense sand and dense sand, respectively.

Table 6.6: r_f values for medium dense and dense sand

	r_f Values	
σ_3 (kPa)	Medium Dense sand	Dense Sand
100	0.74	0.637
150	0.79	0.806
250	0.838	0.789
350	0.886	0.834
r_f Mean Value	0.81	0.767

6.2.9 Parameters M and *l*

In Figure 6.16 and 6.17, the variation of Wp with respect to $\frac{W_p}{f - f_t}$ is presented. $\frac{1}{a}$ = initial slope of the Wp versus (f - ft) relationship and the values for both dense and medium dense sand were given in Table 6.5. Table 6.7 presents the variations of the A values with σ_3.

Table 6.7: Variations of *a* values with σ_3

	A Values	
σ_3 (kPa)	Medium Dense sand	Dense Sand
100	0.1314	0.0891
150	0.3424	0.1644
250	0.5601	0.3298
350	0.7158	0.53

The value of *a* increases with σ_3 with the relationship expressed below:

$$a = M\, p_a \left(\frac{\sigma_3}{p_a}\right)^{l} \qquad (6\text{-}16)$$

where p_a = atmospheric pressure = 101.3 kPa.

The values of a vs σ_3 on log-log scale are plotted in Figure 6.18. Straight lines are fitted to the data, and both M and l are determined, as shown in Table 6.8.

Table 6.8: Variations of M and *l* values with density

	M	*l*
Medium Dense Sand	0.00158	1.3
Dense Sand	0.00091	1.42

6.2.10 Summary of Parameters

Table 6.9 shows the summary of the parameters for Lade's model derived from triaxial compression tests on dense and medium dense crushes quartz sand samples.

Table 6. 9: Parameters for Lade's model

Parameter	Medium dense sand	Dense sand
ϕ	38°	43°
k_1	59.52	76.1
f_t	33	35
A	0.3872	0.43
r_f	0.81	0.767
M	0.00158	0.00091
L	1.3	1.42
K_{ur}	401.9	1033
N	0.4576	0.5807
ν	0.1	0.1

6.3 Back-Calculation of Soil Behaviour in Triaxial Tests

6.3.1 Back-Calculation Procedure

The parameters determined in the previous section are used in the back-calculations of soil behaviour in triaxial tests. The axial stress value σ_1 is increased by increments, $\delta\sigma_1$, from the initial value, which equals to the confining pressure σ_3. The stress level is calculated by using the equation: $f = \frac{I_1^3}{I_3}$, where $I_1 = \sigma_1+\sigma_2+\sigma_3$, and $I_3 = \sigma_1 \cdot \sigma_2 \cdot \sigma_3$. For the present study, σ_2 equals σ_3.

Axial elastic strain increment $\delta\varepsilon_1^e$ is calculated by: $\delta\varepsilon_1^e = \frac{\delta\sigma_1}{E_i}$. While the lateral elastic strain increment $\delta\varepsilon_2^e = \delta\varepsilon_3^e = -\nu \cdot \delta\varepsilon_1^e$, where ν is the Poisson's ratio with the assigned value of 0.1.

The increment in plastic work is calculated from:

$$\delta W_p = \frac{a \cdot df}{\left(1 - r_f \frac{f - f_t}{k_1 - f_t}\right)^2} \qquad (6\text{-}17)$$

The values of the parameter r_f, k_1, and f_t are already known. *df* is the difference in f between two successive stress states. When the stress level f is less than the parameter f_t, which represents the threshold stress level, the plastic work is set to zero. After f increases beyond f_t, the plastic strains occur and the plastic work starts accumulating. This process continues until f value reaches its maximum value k_1.

After the plastic work is determined, the axial and lateral plastic strain increments are calculated by using the plastic stress-strain relationship described as follows:

$$\begin{Bmatrix} \delta\varepsilon_1^{\,p} \\ \delta\varepsilon_2^{\,p} \\ \delta\varepsilon_3^{\,p} \\ \delta\varepsilon_{23}^{\,p} \\ \delta\varepsilon_{31}^{\,p} \\ \delta\varepsilon_{12}^{\,p} \end{Bmatrix} = \frac{K_2}{3(I_1^{\,3} - K_2 \cdot I_3)} \cdot \delta Wp \cdot \begin{Bmatrix} \frac{3}{K_2} \cdot I_1^{\,2} - \sigma_2 \cdot \sigma_3 + \tau_{23}^{\,2} \\ \frac{3}{K_2} \cdot I_1^{\,2} - \sigma_3 \cdot \sigma_1 + \tau_{31}^{\,2} \\ \frac{3}{K_2} \cdot I_1^{\,2} - \sigma_1 \cdot \sigma_2 + \tau_{12}^{\,2} \\ \sigma_1 \cdot \tau_{23} - 2 \cdot \tau_{12} \cdot \tau_{31} \\ \sigma_2 \cdot \tau_{31} - 2 \cdot \tau_{12} \cdot \tau_{31} \\ \sigma_3 \cdot \tau_{12} - 2 \cdot \tau_{12} \cdot \tau_{31} \end{Bmatrix} \qquad (6\text{–}18)$$

where $\delta\varepsilon_1^{\,p}$ is the axial plastic strain increment, $\delta\varepsilon_2^{\,p}$ and $\delta\varepsilon_3^{\,p}$ are the lateral plastic strain increments in the two orthogonal direction. σ_1, σ_2, σ_3 are the current principal stresses. τ_{12}, τ_{13}, and τ_{23} are the shear stress components and should be set to zero because there is no shear stress on the principal stress planes. So the above equations are simplified to:

$$\begin{Bmatrix} \delta\varepsilon_1^{\,p} \\ \delta\varepsilon_2^{\,p} \\ \delta\varepsilon_3^{\,p} \end{Bmatrix} = \frac{K_2}{3(I_1^{\,3} - K_2 \cdot I_3)} \cdot \delta Wp \cdot \begin{Bmatrix} \frac{3}{K_2} \cdot I_1^{\,2} - \sigma_3^{\,2} \\ \frac{3}{K_2} \cdot I_1^{\,2} - \sigma_3 \cdot \sigma_1 \\ \frac{3}{K_2} \cdot I_1^{\,2} - \sigma_1 \cdot \sigma_3 \end{Bmatrix} \qquad (6\text{–}19)$$

The total axial strain increment, $\delta\varepsilon_1^{\,t}$, and the total lateral strain increments $\delta\varepsilon_3^{\,t}$ and $\delta\varepsilon_2^{\,t}$ could be calculated as follows:

$$\delta\varepsilon_1^{\,t} = \delta\varepsilon_1^{\,e} + \delta\varepsilon_1^{\,p}$$

$$\delta\varepsilon_2^{\,t} = \delta\varepsilon_3^{\,t} = \delta\varepsilon_3^{\,e} + \delta\varepsilon_3^{\,p} \qquad (6\text{-}20)$$

By accumulating the strain increments, the axial strain, ε_1, and volumetric strain ε_v, can be obtained:

$$\varepsilon_1 = \Sigma\, \delta\varepsilon_1^{\,t}$$

$$\varepsilon_v = \Sigma\, \delta\varepsilon_1^{\,t} + \Sigma\, \delta\varepsilon_2^{\,t} + \Sigma\, \delta\varepsilon_3^{\,t} \qquad (6\text{-}21)$$

6.3.2 Back-Calculation Results

Figures 6.19 to 6.22 give the results of back-calculations (numerical modelling) of triaxial test data. The experimental triaxial test data are also presented here for comparison purposes.

It could be seen from the modeling results that all the curves, for either the deviator stresses or for the volumetric strains, could be divided into two parts: linear part at the initial stage, and the non-linear part following the end of the elastic parts. The linear part at the initial stage was there because the stress level was below the threshold value. There was no plastic work produced, thus the axial strain is totally composed of elastic strains, and the stress-strain relationship was linear. The relationship between the volumetric strain and axial strain at the initial stage also showed linear behaviour. After the threshold value, plastic strains took place, plastic work started to accumulate and thus the above-mentioned relationships changed to be non-linear.

Fig. 6.19 and 6.21 present the plots of calculated deviator stress vs. axial strain results as well as the experimental results for medium dense sand and dense sand, respectively. Comparisons indicate that the curves agreed very well at high stress levels. But the model overestimates the axial strain before the axial strain reaches about 6%. Because Lade's model cannot model strain softening, for dense sand, underestimation of axial strain is apparent after the axial strain of approximately 6% to 7%.

The modeling results for the relationship between volumetric strain and axial strain are presented in Fig. 6.20 and 6.22 for medium dense sand and dense sand, respectively. They are in reasonably good agreement although there are some scatters. The model simulates the compression as well as the dilation of the sample. However, neither the predicted compression nor dilation curves were in total agreement with the experimental data.

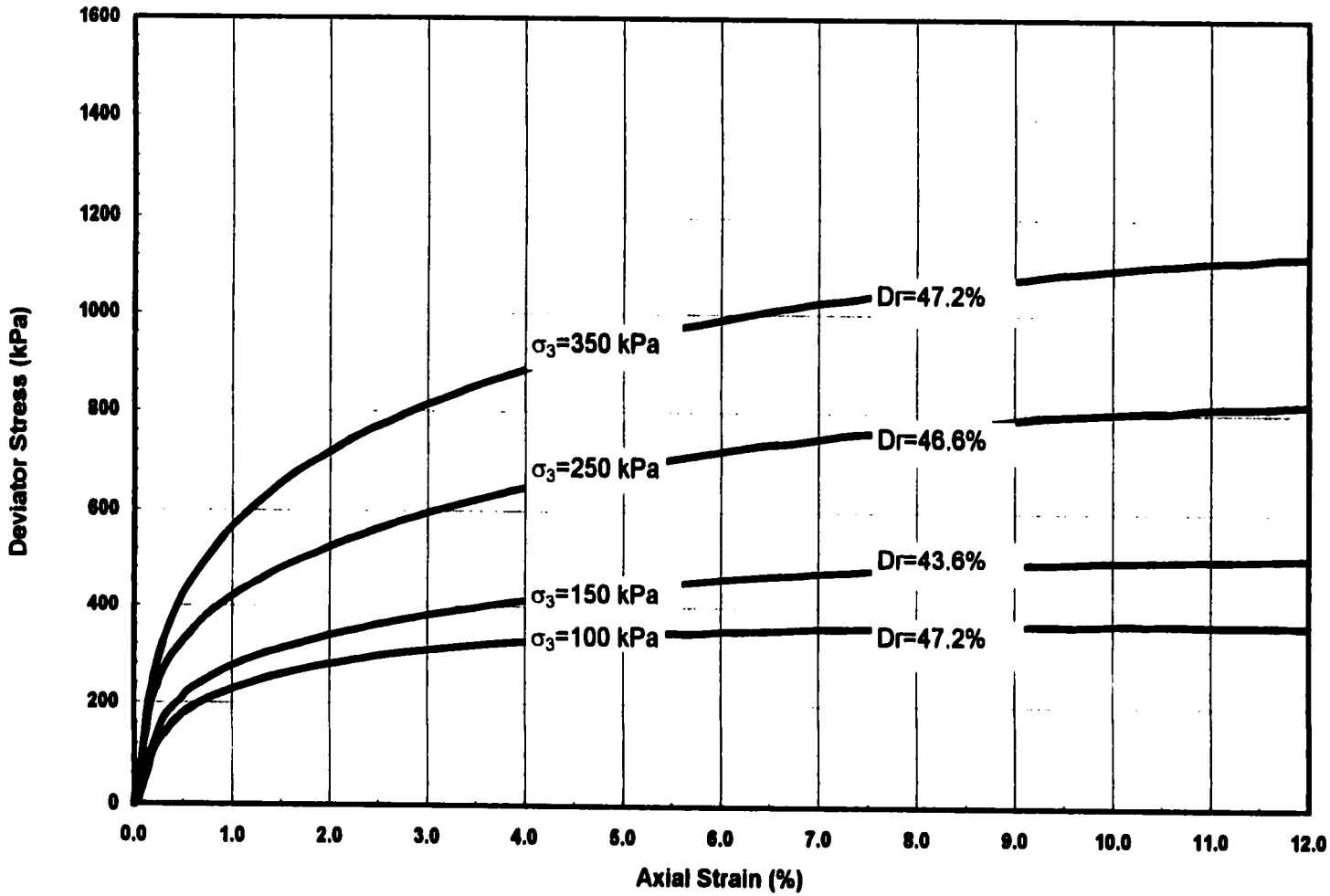

FIG. 6.1 Consolidated drained triaxial test result

Sand: Medium Size Crushed Quartz, D_r = 45.8%
Confining Pressure = 100kPa, 150 kPa, 250kPa, and 350kPa

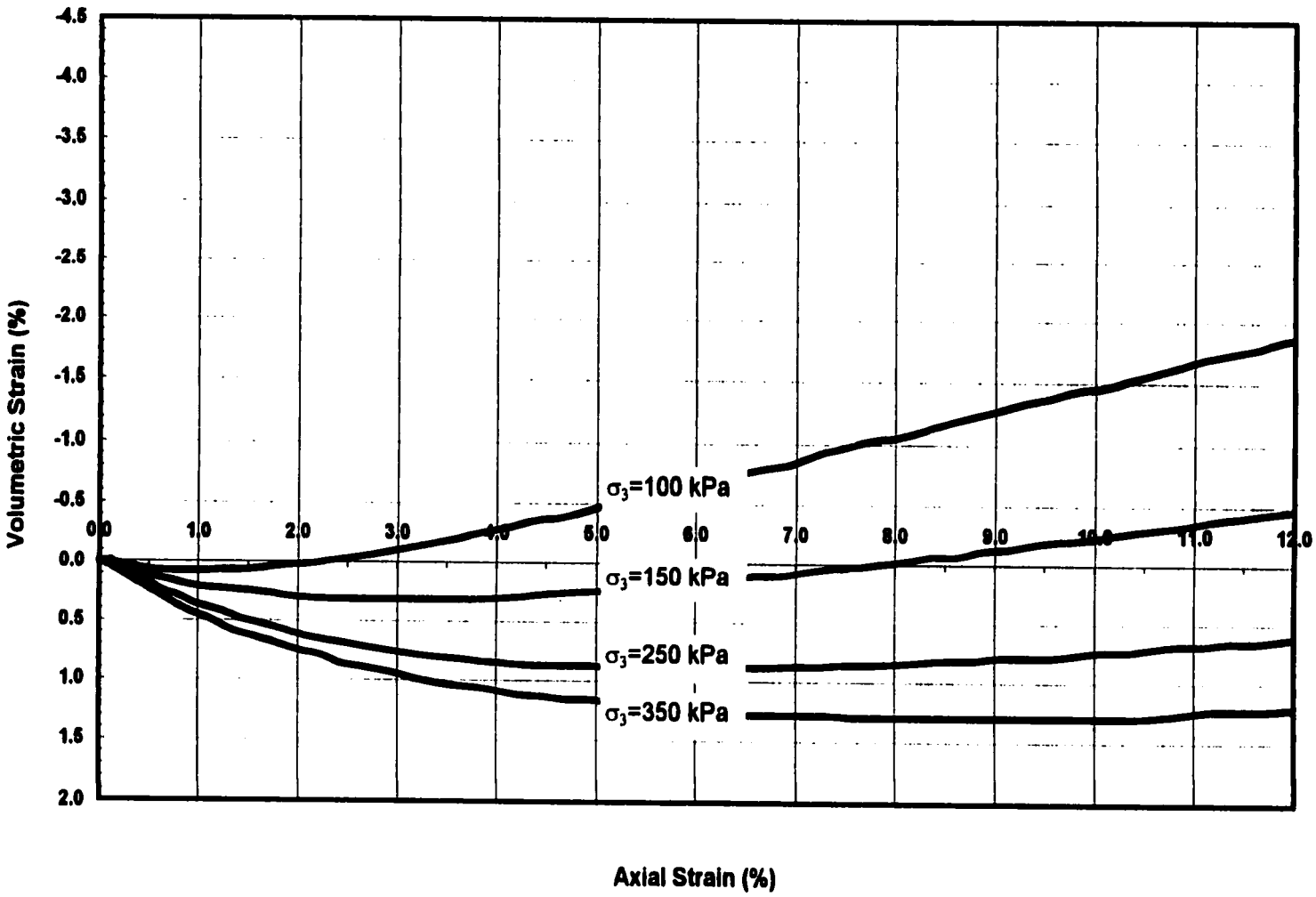

FIG. 6.2 Consolidated drained triaxial test result

Sand: Medium Size Crushed Quartz, Dr = 45.8%
Confining Pressure = 100kPa, 150 kPa, 250 kPa, and 350 kPa

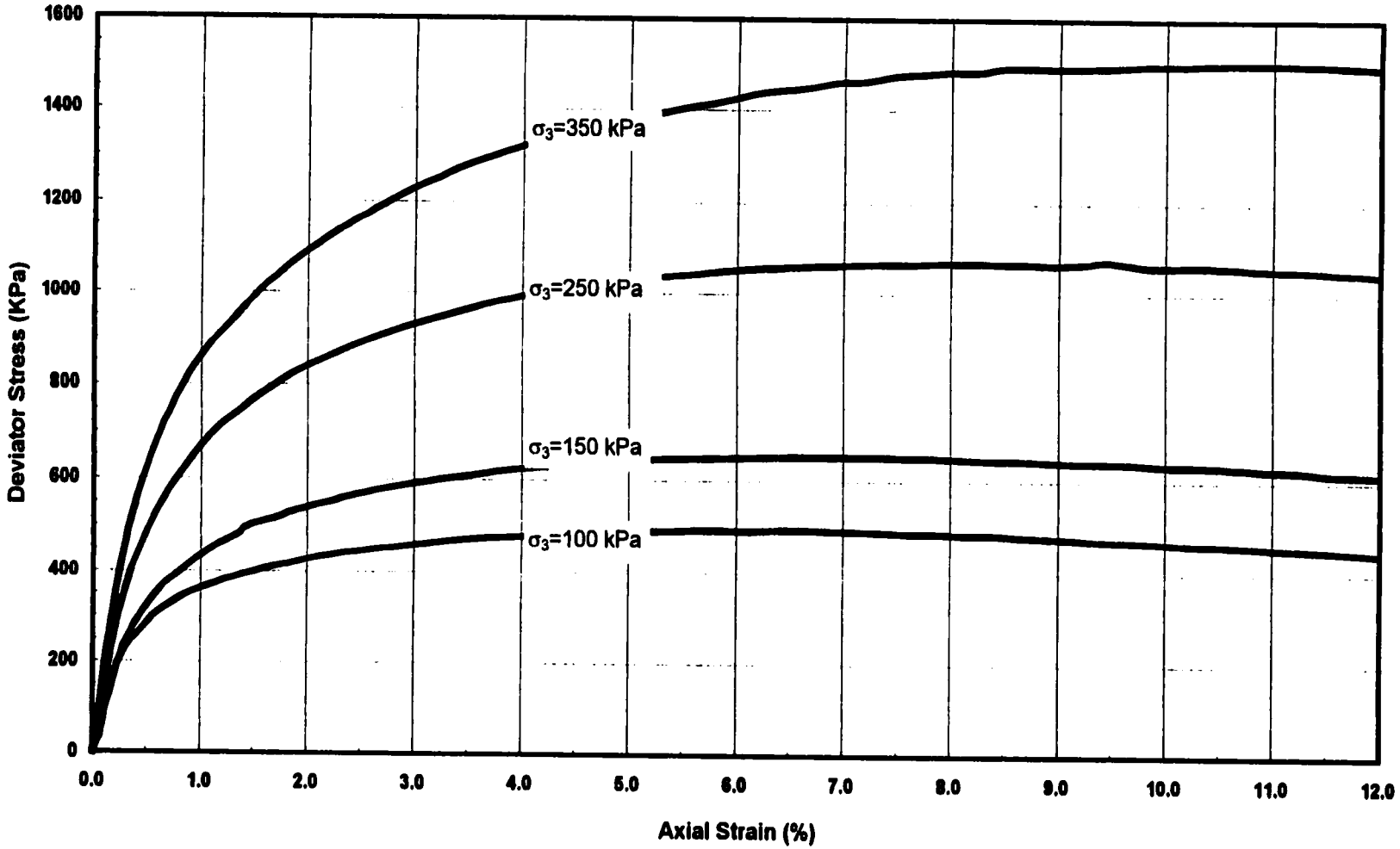

FIG. 6.3 Consolidated drained triaxial test result

Sand: Medium Size Crushed Quartz, Dr = 89%
Confining Pressure = 100 kPa, 150 kPa, 250 kPa, and 350 kPa

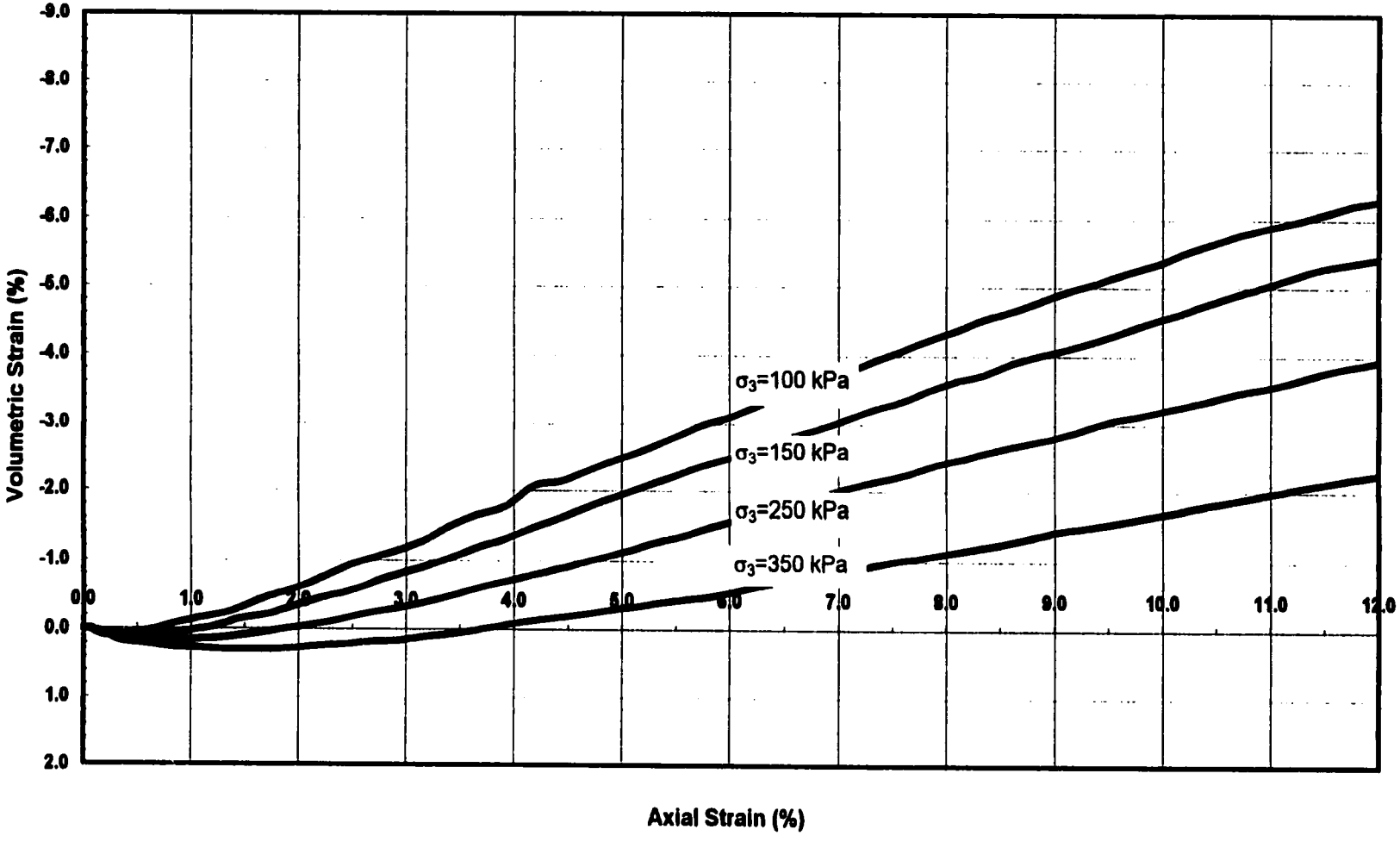

FIG. 6.4 Consolidated drained triaxial test result

Sand: Medium Size Crushed Quatrz, Dr = 89%
Confining Pressure = 100 kPa, 150 kPa, 250 kPa, and 350 kPa

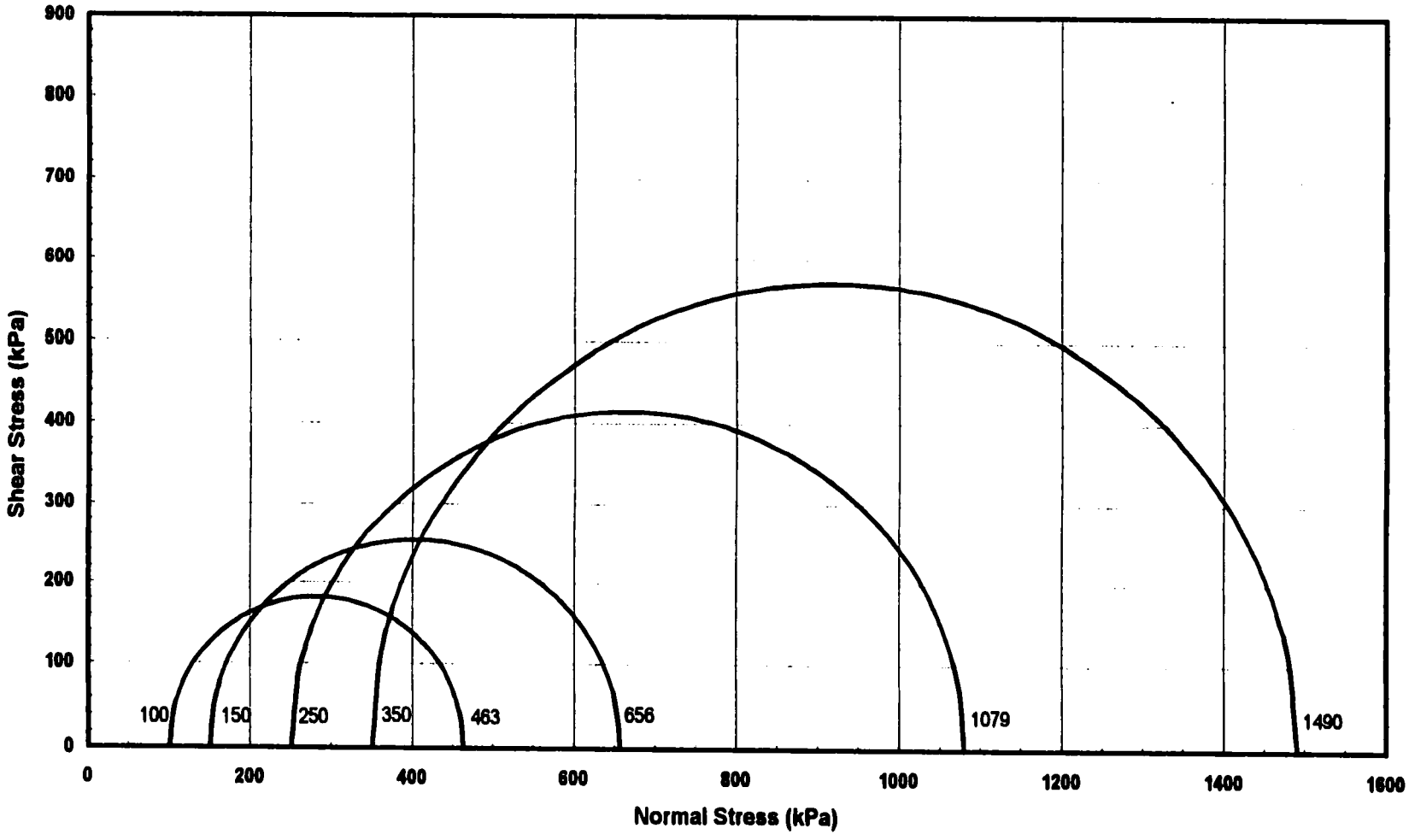

FIG. 6.5 Mohr circles at failure

Sand: Medium Crushed Quartz, D_r = 45.8%
Confining Pressure = 100 kPa, 150 kPa, 250 kPa, and 350 kPa

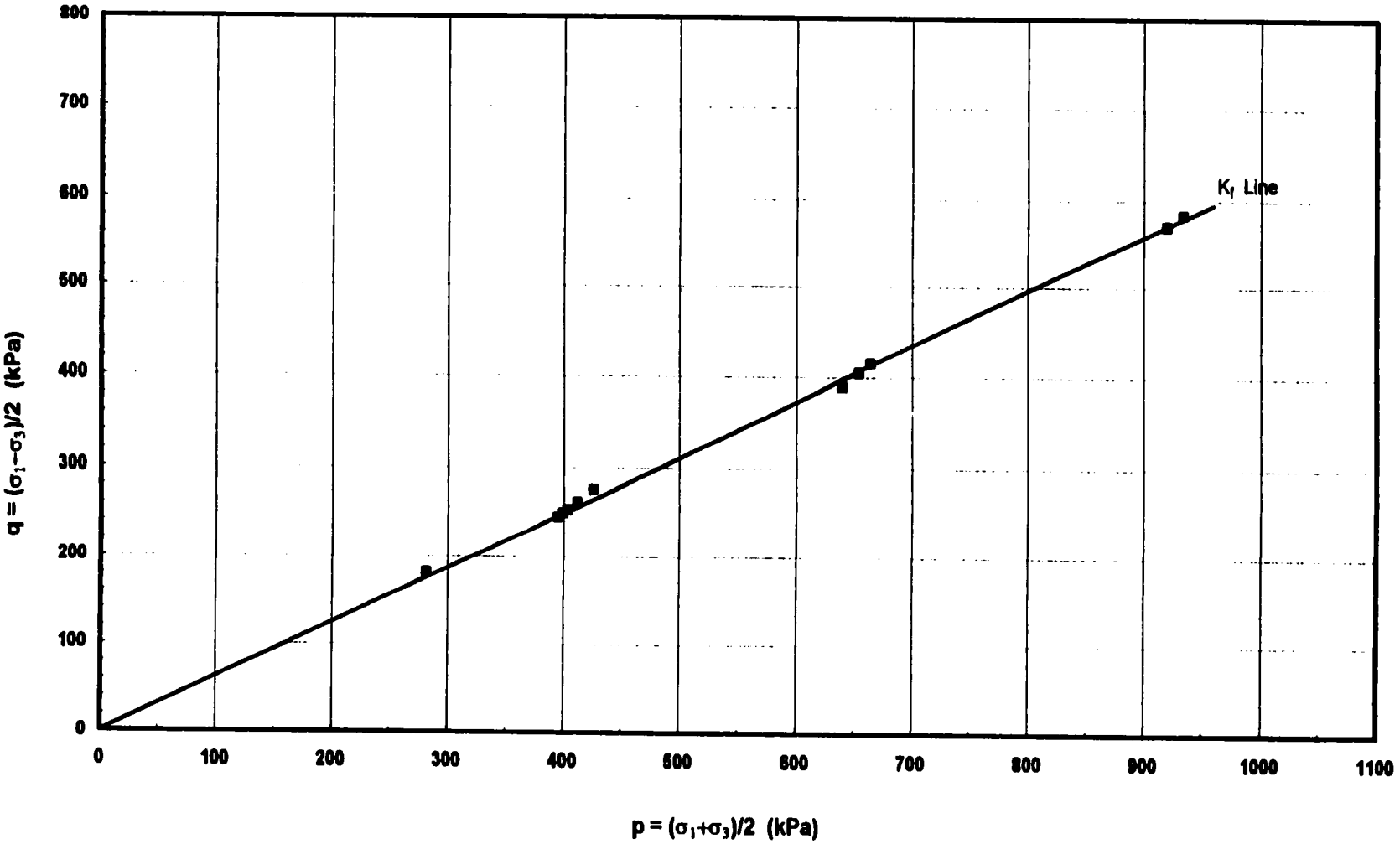

FIG. 6.6 p-q plot and k_f line

Sand: Medium Crushed Quartz, Dr = 45.8%
Confining Pressure = 100 kPa, 150 kPa, 250 kPa, and 350 kPa

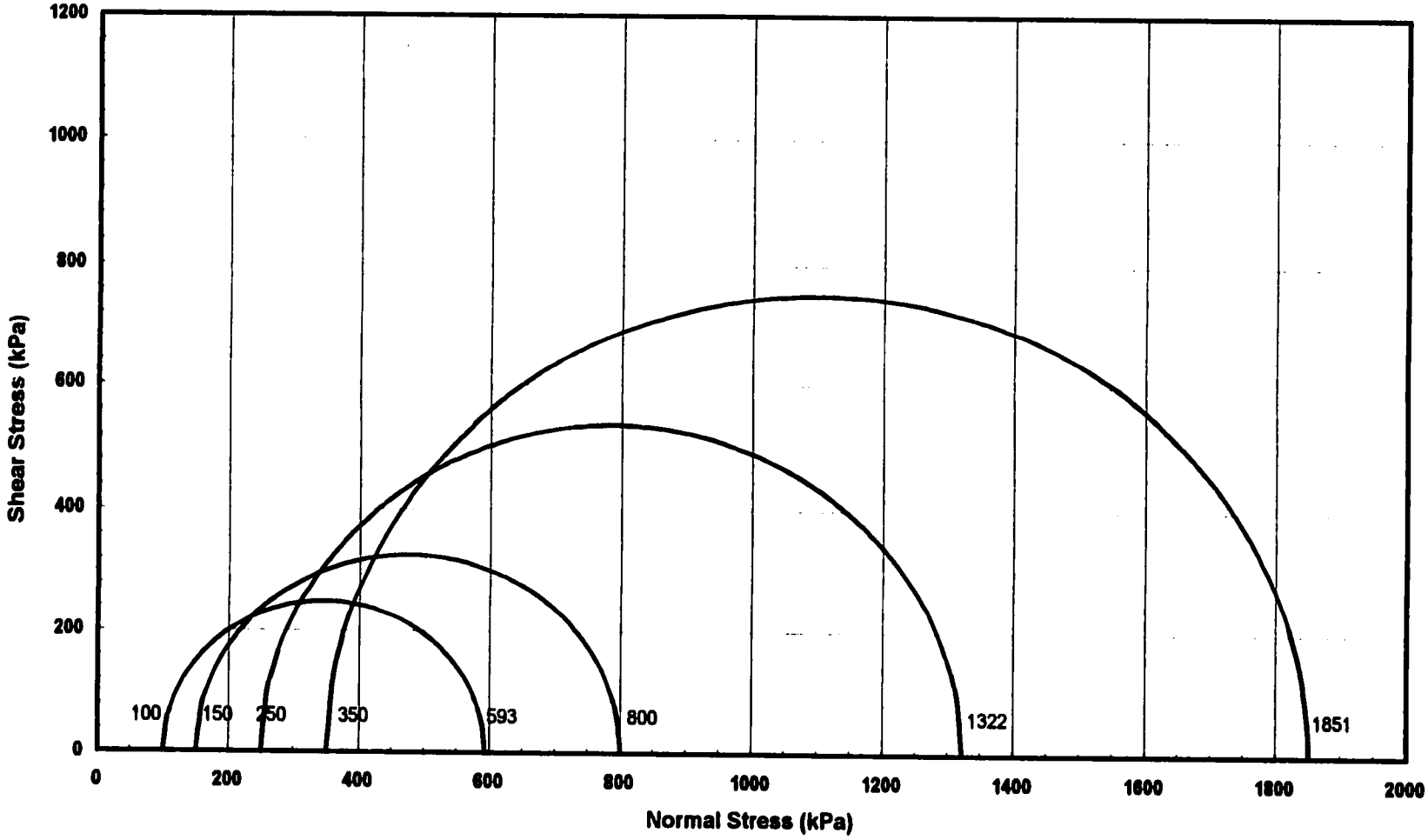

FIG. 6.7 Mohr circles at failure

Sand: Medium Crushed Quartz, Dr = 89%
Confining Pressure = 100 kPa, 150 kPa, 250 kPa, and 350 kPa

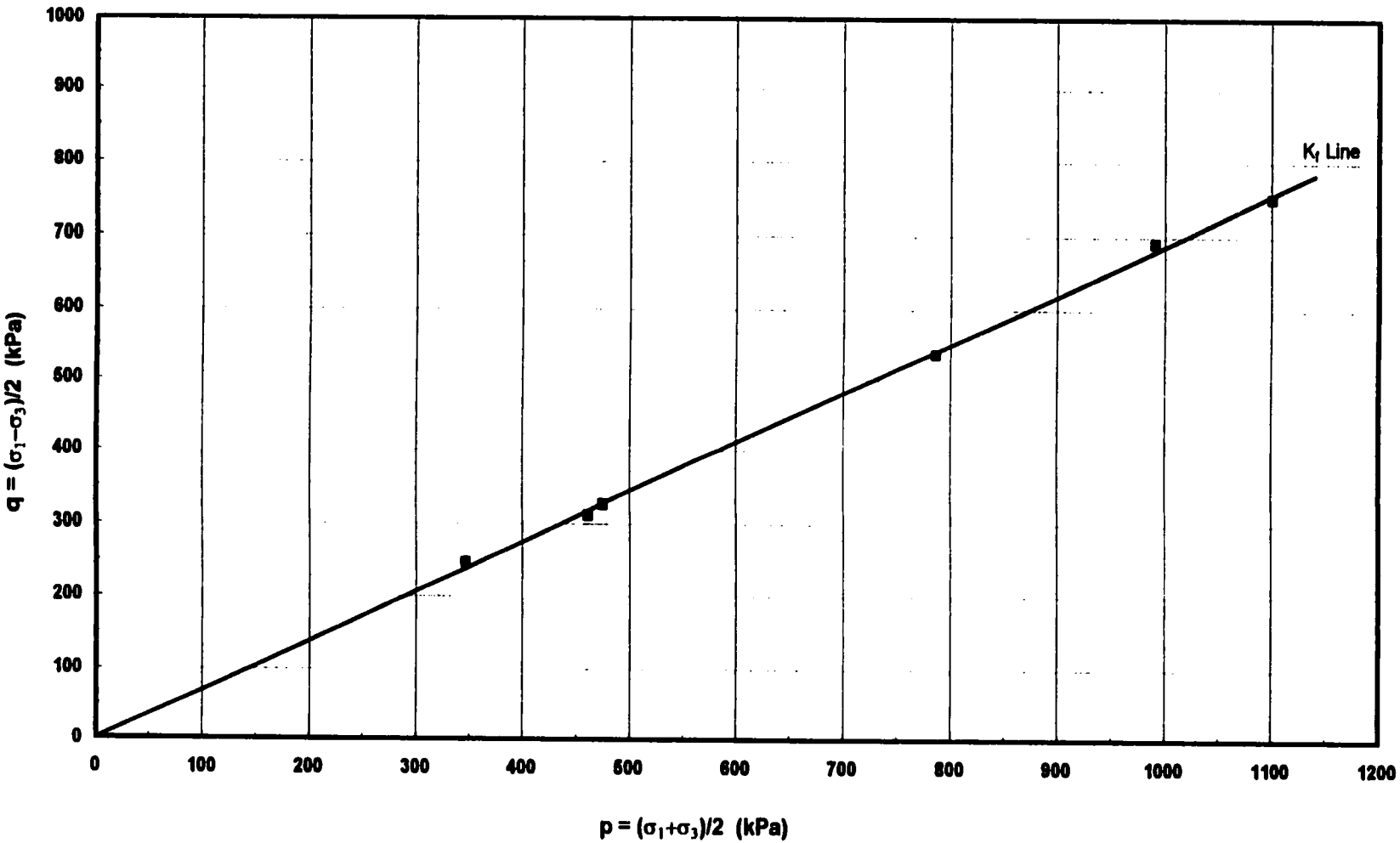

FIG. 6.8 p-q plot and k_f line

Sand: Medium Crushed Quartz, Dr = 89%
Confining Pressure = 100 kPa, 150 kPa, 250 kPa, and 350 kPa

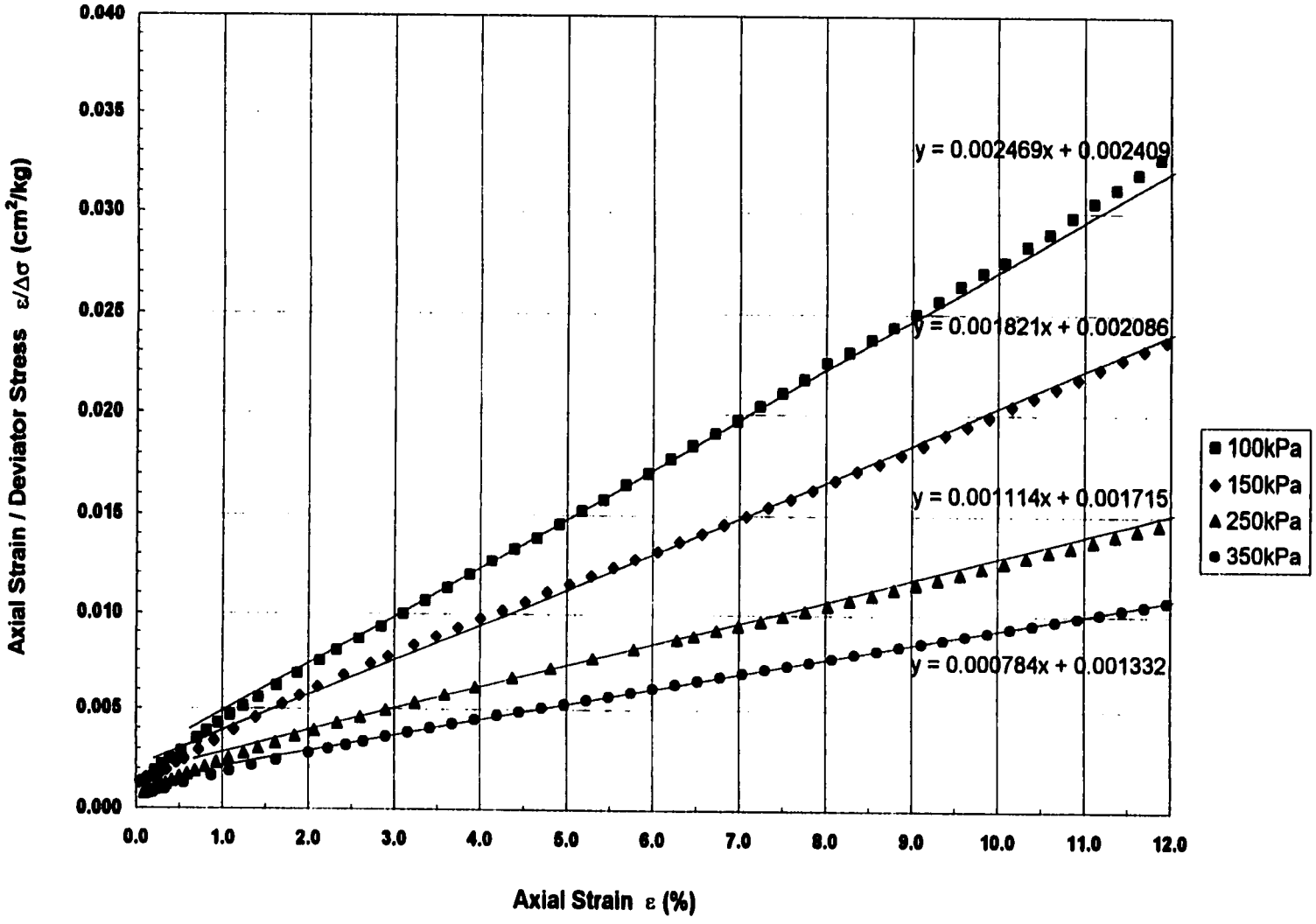

FIG. 6.9 Transformed hyperbolic stress-strain curve

Sand: Medium Size Crushed Quartz, D_r = 45.8%

Confining Pressure = 100 kPa, 150 kPa, 250 kPa, and 350 kPa

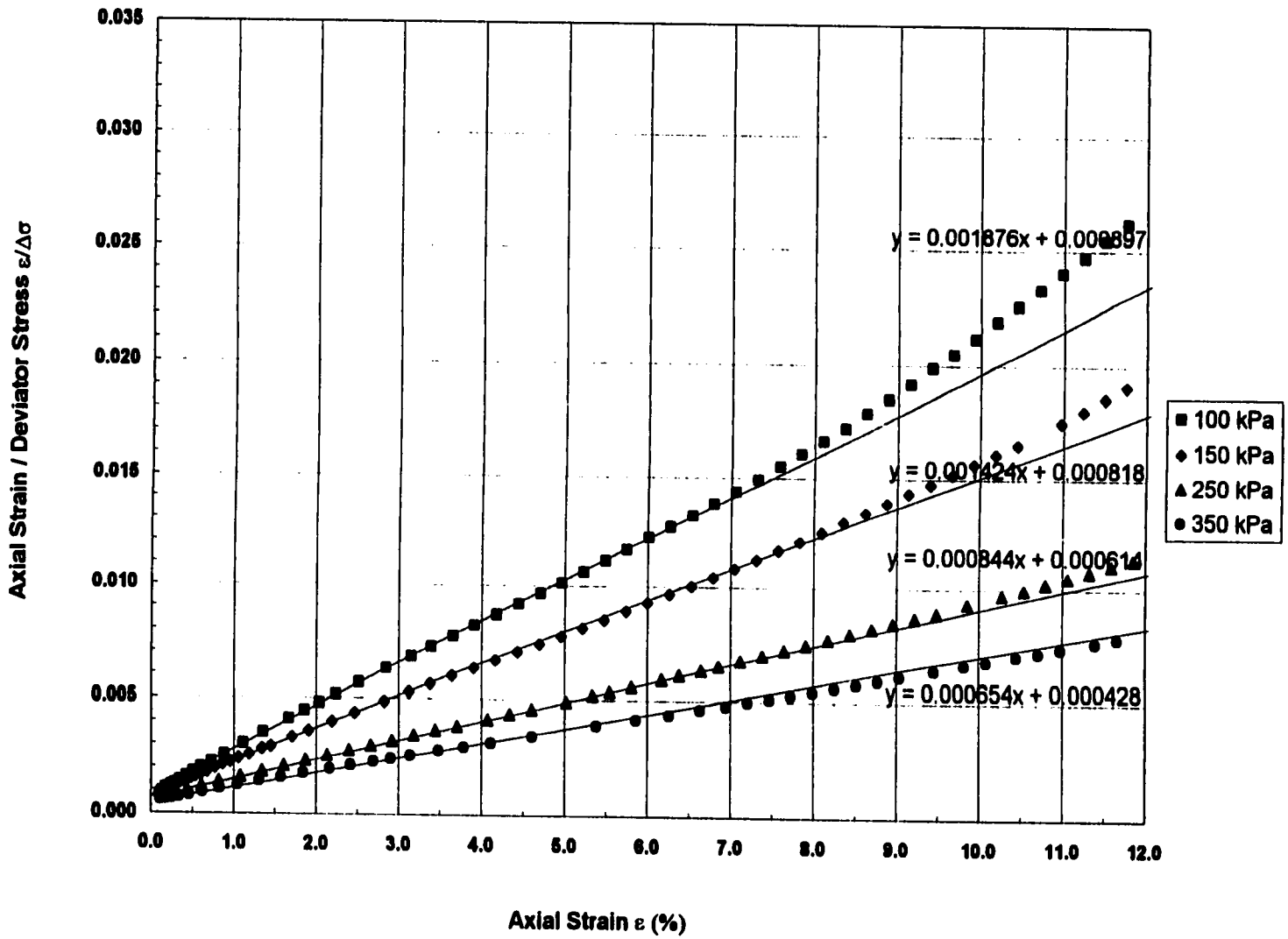

FIG. 6.10 Transformed hyperbolic stress-strain curve

Sand: Medium Crushed Quartz, Dr = 89%

Confining Pressure = 100 kPa, 150 kPa, 250 kPa, and 350 kPa

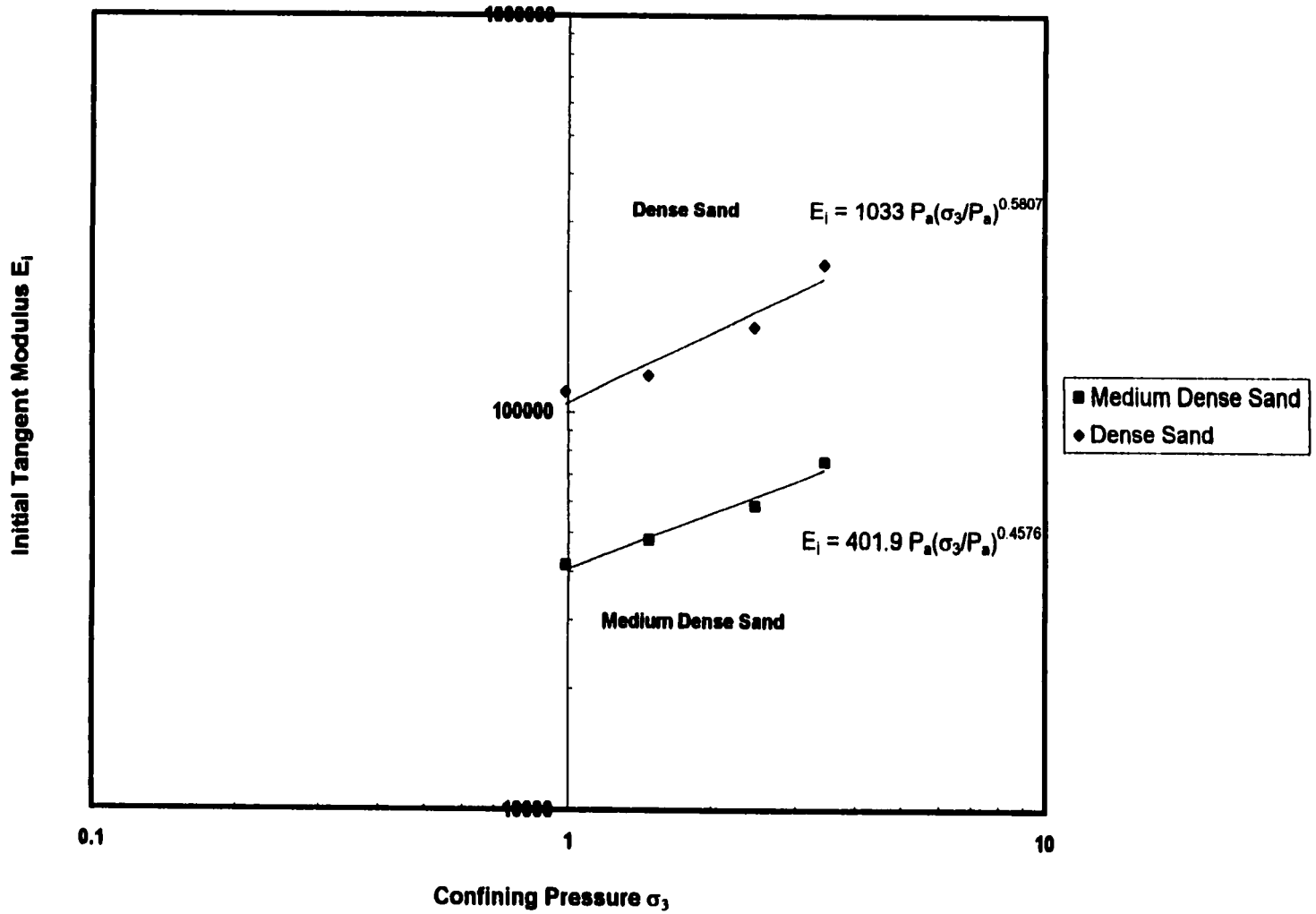

FIG. 6. 11 Variations of E_i with σ_3

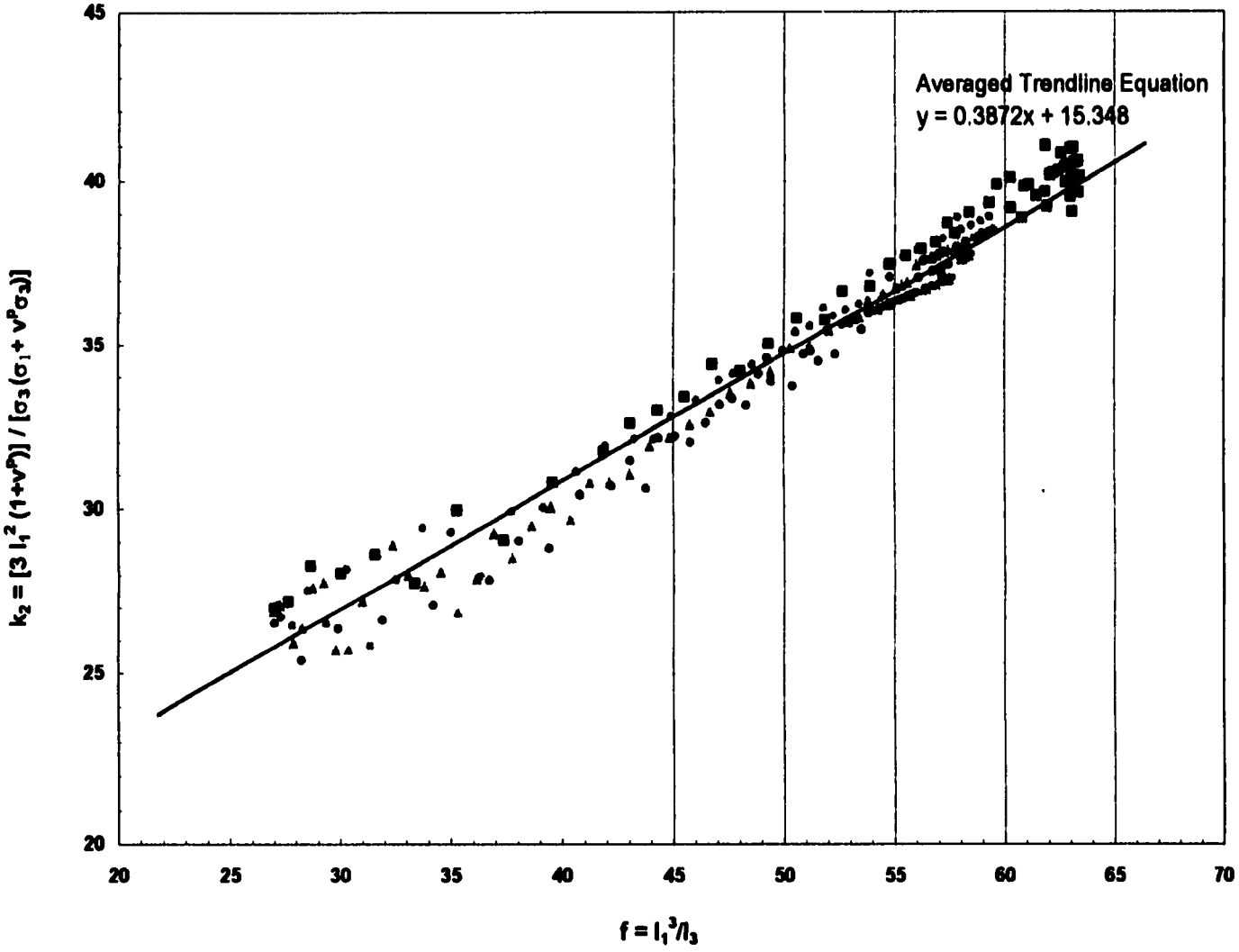

FIG. 6. 12 Variation of k_2 with stress level f for medium dense sand

Confining pressure σ_3 = 100 kPa, 150 kPa, 250 kPa, 350 kPa

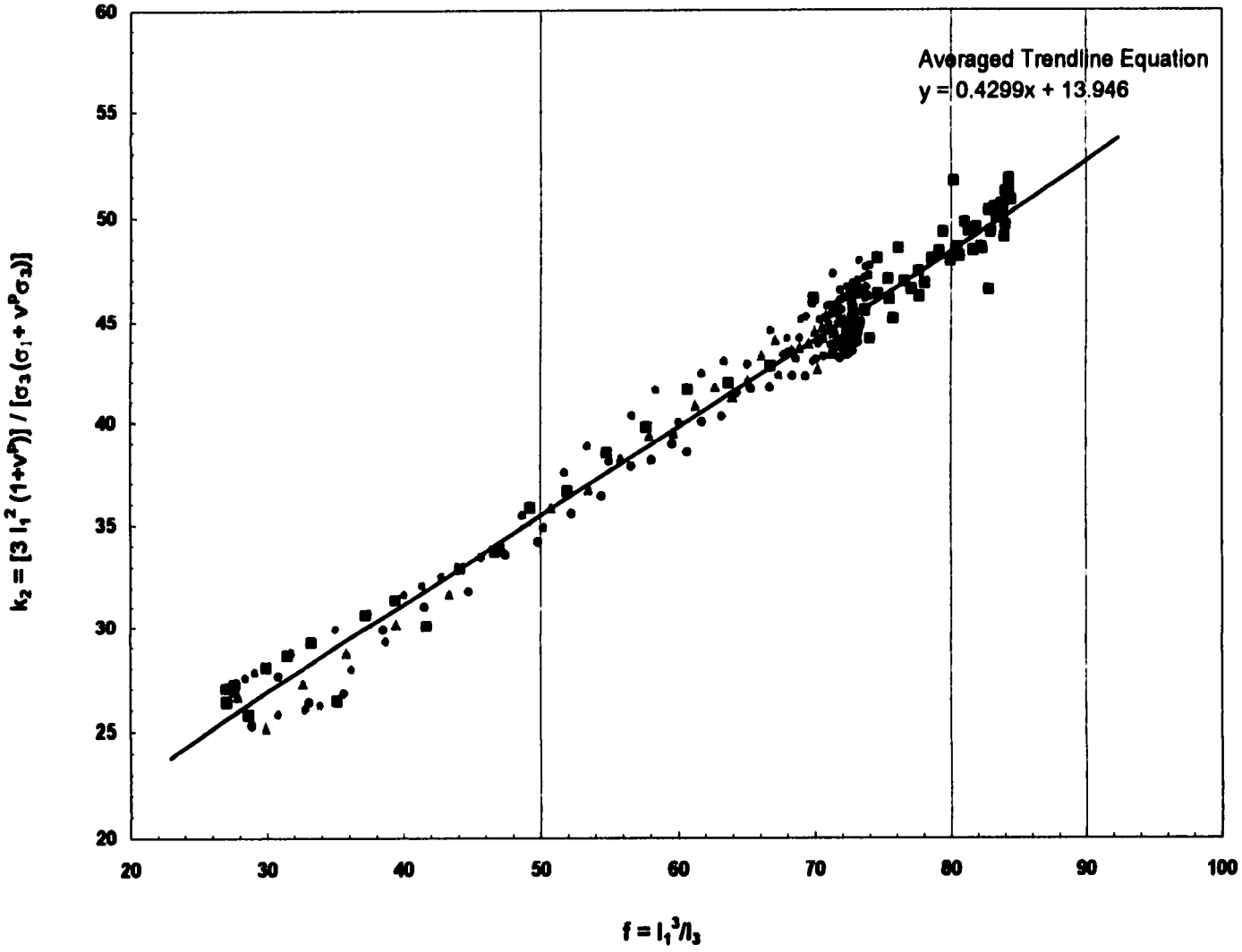

FIG. 6. 13 Variation of k_2 with stress level f for dense sand

Confining pressure σ_3 = 100 kPa, 150 kPa, 250 kPa, 350 kPa

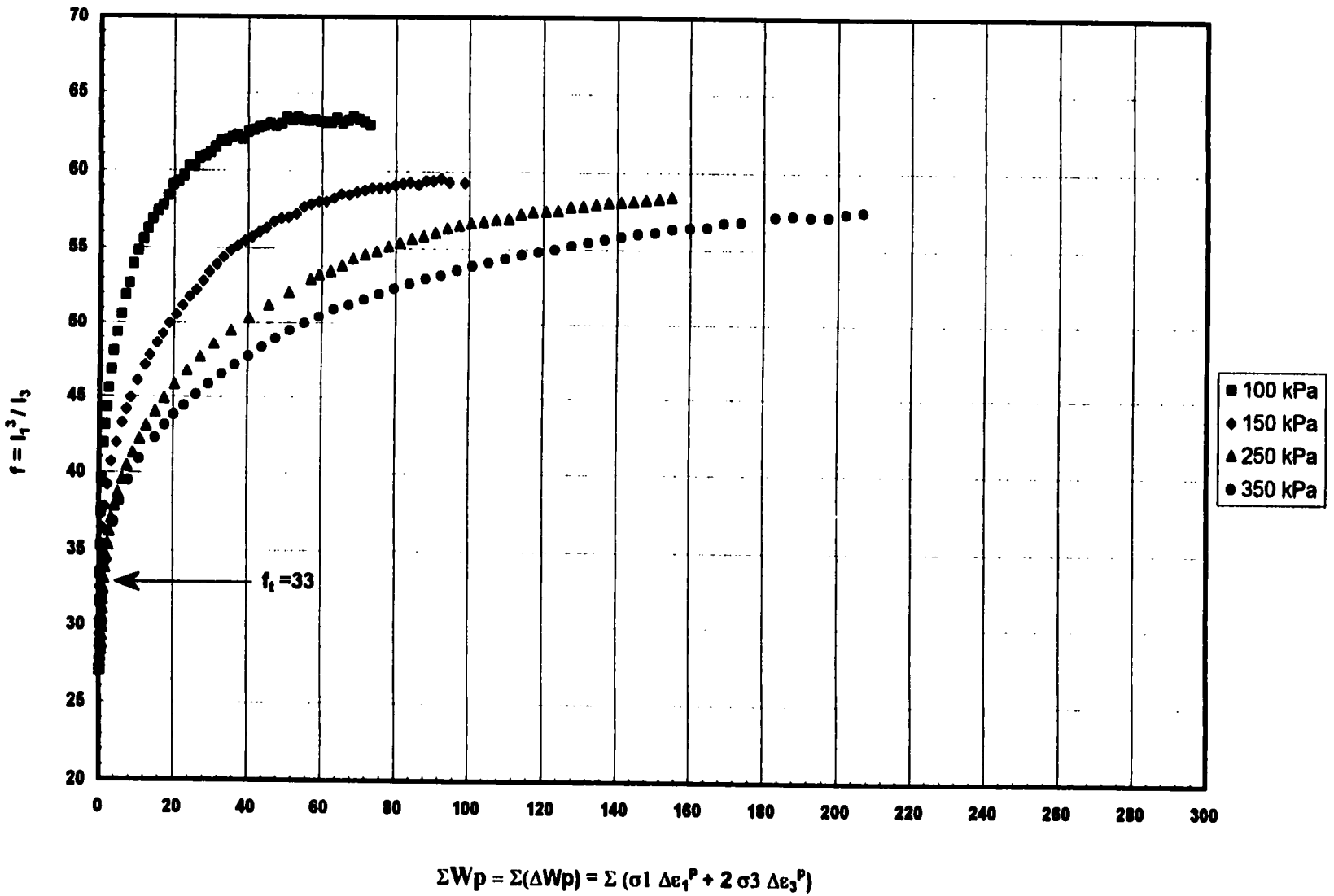

FIG. 6. 14 Plastic work ΣW_p versus stress level f for medium dense sand

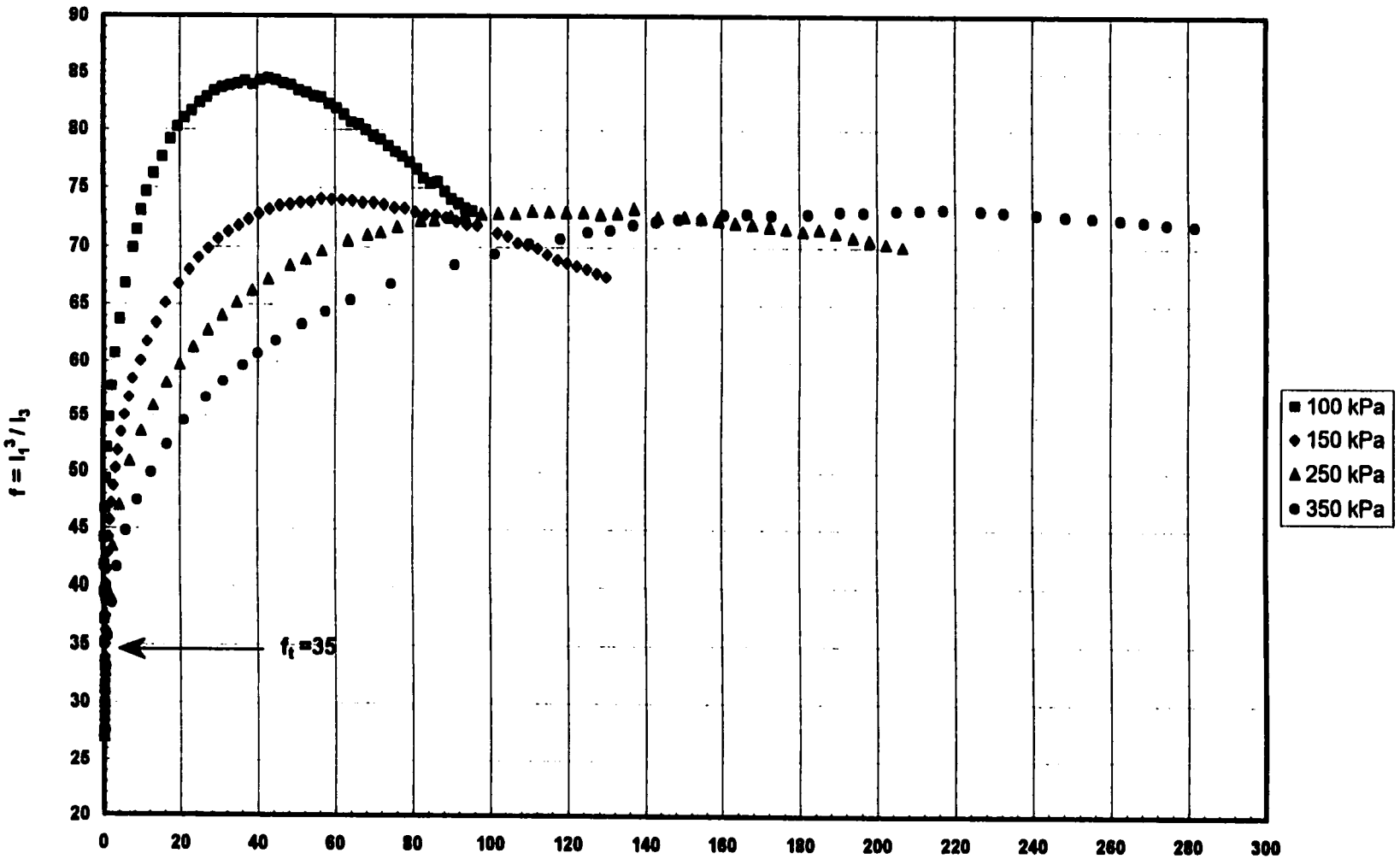

FIG. 6. 15 Plastic work ΣW_p versus stress level f for dense sand

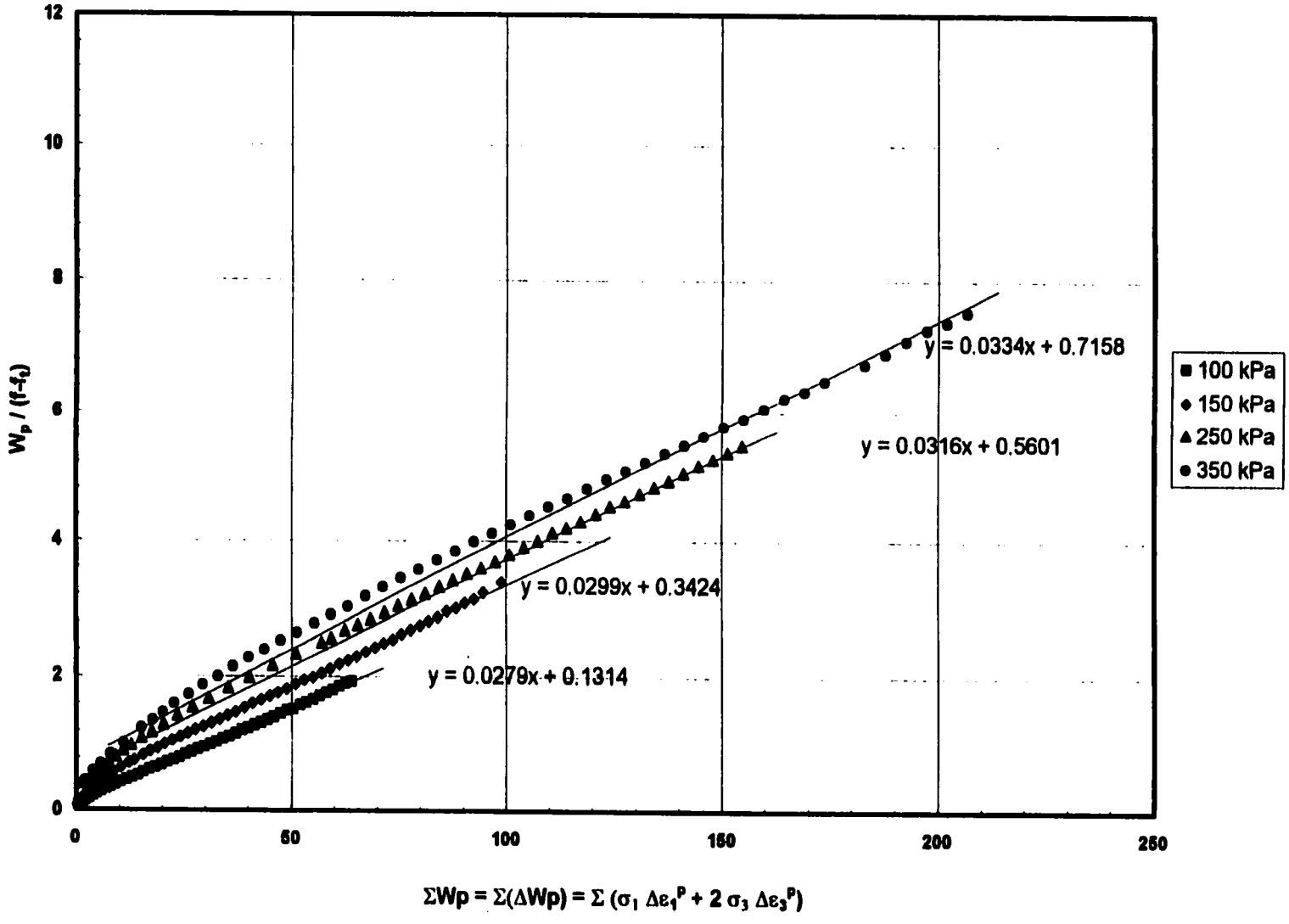

FIG. 6. 16 W_p versus $W_p / (f-f_t)$ for medium dense sand

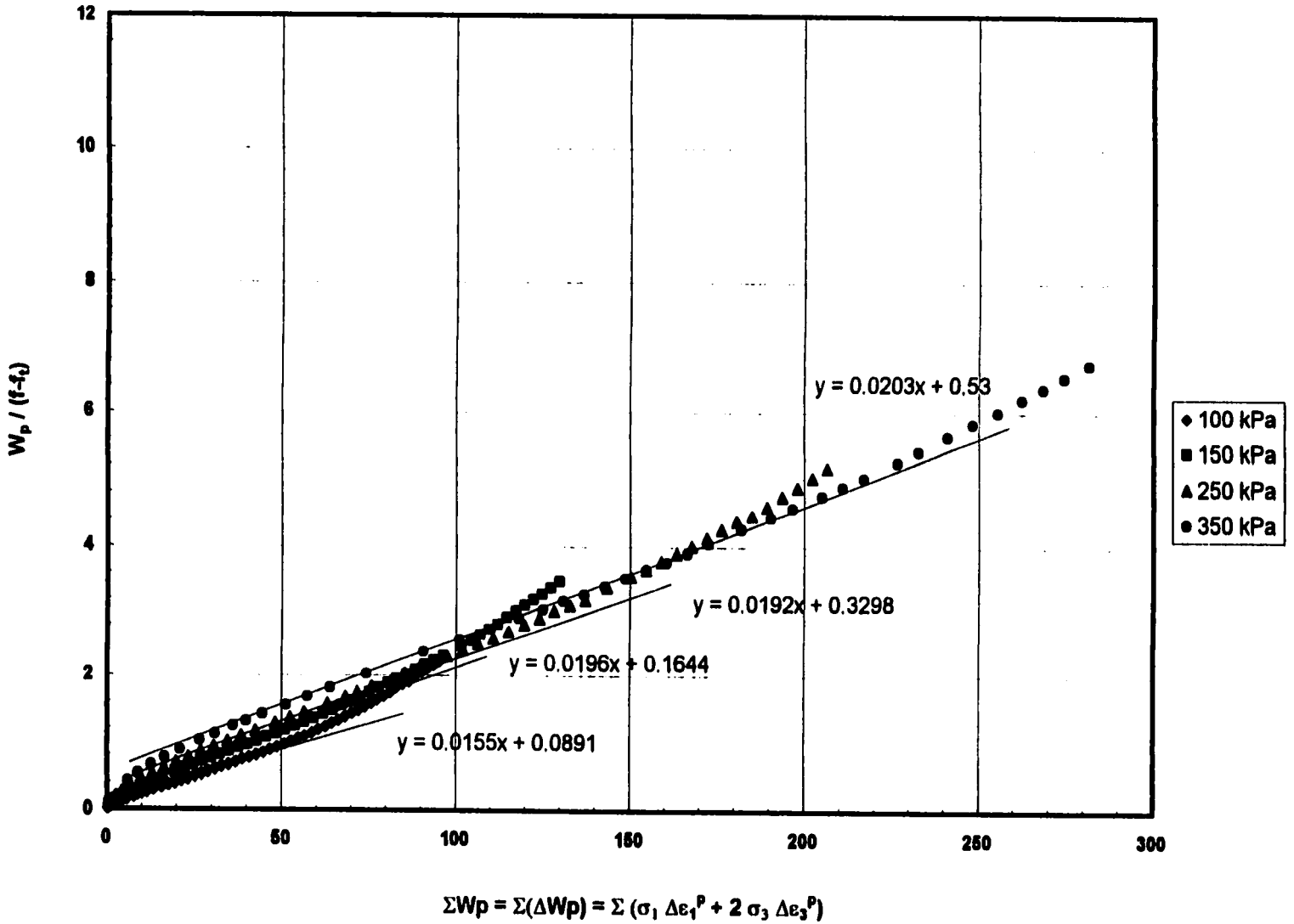

FIG. 6. 17 W_p versus $W_p / (f-f_t)$ for dense sand

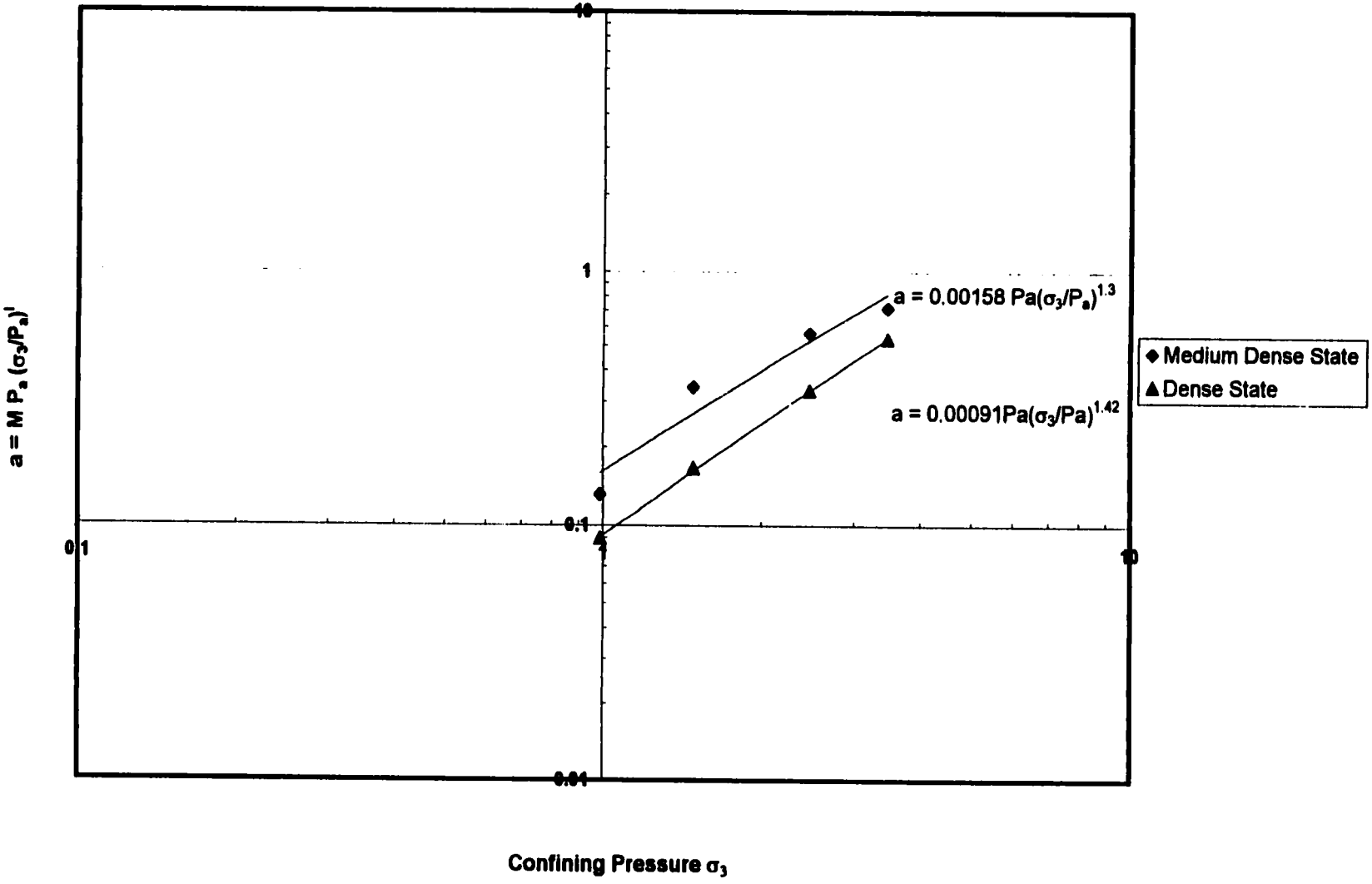

FIG. 6. 18 Variations of a with σ_3

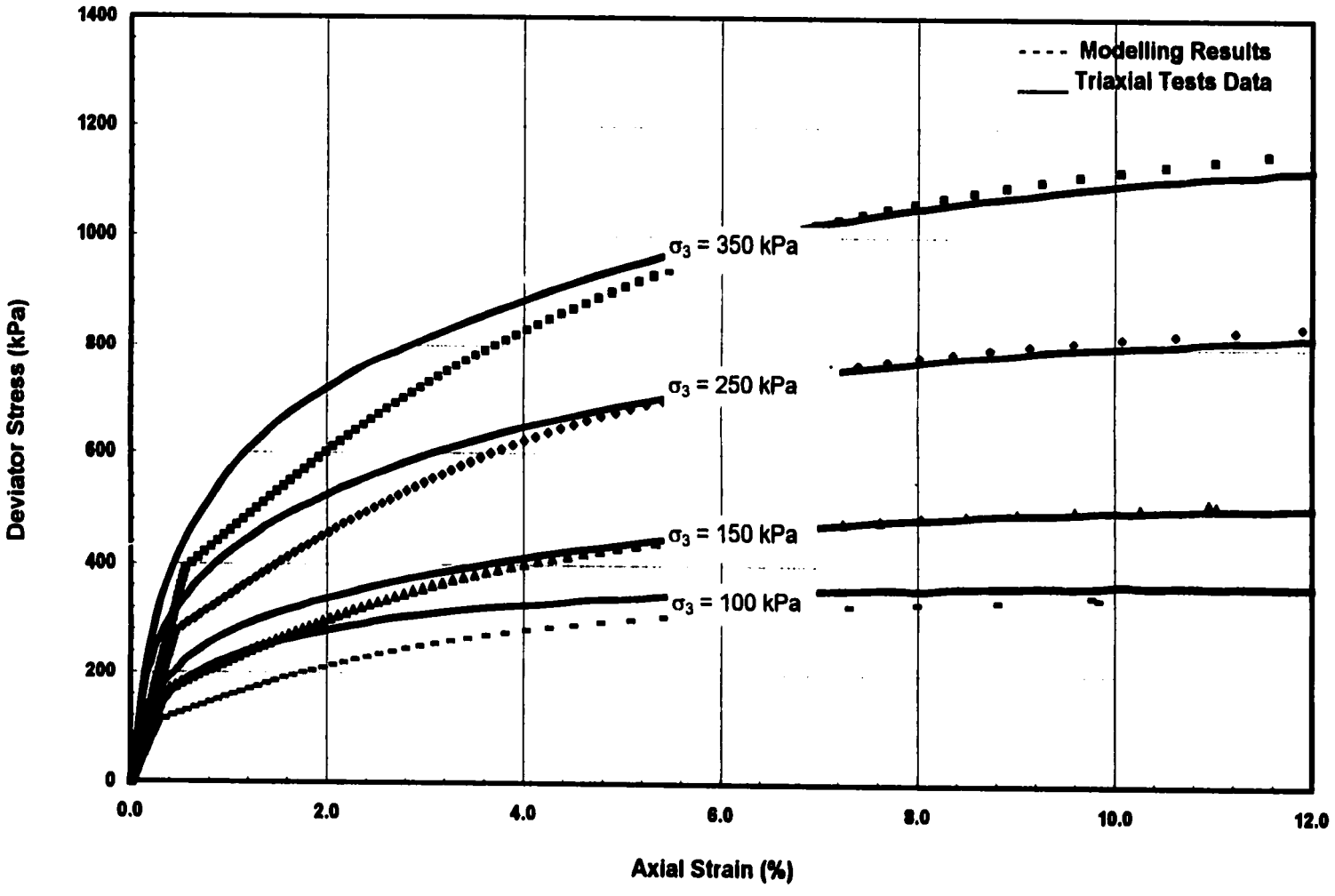

FIG. 6.19 Comparison between modelling result and triaxial test data

Sand: Medium Size Crushed Quartz
Relative Density: 45.8%
Confining Pressure = 100 kPa, 150 kPa, 250 kPa, and 350 kPa

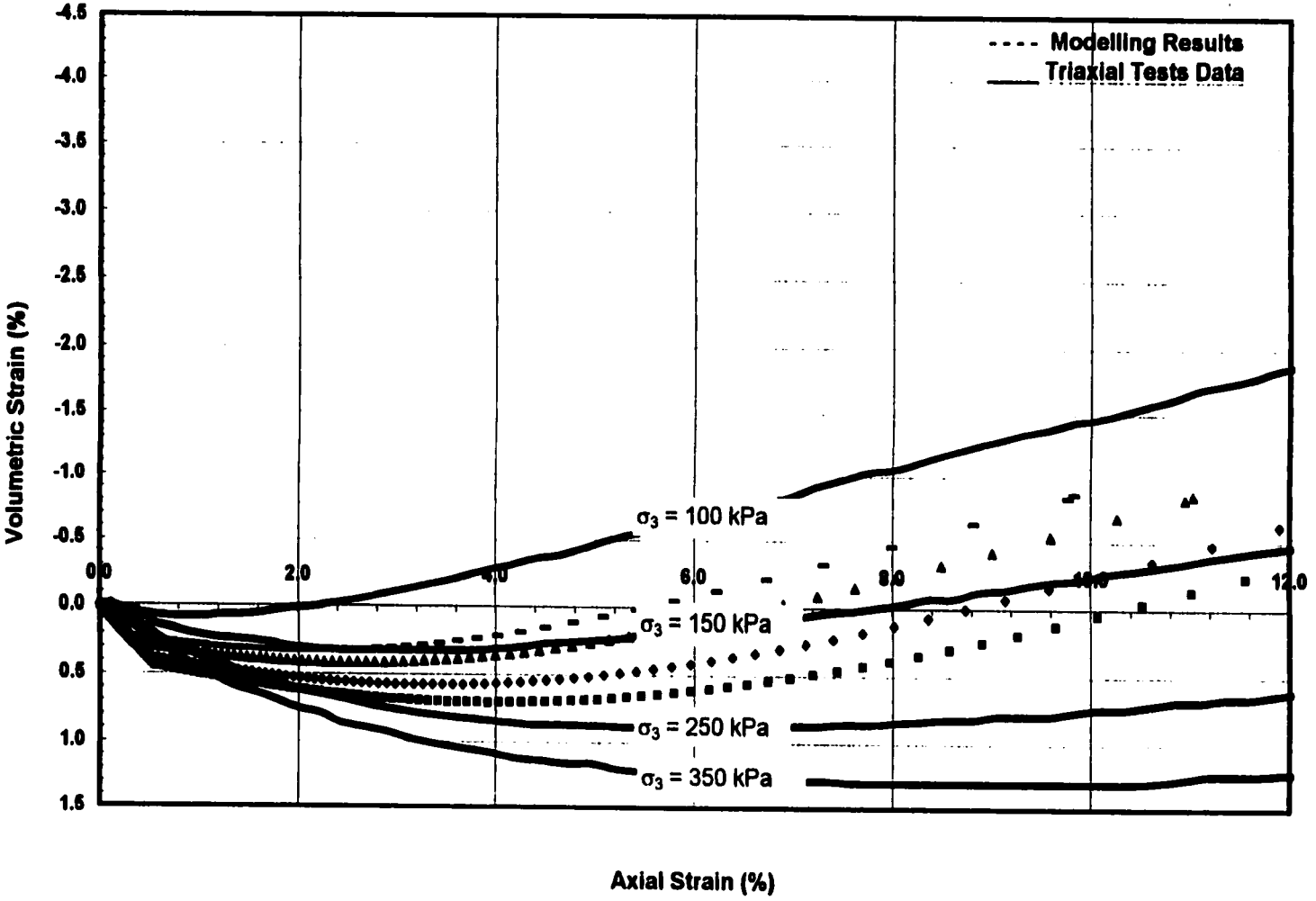

FIG. 6.20 Comparison between modelling result and triaxial test data

Sand: Medium Crushed Quartz
Relative Density: 45.7%
Confining Pressure = 100 kPa, 150 kPa, 250 kPa, and 350 kPa

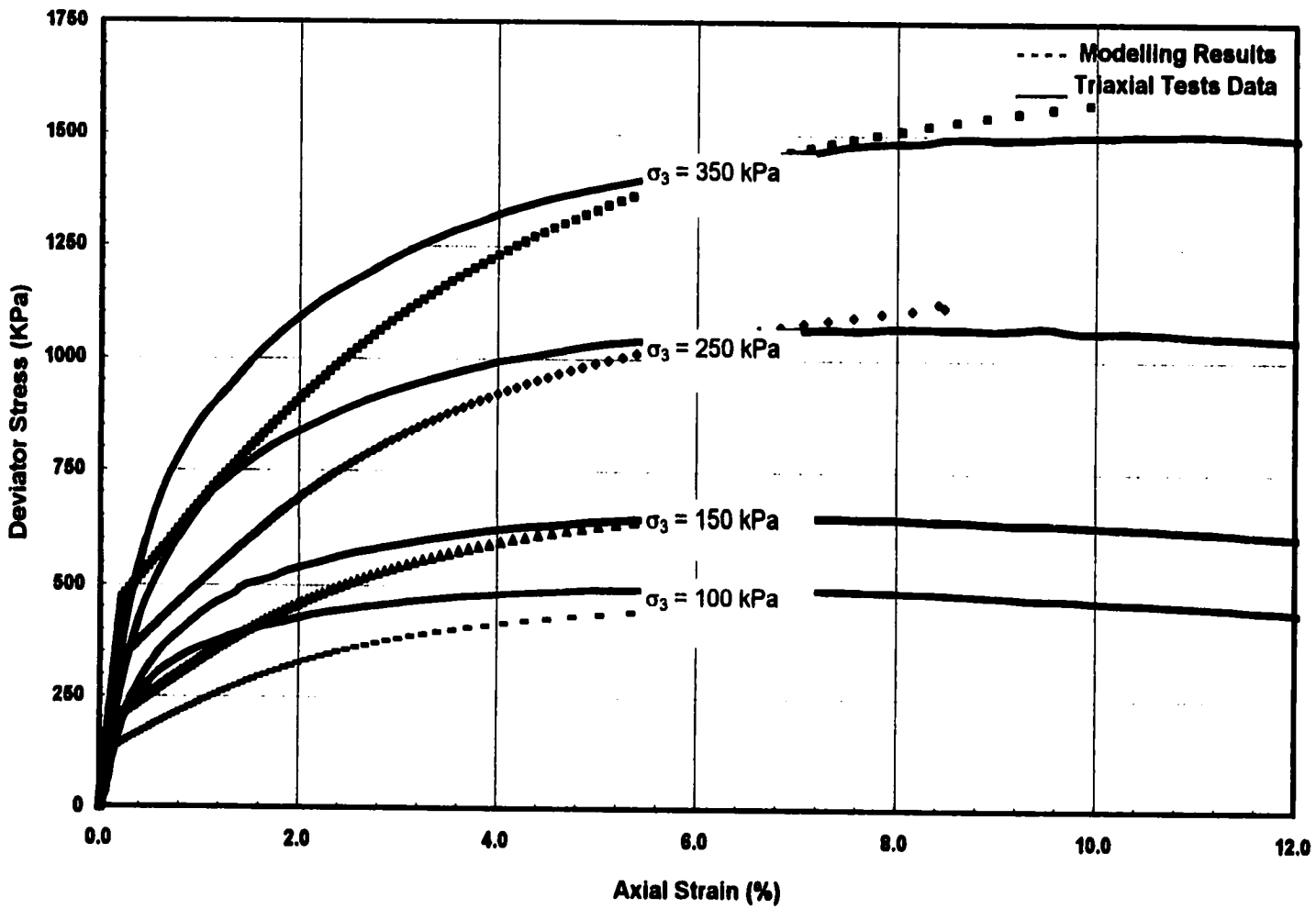

FIG. 6.21 Comparison between modelling result and triaxial test data

Sand: Medium Crushed Quartz
Relative Density: 89%
Confining Pressure = 100 kPa, 150 kPa, 250 kPa, and 350 kPa

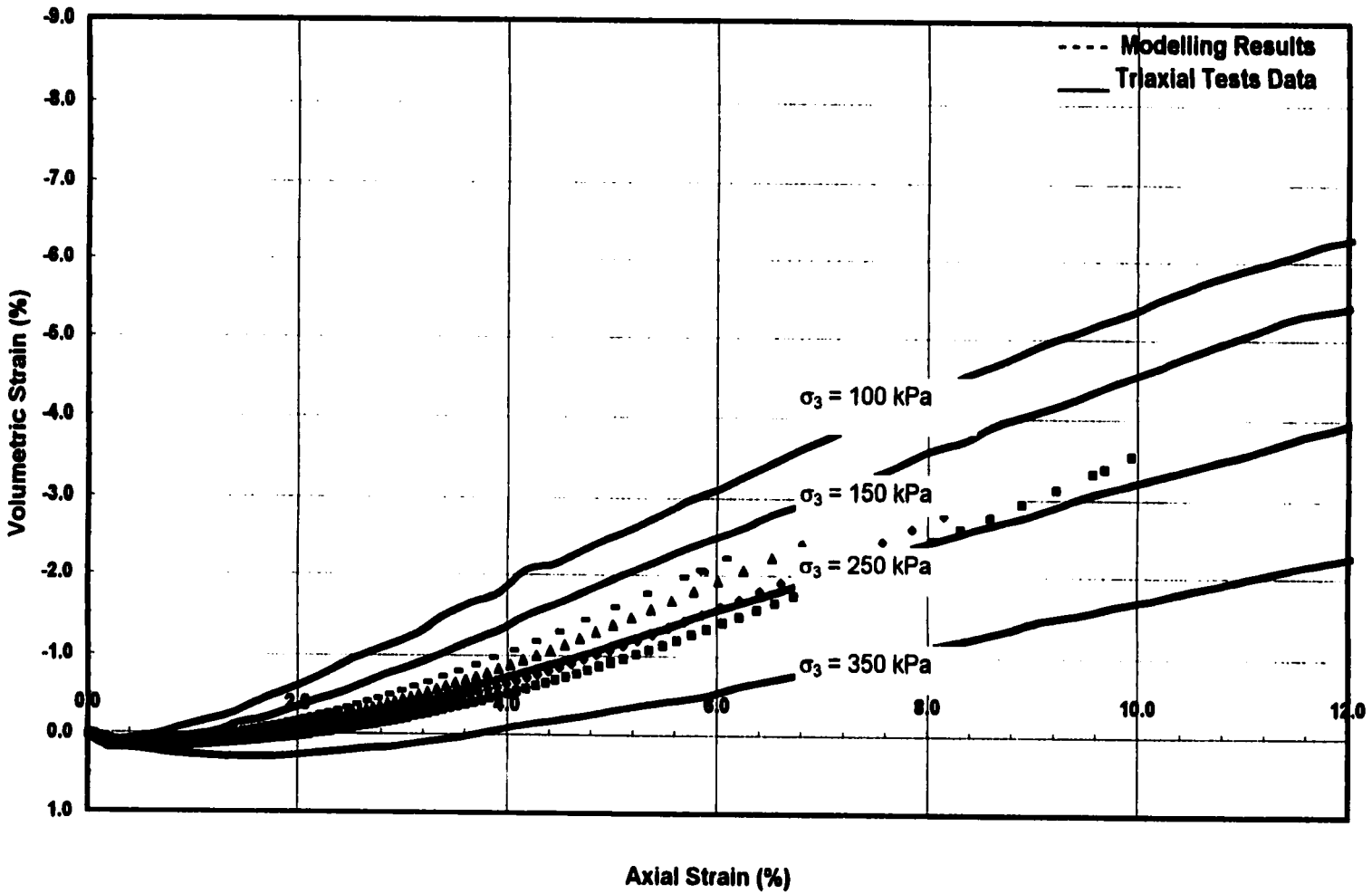

FIG. 6.22 Comparison between modelling result and triaxial test data

Sand: Medium Crushed Quatrz
Relative Density: 89%
Confining Pressure = 100 kPa, 150 kPa, 250 kPa, and 350 kPa

CHAPTER 7

NUMERICAL MODEL FOR SAND-STEEL INTERFACE BEHAVIOUR

In this Chapter, Lade's model is used to simulate the stress-displacement behaviour of interfaces. First the modelling procedure is described. Then the modelling results for the soil mass as well as for the interface layer are presented. Finally the results from the numerical modelling method are compared with the experimental results presented in Chapter 4.

7.1 Introduction

The numerical simulations presented in this chapter were performed for two constant normal stress interface tests. The magnitudes of the normal stress in these tests were 100 kPa and 300 kPa. Variations of maximum interface thickness with two different normal stress σ_z values are summarized in Table 7.1.

In the sand-steel interface tests, sand samples in the soil container are divided into two parts: (1) the soil mass at the upper part, and (2) the interface layer at the lower part, as shown in Fig. 7.1. The total tangential displacement, which is represented by δ in Figure 7.1, is composed of the displacement due to the soil mass deformation, δ_1, the displacement due to the interface deformation δ_2, and the sliding displacement at the interface, δ_3. All three displacement components were measured during the experiments.

Table 7.1: Variations of maximum interface thickness (mm) with normal stress σ_x

	σ_3 = 100 kPa	σ_3 = 300 kPa
Medium Dense Sand	4.5	4
Dense Sand	3	2.5

As explained in Chapter 6, medium crushed quartz sand was used in the triaxial tests, and the parameters of Lade's model were determined from the experimental data. The interface tests were carried out using the same sand at the same relative densities. Therefore, the model parameters can be directly used for the numerical simulation of sand mass behaviour in the interface tests. One of the model parameters is modified for the modeling of the stress-displacement behaviour at the interface layer.

7.2 Numerical Modelling Procedure

7.2.1 Stress Level

The stress level is calculated by using the equation:

$$f = \frac{I_1^3}{I_3} \tag{7-1}$$

where $I_1 = \sigma_x+\sigma_y+\sigma_z$ and $I_3 = \sigma_x \cdot \sigma_y \cdot \sigma_z$

σ_x is the normal stress in the horizontal direction, x

σ_y is the normal stress in the horizontal direction, y

σ_z is the normal stress in the vertical direction, z

(1) Normal Stress in Vertical Direction

In the interface tests, the normal stress in the vertical direction, σ_z, is kept constant at 100 kPa or 300 kPa.

(2) Normal Stress in X-Direction

The initial normal stress in the x-direction, σ_x, is calculated by using the following equation:

$$\sigma_x = K_0 \cdot \sigma_z \qquad (7\text{-}2)$$

where $K_0 = 1\text{-}\sin(\phi)$ (Jaky, 1948)

ϕ = friction angle of sand mass

$\phi = 38°$ for medium dense state Dr = 45.7%

$\phi = 43°$ for dense state Dr = 88%

The term "initial" is used here to represent the state of the sample before the shearing of the interface is initiated. In the numerical model, it is assumed that σ_x remains at its initial value during shearing.

(3) Normal Stress in Y-Direction

In the y-direction, the normal stress, σ_y, is calculated by using the Mohr circles shown in Fig.7.2. The initial value of σ_y is calculated by using an equation similar to Equation 7.2. During the interface test, the shear stress τ_{zy} increases from zero to the peak value τ_f. In Fig.7.2, Mohr circles develop from the initial condition to the failure state. The states of stress between the initial and failure states are not known. By using the Mohr circle corresponding to failure, τ_f and σ_{yf} are calculated.

For the soil mass which resides in the upper part of the soil container, the peak shear stress acting on the horizontal plane and the corresponding σ_y can be calculated from:

$$\tau_f = \sigma_z \cdot \tan(\phi) \qquad (7\text{-}3)$$

$$\sigma_{yf} = \sigma_z + 2 \cdot \frac{\tau_f}{\tan(90^0 - \phi)} \qquad (7\text{-}4)$$

where τ_f = maximum shear stress for the soil mass

σ_{yf} = maximum normal stress in the y-direction for the soil mass

For the interface layer, which resides on the sand-steel contact surface, the maximum value of τ_f is determined from the interface tests, so the maximum normal stress σ_{yf} is calculated by:

$$\sigma_{yf} = \sigma_z + 2 \cdot \frac{\tau_f}{\tan\left[90^0 - \arctan\left(\frac{\tau_f}{\sigma_z}\right) \right]} \qquad (7\text{-}5)$$

It is assumed that, accompanied by the increment of shear stress, σ_y increases linearly from the value of $\sigma_y = K_0 \cdot \sigma_z$ to the maximum value σ_{yf}. During the modelling, the following equation is used for calculating σ_y:

$$\sigma_y = \sigma_z \cdot K_0 + \left(\frac{\sigma_{yf} - \sigma_z K_0}{\tau_f} \right) \cdot \tau \qquad (7\text{–}6)$$

It should be noted that τ_f has a different value in the soil mass than that in the interface layer.

(4) k_1 Value at Failure

k_1 is calculated as the f value at failure:

$$k_1 = \frac{I_1^3}{I_3} = \frac{(\sigma_x + \sigma_{yf} + \sigma_z)^3}{\sigma_x \cdot \sigma_{yf} \cdot \sigma_z} \qquad (7\text{-}7)$$

The Equations 7-4 and 7-5 represents the σ_{yf} values for the soil mass and for the interface layer respectively. Therefore the value of the parameter k_1 for the soil mass is different from the value of k_1 for the interface.

7.2.2 Elastic Strain Increments

The components of elastic strain increments are calculated by:

$$\delta\varepsilon_x^e = -\nu \cdot \frac{\delta\sigma_y}{E_i}$$

$$\delta\varepsilon_y^e = \frac{\delta\sigma_y}{E_i} \qquad (7\text{-}8)$$

$$\delta\varepsilon_{xy}^e = \frac{\delta\tau_{xy}}{2 \cdot G}$$

where E_i is the elastic modulus, $E_i = K_{ur} \cdot p_a \cdot (\frac{\sigma_3}{p_a})^n$

G is the shear modulus, $G = \frac{E_i}{2 \cdot (1+\nu)}$

ν is the Poisson's ratio. The values of ν and K_{ur} are listed in Table 6.9.

7.2.3 Plastic Strain Increments

(1) Plastic Work Increment

The increment in plastic work is calculated from:

$$\delta W_p = \frac{a \cdot df}{\left(1 - r_f \frac{f - f_t}{k_1 - f_t}\right)^2} \qquad (7\text{-}9)$$

where a is calculated as: $a = M\ Pa\ (\frac{\sigma_3}{p_a})^l$

df is the difference in f between two successive stress states

the values for the parameters r_f, k_1, l, and f_t are already known (listed in Table 6.9)

(2) Plastic Strain Increments

The variation of k_2 is calculated by:

$$k_2 = A\ f + 27\ (1\text{-}A) \qquad (7\text{-}10)$$

where the value of A is given in Table 6.9.

The plastic strain increments are calculated by using the plastic stress-strain relationship described as follows:

$$\begin{Bmatrix} \delta\varepsilon_x^{\,p} \\ \delta\varepsilon_y^{\,p} \\ \delta\varepsilon_{xy}^{\,p} \end{Bmatrix} = \frac{K_2}{3(I_1^3 - K_2 \cdot I_3)} \cdot \delta Wp \cdot \begin{Bmatrix} \frac{3}{K_2} \cdot I_1^2 - \sigma_y \cdot \sigma_z \\ \frac{3}{K_2} \cdot I_1^2 - \sigma_z \cdot \sigma_x \\ \sigma_z \cdot \tau_{xy} \end{Bmatrix} \qquad (7\text{–}11)$$

7.2.4 Total Strain

The components of the total strain increments are calculated by:

$$\begin{aligned} \delta\varepsilon_x^{\,t} &= \delta\varepsilon_x^{\,e} + \delta\varepsilon_x^{\,p} \\ \delta\varepsilon_y^{\,t} &= \delta\varepsilon_y^{\,e} + \delta\varepsilon_y^{\,p} \\ \delta\varepsilon_{xy}^{\,t} &= \delta\varepsilon_{xy}^{\,e} + \delta\varepsilon_{xy}^{\,p} \end{aligned} \qquad (7\text{-}12)$$

The components of the total strains are the accumulation of the total strain increments.

$$\begin{aligned} \varepsilon_x &= \Sigma\, \delta\varepsilon_x^{\,t} \\ \varepsilon_y &= \Sigma\, \delta\varepsilon_y^{\,t} \\ \varepsilon_{xy} &= \Sigma\, \delta\varepsilon_{xy}^{\,t} \end{aligned} \qquad (7\text{-}13)$$

7.3 Modelling Results

A Fortran program is written for the calculation of soil mass behaviour based on Lade's model. In the program, shear stress is increased at small intervals, which brings the sand-steel interface plus the soil mass system to continuously increased stress levels, until the shear stress reaches the maximum (peak) value, which is obtained from the interface tests.

For the soil mass located at the upper part of the soil container, the parameters for Lade's model have already been determined in Chapter 6. They are used directly in the Fortran program for calculations.

For the modelling of the interface layer, all the parameters of Lade's model are also directly used in the Fortran program, except for the parameter k_1. The value of the parameter k_1 for the interface layer is calculated by using Equation 7-7.

The calculations give the shear strains. Multiplying them by the thickness of the soil mass, or the thickness of the interface, the displacements are obtained.

Figure 7.3 presents the modelling results of the stress-displacement relationships. The horizontal axis represents the displacement due to the deformation of the sand mass and also the interface layer. The measured results are also presented here for comparison purposes. When the shear stress is small, not much displacement is developed. With increasing shear stress, the tangential displacement becomes large.

Even though the modelling results generally agree very well with the measured data for samples with low relative densities, there exist some discrepancies when the relative density of soil is high. By using Lade's model, strain softening could not be modelled. This is apparent for sand samples with high relative density. The reason for this is because Lade's model is developed on the basis of the hyperbolic theory. The non-linear stress-strain curves always approach an asymptote at peak stress level without softening after the peak.

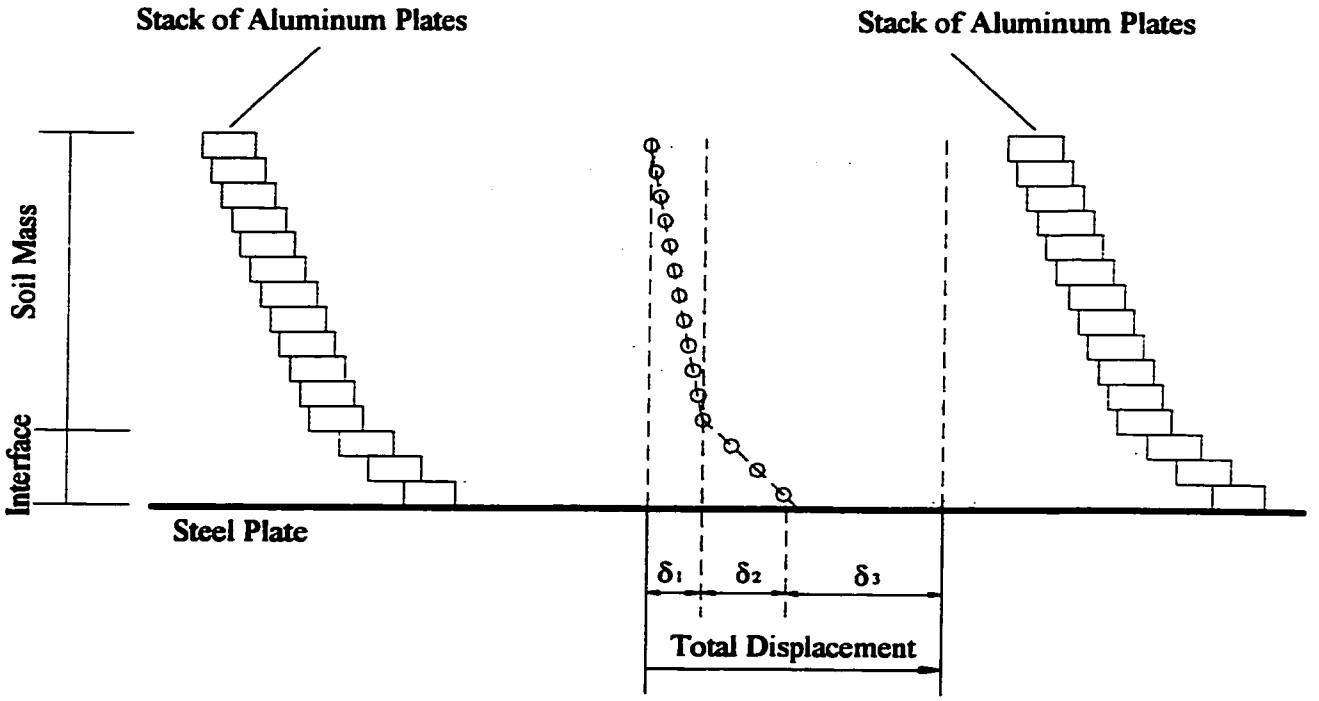

FIG. 7.1 Idealized sand-steel interface system

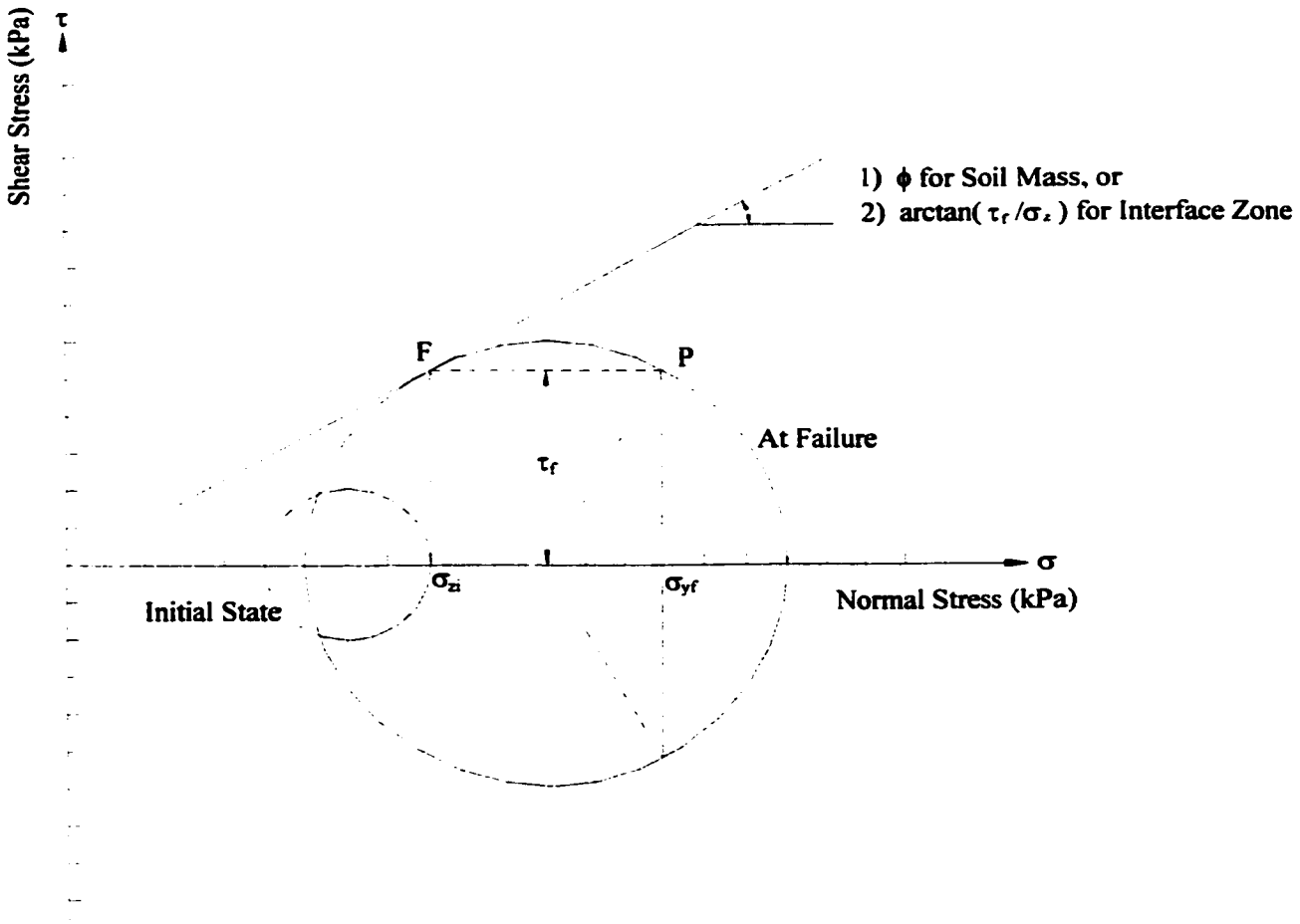

FIG. 7.2 Mohr diagram

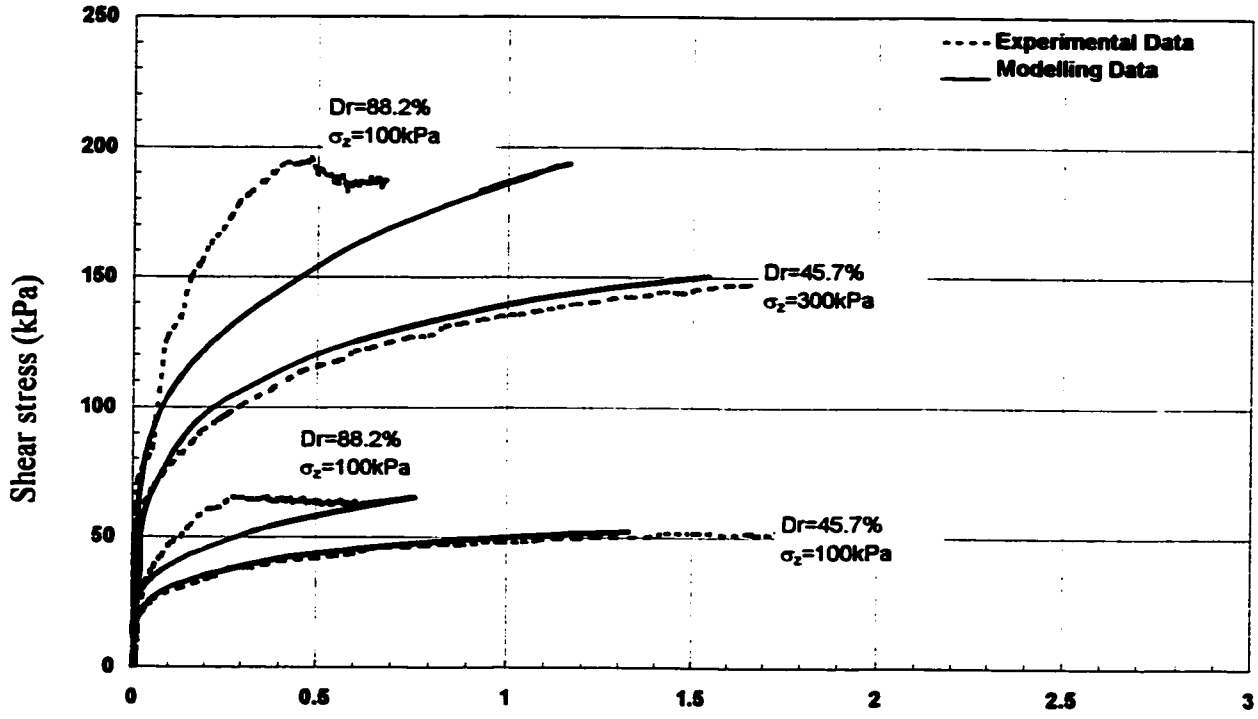

FIG. 7.3 Comparison between the model predictions of shear stress vs displacement and the experimental results

Sand: Medium crushed quartz, Dr = 88.2% and 45.7%
Normal stress σ_z= 100 kPa and 300 kPa

CHAPTER 8
SUMMARY, CONCLUSIONS, AND RECOMMENDATIONS FOR FURTHER RESEARCH

8.1 Summary

In an interface test, the soil sample consists of two parts: 1) the soil mass and 2) the interface layer. The main objective of this research was to determine the stress-deformation behaviour of soil in the interface layer. The existing interface apparatus, C3DSSI, was set up to measure the tangential displacement due to the deformation of the sand sample, which includes the soil mass and the interface layer, and the displacement due to sliding at the contact surface. It was not possible to observe separately the soil deformations in the sand mass and in the interface zone with the existing apparatus without modifications.

In order to achieve the described objective, some modifications were made on the C3DSSI apparatus. A digital camera was used to take photographs of the movements of the stack of plates, which made up the soil container. The photographs were then digitized to plot a series of deformation curves. With this method, satisfactory observations were made for the deformations of the sand in the sand mass and in the interface zone. The thickness of the interface layer was also determined.

Lade's model was used for the numerical simulation of the sand-steel interface behaviour. A computer program containing Lade's model was written in Fortran language. By conducting a series of triaxial compression tests, the values of parameters for Lade's model were found. The simulation of the sand-steel interface behaviour consisted of two sections: 1) the

simulation of the behaviour of sand mass, and 2) the simulation of the sand behaviour in the interface zone. Comparisons were made between the results of the numerical modelling and the experimental results.

8.2 Conclusions

Based on the results of the experimental investigation and the numerical modelling of the sand-steel interface behaviour, the following conclusions are drawn:

1) The stress-strain behaviour of soil in the interface layer is different than the behaviour of soil in the soil mass.

2) Strain localization takes place in the interface layer.

3) The thickness of the interface layer increases from zero to its maximum value as the shear stress increases.

4) Digital photography and subsequent processing is a simple but effective method to observe the behaviour of soil in the interface tests.

5) Lade's work hardening model can be used with moderate success for the simulation of interface behaviour. The model, however, has some limitations. The strain softening cannot be simulated. In addition, sample dilation or compression is not predicted with a reasonable accuracy.

8.3 Recommendations for Future Research

Based on the literature review and the present research, the following recommendations are made for future research.

1) Future tests should include measurements of normal stresses acting at the sample boundaries in the x- and y-directions. These measurements will provide continuous information about the stress state in the sample.

2) Measurements of translations and rotations of sand grains in the interface layers would produce necessary information for the development of more advanced models.

3) A soil model, different than Lade's work hardening model, should be used to simulate the strain softening behaviour at interfaces.

REFERENCES

Atkinson, J. H. (1993). An introduction to the mechanics of soils and foundations through critical state soil mechanics. McGraw–Hill international series in civil engineering.

Andrawes, K. Z. and Butterfield, R. (1973). The measurement of planar displacement of sand grains. Geotechnique, Vol. 23, No. 4, 571-576

Been, K. and Jefferies, M. G., Hachey, J. (1991). The critical state of sands. Geotechnique, Vol. 41, No. 3, 365-381

Boulon, M. and Plytas, C. (1986). Soil structure directionally dependent interface constitutive equations - Application to the prediction of shaft friction along piles. Proceedings, 2nd International Symposium on Numerical Models in Geomechnics, 43-54

Bowles, J. E. (1992). Engineering properties of soils and their measurement. 4th edition. McGraw–Hill international series in civil engineering.

Britto, A. M. and Gunn, M. J. (1987). Critical state soil mechanics via finite elements. Ellis Horwood Series in Civil Engineering.

Brumund, W. F. and Leonards, G. A. (1973). Experimental study of static and dynamic friction between sand and typical construction materials. Journal of Testing and Evaluation. JTEVA, 1 (2), 162-165

Butterfield, R., Harkness, R. M. and Andrawes, K. Z. (1970). A stereo-photogrammetric method for measuring displacement fields. Geotechnique, Vol. 20, No. 3, 308-314

Chang, C.-Y. and Duncan, J. M. (1970). Analysis of soil movement around a deep excavation. Journal of the Soil Mechanics and Foundations Division, ASCE, Vol. 96, No. SM 5, proc. Paper 7512, Sept., 1655-1681

Chu, J., Lo, S. –C. R. and Lee, I. K. (1996). Strain softening and shear band formation of sand in multi-axial testing. Geotechnique, Vol. 46, No. 1, 63-82

De Pater, C. J. and Nieuwenhuis, J. D. (1986). Method for measuring the deformation of a sand surface. Geotechnique, Vol. 36, No.4, 581-585

Desai, C. S. (1980). A general basis for yield, failure and potential functions in plasticity. Int. J. Numer. and Analyt. Methods in Geomech., Vol. 4, 361-375

Desai, C. S. (1981). Behaviour of interfaces between structural and geologic media. Proceedings, International conference on recent advances in geotechnical earthquake engineering and soil dynamics. Vol. 2, 619-638

Desai, C. S., Drumm, E. C. and Zaman, M. M. (1985). Cyclic testing and modeling of interfaces. ASCE, Journal of Geotechnical Engineering. Vol. 111, No. 6, 793-815

Desai, C. S. and Fishman, K. L. (1991). Plasticity-based constitutive model with associated testing for joints. Int. J. Rock Mech. and Min. Sci., 28 (1), 15-26

Desai, C. S. and Siriwardance, H. J. (1984). Constitutive laws for engineering materials with emphasis on Geologic materials. Prentice-Hall, Inc., Engewood Cliffs, NJ 07632

Drucker, D. C., Gibson, R. E. and Hentel, D. J. (1957). Soil mechanics and work-hardening theories of plasticity. J. Soil Mech. Fdn. Engng. Div. Am. Soc. Civ. Engrs 122, 338-346

Duncan, J. M. and Chang, C. Y. (1970). Nonlinear analysis of stress and strain in soils. Journal of the Soil Mechanics and Foundations Division. Proceedings of the American Society of Civil Engineering. 1629-1653

Evgin, E and Fakharian, K. (1993). A three-dimensional apparatus for cyclic testing of interfaces. Proceedings, 46th Annual Canadian Geotechnical Conference, Saskatoon, Canada, 485-493

Fakharian, K. (1996). Three-dimensional monotonic and cyclic behaviour of sand-steel interfaces: testing and modelling. PhD thesis, University of Ottawa, Canada

Fakharian, K. and Evgin, E. (1996). An automated apparatus for three-dimensional monotonic and cyclic testing of interfaces. Geotechnical Testing Journal, GTJODJ, Vol. 19, No. 1, 22-31

Finno, R. J., Harris, W. W., Mooney, M. A. and Viggiani, G. (1997). Shear bands in plane strain compression of loose sand. Geotechnique, Vol. 47, No. 1, 149-165

Fishman, K. L. and Desai, C. S. (1987). A constitutive model for hardening behaviour of rock joints. Desai et al., Editors. Constitutive Laws for Engineering Materials: Theory and Applications. 1043-1050

Fu, T. (1998). Experimental study and discrete element simulation of sand-steel interface behaviour. M. A. Sc. thesis, University of Ottawa, Canada

Ghaboussi, J. and Wilson, E. L. (1973). Finite element for rock joints and interfaces. Journal of the Soil Mechanics and Foundations Division, ASCE, 99 (SM10), 833-848

Huck, P. J., Liber, T., Chiapetta, R. L., Thomopoulos, N. T. and Singh, N. M. (1973). Dynamic response of soil / concrete interfaces at high pressure. Report AFWL-TR-73-264, Air Force Weapons Laboratory, New Mexico

Huck, P. J. and Saxena, S. K. (1981). Response of soil-concrete interface at high pressure. In Proc. of 10th ICSMFE, Sockholm, Sweden

Idriss, I. M., Dobry, R. and Singh, R. D. (1978). Nonlinear behaviour of soft clays during cyclic loading. Journal of the Geotechnical Engineering Division, ASCE, 104 (GT12), 1427-1447

Jaky, J. (1948). Earth pressure in soils. Proceedings of the Second International Conference on Soil Mechanics and Foundation Engineering, Rotterdam, Vol. I, pp. 103-107.

Jefferies, M. G. (1993). Norsand: a simple critical state model for sand. Geotechnique, Vol. 43, No. 1, 91-103

Kishida, H. and Uesugi, M. (1987). Tests of the interface between sand and steel in the simple shear apparatus. Geotechnique, Vol. 37, No. 1, 45-52

Kolar, v. and Nemec, I. (1989). Modeling of soil-structure interaction. Developments in Geotechnical Engineering, Vol. 58

Kulhawy, F.H., Duncan, J. M. and Seed, H. B. (1969). Finite element analysis of stresses and movements in embankments during construction. Report No.TE69-4, College of Engineering, Office of Research Services, University of California, Berkeley, Calif.

Lade, P. V. and Duncan, J. M. (1975). Elastoplastic stress-strain theory for cohesionless soil. Journal of the Geotechnical Engineering Division. 1037-1053

Lemos, L. J. L. and Vaughan, P. R. (2000). Clay-interface shear resistance. Geotechnique, Vol. 50, No. 1, 55-64

Muhlhaus, H. –B. and Vardoulakis, I. (1987). The thickness of shear bands in granular materials. Geotechnique, Vol. 37, No. 3, 271-283

Navayogarajah, N., Desai, C. S. and Kiousis, P. D. (1992). Hierarchical single-surface model for static and cyclic behaviour of interfaces. Journal of Engineering Mechanics, ASCE, 118 (5), 990-1011

Nogami, T. (1997). Observation and Modeling in Numerical Analysis and Model Tests in Dynamic Soil-Structure Interaction Problems. Proceedings of sessions held in conjunction with Geo-Logan '97, Geotechnical Special Publication, No. 64.

Potyondy, J. G. (1961). Skin friction between various soils and construction materials. Geotechnique, Vol. 14, No. 4, 39-53

Ramberg, W. and Osgood, W. R. (1943). Description of stress-strain curves by three parameters. Technical Note 902, National Advisory Committee for Aeronautics, Washington, D. C.

Rowe, P. W. (1962). The stress-dilatancy relation for static equilibrium of an assembly of particles in contact. Proceedings of the Royal Society, Vol. 269, Series A, London, England, 500-527

Schofield, A. N. and Wroth, C. P. (1968). Critical state soil mechanics. McGraw-Hill, London

Saada, A. S., Liang, L., Figueroa, J. L. and Cope, C. T. (1999). Bifurcation and shear band propagation in sands. Geotechnique, Vol. 49, No. 3, 367-385

Streeter, V. L., Wylie, E. B. and Richart, F. E. (1974). Soil motion computations by characteristics method. Journal of Geotechnical Engineering Division, ASCE, 100 (GT3), 247-263

Stroud, M. A. (1971). The behaviour of sand at low stress levels in the simple shear apparatus. PhD thesis. University of Cambridge, UK.

Tejchman, J. and Wu, W. (1995). Experimental and numerical study of sand-steel interfaces. Int. J. for Num. and Anal. Mech. in Geotech., 19, 513-536

Uesugi, M. and Kishida, H. (1985). Cyclic testing and modeling of interfaces (discussion). Journal of Geotechnical Engineering, ASCE 113 (9), 1086-1087

Uesugi, M. and Kishida, H. (1986a). Influential factors of friction between steel and dry sands. Soils and Foundations, Vol. 26, No. 2, 33-46

Uesugi, M. and Kishida, H. (1986b). Frictional resistance at yield between dry sand and mild steel. Soils and Foundations, Vol. 26, No. 4, 139-149

Uesugi, M., Kishida, H. and Tsubakihara, Y. (1988). Behavior of sand particles in sand-steel friction. Soils and Foundations, Vol. 28, No. 1, 107-118

Uesugi, M., Kishida, H. and Tsubakihara, Y. (1989). Friction between sand and steel under repeated loading. Soils and Foundations, Vol. 29, No. 3, 127-137

Uesugi, M., Kishida, H. and Uchikawa, Y. (1990). Friction between dry sand and concrete under monotonic and repeated loading. Soils and Foundations, Vol. 30, No. 1, 115-128

Uesugi, M. and Kishida, H. (1991). Cyclic axial loading analysis of piles in sand. (discussion). Journal of Geotechnical Engineering, ASCE 115 (6), 1435-1437

Unterreiner, P., Sulem, J., Vardoulakis, I. and Boulon, M. (1994). Essential features of a Cosserat continuum in interfacial localization. Localization and Bifurcation Theory for Soils and Rocks, Chambon, Desrues, Vardoulakis (eds)

Vardoulakis, I. and Unterreiner, P. (1995). interfacial localization in simple shear tests on a granular medium modelled as a Cosserat continuum. Mechanics of Geomaterial Interfaces, Selvadurai, A. P. S. and Boulon, M. J. (Editors)

Wroth, C. P. And Bassett, R. H. (1965). A stress-strain relationship for the shearing behaviour of a sand. Geotechnique, Vol. 15, No. 1, 32-56

Yoshida, T., Tatsuoka, F., Siddiquee, M. S. A., Kamegai, Y. and Park, C.-S. (1994). Shear banding in sands observed in plane strain compression. Localization and Bifurcation Theory for Soils and Rocks, Chambon, Desrues, Vardoulakis (eds)

Yoshimi, Y. and Kishida, T. (1981a). A ring torsion apparatus for evaluating friction between soil and metal surfaces. Geotechnical Testing Journal, Vol. 4, No. 4, 145-152

Yoshimi, Y. and Kishida, T. (1981b). Friction between sand and metal surface. Proceedings of 10th International Conference on Soils Mechanics and Foundation Engineering. Vol.1, 831-834

Yoshimi, Y. and Oh-oka, H. (1973). A ring torsion apparatus for simple shear tests. Proceedings of 8th International Conference on Soil Mechanics and Foundation Engineering, (1.2), 501-506

Zhang, H. (1997). Steady state behaviour of sands and limitations of the triaxial test. PhD thesis, University of Ottawa, Canada